

**An *ab Initio* Study of Cobalt(II) Complexes as Possible Corrosion Products in a
CANDU Supercritical Water-cooled Reactor (SCWR)**

by

Daniel Charles Murray Whynot

**A Thesis Submitted to Saint Mary's University, Halifax, Nova Scotia,
in Partial Fulfillment of the Requirements for the
Degree of Master of Science in Applied Science**

January 2012, Halifax, Nova Scotia

© Daniel Charles Murray Whynot, 2012

**Approved: Dr. Cory Pye
Supervisor
Department of Chemistry**

**Approved: Dr. Khashayar Ghandi
External Examiner
Department of Chemistry and Biochemistry
Mount Allison University**

**Approved: Dr. Jason Clyburne
Supervisory Committee Member
Department of Chemistry**

**Approved: Dr. Jacob Hanley
Supervisory Committee Member
Department of Geology**

**Approved: Dr. Jason Masuda
Graduate Studies Representative**

Date: January 19, 2012



Library and Archives
Canada

Published Heritage
Branch

395 Wellington Street
Ottawa ON K1A 0N4
Canada

Bibliothèque et
Archives Canada

Direction du
Patrimoine de l'édition

395, rue Wellington
Ottawa ON K1A 0N4
Canada

Your file Votre référence

ISBN: 978-0-494-83807-5

Our file Notre référence

ISBN: 978-0-494-83807-5

NOTICE:

The author has granted a non-exclusive license allowing Library and Archives Canada to reproduce, publish, archive, preserve, conserve, communicate to the public by telecommunication or on the Internet, loan, distribute and sell theses worldwide, for commercial or non-commercial purposes, in microform, paper, electronic and/or any other formats.

The author retains copyright ownership and moral rights in this thesis. Neither the thesis nor substantial extracts from it may be printed or otherwise reproduced without the author's permission.

AVIS:

L'auteur a accordé une licence non exclusive permettant à la Bibliothèque et Archives Canada de reproduire, publier, archiver, sauvegarder, conserver, transmettre au public par télécommunication ou par l'Internet, prêter, distribuer et vendre des thèses partout dans le monde, à des fins commerciales ou autres, sur support microforme, papier, électronique et/ou autres formats.

L'auteur conserve la propriété du droit d'auteur et des droits moraux qui protègent cette thèse. Ni la thèse ni des extraits substantiels de celle-ci ne doivent être imprimés ou autrement reproduits sans son autorisation.

In compliance with the Canadian Privacy Act some supporting forms may have been removed from this thesis.

While these forms may be included in the document page count, their removal does not represent any loss of content from the thesis.

Conformément à la loi canadienne sur la protection de la vie privée, quelques formulaires secondaires ont été enlevés de cette thèse.

Bien que ces formulaires aient inclus dans la pagination, il n'y aura aucun contenu manquant.

Canada

TABLE OF CONTENTS

	Page
Abstract	i
Acknowledgements	ii
List of Abbreviations	iii
List of Figures	iv
List of Tables	ix
Chapter 1: Introduction	
1.1	Supercritical Water-cooled Reactor (SCWR) 1
1.2	Cobalt 2
1.2.1	The Importance of Studying Cobalt in Relation to SCWRs 4
1.3	Quantum Mechanics 6
1.4	Computational Chemistry 9
1.4.1	Born-Oppenheimer Approximation 9
1.4.2	Basis Sets 10
1.4.3	Hartree-Fock Method 14
1.4.4	Self-Consistent Field 18
1.4.5	Møller-Plesset Perturbation Theory 19
1.4.6	Density Functional Theory 21
1.5	Conductor-like Screening Model (COSMO) 25
1.6	Research Objectives 26
Chapter 2: Methods	
2.1	Computational Methods 28

Chapter 3: Hydrated Cobalt(II) and Single Ligand Complexes

3.1	Water, Chloride, Hydroxide and Ammonia Ligands	32
3.2	Aquacobalt(II) Complexes, $[\text{Co}(\text{H}_2\text{O})_n]^{2+}$, where $n=1-6$	33
3.2.1	Results	34
3.2.2	Discussion/Literature Comparison	36
3.3	Chlorocobalt(II) Complexes, $[\text{CoCl}_n(\text{H}_2\text{O})_m]^{2-n}$, where $n=1-4$, $m=0-(6-n)$	46
3.3.1	Results	47
3.3.2	Discussion/Literature Comparison	51
3.4	Hydroxocobalt(II) Complexes, $[\text{Co}(\text{OH})_n(\text{H}_2\text{O})_m]^{2-n}$, where $n=1-4$, $m=0-(6-n)$	57
3.4.1	Results	58
3.4.2	Discussion/Literature Comparison	62
3.5	Ammincobalt(II) Complexes, $[\text{Co}(\text{NH}_3)_n(\text{H}_2\text{O})_m]^{2+}$, where $n=1-6$, $m=0-(6-n)$	69
3.5.1	Results	70
3.5.2	Discussion/Literature Comparison	75

Chapter 4: Hydrated Cobalt(II) Mixed-Ligand Complexes

4.1	Cobalt(II) Mixed-Ligand Complexes	82
4.2	Chlorohydroxocobalt(II) Complexes, $[\text{CoCl}_n(\text{OH})_m(\text{H}_2\text{O})_l]^{2-n-m}$, where $n=1-3$, $m=1-(4-n)$ and $l=0-(6-n-m)$	83
4.2.1	Results	83
4.2.2	Discussion/Literature Comparison	89
4.3	Chloroammincobalt(II) Complexes, $[\text{CoCl}_n(\text{NH}_3)_m(\text{H}_2\text{O})_l]^{2-n}$, where $n=1-4$, $m=1-(6-n)$ and $l=0-(6-n-m)$	94
4.3.1	Results	94
4.3.2	Discussion/Literature Comparison	96
4.4	Hydroxoammincobalt(II) Complexes, $[\text{Co}(\text{NH}_3)_n(\text{OH})_m(\text{H}_2\text{O})_l]^{2-m}$, where $n=1-5$, $m=1-(6-n)$ and $l=0-(6-n-m)$	104
4.4.1	Results	104

4.4.2	Discussion/Literature Comparison	109
Chapter 5: Conclusions and Future Work		
5.1	Conclusions	114
5.1.1	Aquacobalt(II)	115
5.1.2	Chlorocobalt(II)	115
5.1.3	Hydroxocobalt(II)	116
5.1.4	Ammincobalt(II)	116
5.1.5	Chlorohydroxocobalt(II)	116
5.1.6	Chloroammincobalt(II)	117
5.1.7	Hydroxoammincobalt(II)	118
5.2	Future Work	118
References		120
Chapter 3 Appendix A – Supplementary Materials		
Chapter 4 Appendix A – Supplementary Materials		

An ab Initio Study of Cobalt(II) Complexes as Possible Corrosion Products in a
CANDU Supercritical Water-cooled Reactor (SCWR)

by Daniel Charles Murray Whynot

Abstract

Atomic Energy of Canada Limited and CANDU are currently developing a Gen-IV Supercritical Water-cooled Reactor (SCWR). The SCWR offers advantages of increased thermal efficiency and sustainability, but at the cost of operating under extreme conditions (650°C and 25 MPa). Under these conditions, transition metals from the construction materials could dissolve and form complexes with surrounding anions and reprecipitate on the pipes and valves of the reactor, causing corrosion. Cobalt is one transition metal of interest because it exists in small quantities in many metal alloys and becomes highly reactive when bombarded with neutrons. Comprehensive *ab initio* computational studies were performed on cobalt(II) complexes containing water, chloride, hydroxide and ammonia ligands. For all molecules studied, optimized geometries were obtained as well as vibrational stretching frequencies, which were compared to experimental data, where possible, so that the most likely species to exist inside the reactor could be predicted.

January 19, 2012

ACKNOWLEDGEMENTS

Firstly, I would like to thank my thesis supervisor Dr. Cory Pye for his support throughout this whole process. It was his encouragement that made me want to pursue a Master's degree in the first place. This great opportunity will definitely have a positive influence on my future.

Secondly, I would like to thank the Natural Sciences and Engineering Research Council (NSERC), Atomic Energy of Canada Limited (AECL) and Natural Resources Canada (NRCan) for funding the research project that I am so appreciative to have been a part of. I am also grateful to the Saint Mary's University Faculty of Graduate Studies and Research for partially funding my graduate experience at SMU. Also, thanks to the Atlantic Computational Excellence network (ACEnet) for computer time.

I would also like to thank my lab group; Yaoting Zhang, Jane Ferguson, Barb Goodall, and Liwei Cheng, who have been great friends throughout this, sometimes frustrating, process. Also the "group meetings" and excursions during our summers together have solidified this experience as one of the best in my life to date. Jane also deserves a special mention as she provided me with many of the calculations for the complexes containing water and chloride.

Most importantly I want to thank my family, especially my wife Alyssa, who have been there during the most trying times of this whole experience and have provided me with all the support and encouragement that I needed to complete it.

LIST OF ABBREVIATIONS

ACEnet	Atlantic Computational Excellence Network
AECL	Atomic Energy of Canada Limited
B3LYP	Becke 3-Parameter Lee-Yang-Parr Hybrid Functional
CANDU	Canada Deuterium Uranium
COSMO	Conductor-like Screening Model
C-PCM	Conductor-like Polarizable Continuum Model
DFT	Density Functional Theory
GTO	Gaussian-Type Orbital
HF	Hartree-Fock
HPC	High-Performance Computing
IP	Ion Pair
LCAO	Linear Combination of Atomic Orbitals
LWR	Light Water Reactor
MO	Molecular Orbital
MP2	Second-order Møller-Plesset Perturbation Theory
NMR	Nuclear Magnetic Resonance
PCM	Polarizable Continuum Model
SAS	Solvent Accessible Surface
SCF	Self-Consistent Field
SCWR	Supercritical Water-cooled Reactor
STO	Slater-Type Orbital
UV/Vis	Ultraviolet/Visible

LIST OF FIGURES

- Figure 3-1:** The cobalt(II) and chloride ions as well as optimized MP2 and B3LYP geometries for the remaining ligands used in the calculations of cobalt(II) complexes. 32
- Figure 3-2:** Optimized MP2 and B3LYP geometries for $[\text{Co}(\text{H}_2\text{O})_n]^{2+}$, where $n=1 - 6$. All structures are similar with the exception of the trihydrate which is C_1 at MP2 and D_3 at B3LYP (indicated by “**”). 35
- Figure 3-3:** Co-O bond lengths (left) and vibrational stretching frequencies (right) for $[\text{Co}(\text{H}_2\text{O})_n]^{2+}$, where $n=1 - 6$, calculated at the HF/6-31+G* level. 40
- Figure 3-4:** Co-O bond lengths (left) and vibrational stretching frequencies (right) for $[\text{Co}(\text{H}_2\text{O})_n]^{2+}$, where $n=1 - 6$, calculated at the MP2/6-31+G* level. 41
- Figure 3-5:** Co-O bond lengths (left) and vibrational stretching frequencies (right) for $[\text{Co}(\text{H}_2\text{O})_n]^{2+}$, where $n=1 - 6$, calculated at the B3LYP/6-31+G* level. 42
- Figure 3-6:** Simulated Raman plot based on our HF/6-31+G* frequency calculation. 43
- Figure 3-7:** Hexaaquacobalt(II) dodecahydrate optimized at HF/6-31+G* with T (chiral tetrahedral) symmetry. 44
- Figure 3-8:** Optimized MP2 and B3LYP geometries for $[\text{CoCl}_n(\text{H}_2\text{O})_m]^{2-n}$, where $n=1 - 2$ and $m=0 - (6-n)$. All symmetries marked with “**” indicate B3LYP otherwise all MP2 and B3LYP structures are similar. 48

- Figure 3-9:** Optimized MP2 and B3LYP geometries for $[\text{CoCl}_n(\text{H}_2\text{O})_m]^{2-n}$, where $n=3 - 4$ and $m=0 - (6-n)$. There was no distinction between structures for MP2 and B3LYP. 49
- Figure 3-10:** Co-O and Co-Cl (highlighted in red) bond lengths (left) and vibrational stretching frequencies (right) for $[\text{CoCl}_n(\text{H}_2\text{O})_m]^{2-n}$, where $n=1 - 4$ and $m=0 - (6-n)$, calculated at the HF/6-31+G* level. 53
- Figure 3-11:** Co-O and Co-Cl (highlighted in red) bond lengths (left) and vibrational stretching frequencies (right) for $[\text{CoCl}_n(\text{H}_2\text{O})_m]^{2-n}$, where $n=1 - 4$ and $m=0 - (6-n)$, calculated at the MP2/6-31+G* level. 54
- Figure 3-12:** Co-O and Co-Cl (highlighted in red) bond lengths (left) and vibrational stretching frequencies (right) for $[\text{CoCl}_n(\text{H}_2\text{O})_m]^{2-n}$, where $n=1 - 4$ and $m=0 - (6-n)$, calculated at the B3LYP/6-31+G* level. 55
- Figure 3-13:** Optimized MP2 and B3LYP geometries for $[\text{Co}(\text{OH})(\text{H}_2\text{O})_m]^+$ (top) and $[\text{Co}(\text{OH})_2(\text{H}_2\text{O})_m]$ (bottom). “*” indicates B3LYP geometry is different than MP2. 59
- Figure 3-14:** Optimized MP2 and B3LYP geometries for $[\text{Co}(\text{OH})_3(\text{H}_2\text{O})_m]$ (top) and $[\text{Co}(\text{OH})_4(\text{H}_2\text{O})_m]^{2-}$ (bottom). “*” indicates B3LYP geometry if different than MP2. 61
- Figure 3-15:** Co-O bond lengths (left) and vibrational stretching frequencies (right) for $[\text{Co}(\text{OH})_n(\text{H}_2\text{O})_m]^{2-n}$, where $n=1 - 4$ and $m=0 - (6-n)$, calculated at the HF/6-31+G* level. 64
- Figure 3-16:** Co-O bond lengths (left) and vibrational stretching frequencies (right) for $[\text{Co}(\text{OH})_n(\text{H}_2\text{O})_m]^{2-n}$, where $n=1 - 4$ and $m=0 - (6-n)$, calculated at the MP2/6-31+G* level. 65

- Figure 3-17:** Co-O bond lengths (left) and vibrational stretching frequencies (right) for $[\text{Co}(\text{OH})_n(\text{H}_2\text{O})_m]^{2-n}$, where $n=1-4$ and $m=0-(6-n)$, calculated at the B3LYP/6-31+G* level. 66
- Figure 3-18:** Optimized MP2 and B3LYP geometries for $[\text{Co}(\text{NH}_3)_n(\text{H}_2\text{O})_m]^{2+}$, where $n=1-2$, $m=0-(6-n)$. “*” indicates only stable at MP2, “a” indicates only stable at B3LYP. 72
- Figure 3-19:** Optimized MP2 and B3LYP geometries for $[\text{Co}(\text{NH}_3)_n(\text{H}_2\text{O})_m]^{2+}$, where $n=3-6$, $m=0-(6-n)$. “*” indicates only stable at MP2, “a” indicates only stable at B3LYP. 73
- Figure 3-20:** Co-N (+) and Co-O (l) bond lengths (left) and vibrational stretching frequencies (right) for $[\text{Co}(\text{NH}_3)_n(\text{H}_2\text{O})_m]^{2+}$, where $n=1-6$ and $m=0-(6-n)$, calculated at the HF/6-31+G* level. 78
- Figure 3-21:** Co-N (+) and Co-O (l) bond lengths (left) and vibrational stretching frequencies (right) for $[\text{Co}(\text{NH}_3)_n(\text{H}_2\text{O})_m]^{2+}$, where $n=1-6$ and $m=0-(6-n)$, calculated at the MP2/6-31+G* level. 79
- Figure 3-22:** Co-N (+) and Co-O (l) bond lengths (left) and vibrational stretching frequencies (right) for $[\text{Co}(\text{NH}_3)_n(\text{H}_2\text{O})_m]^{2+}$, where $n=1-6$ and $m=0-(6-n)$, calculated at the B3LYP/6-31+G* level. 80
- Figure 4-1:** Optimized MP2 and B3LYP geometries for $[\text{CoCl}(\text{OH})_m(\text{H}_2\text{O})_l]^{1-m}$, where $m=1-2$, $l=0-(5-m)$. “*” indicates only stable at MP2, “a” indicates only stable at B3LYP. 84
- Figure 4-2:** Optimized MP2 and B3LYP geometries for $[\text{CoCl}_n(\text{OH})_m(\text{H}_2\text{O})_l]^{1-n-m}$, where $n=1-3$, $m=1-3$, $l=0-(6-n-m)$. 86

- Figure 4-3:** Co-Cl (+) and Co-O (l) bond lengths (left) and vibrational stretching frequencies (right) for $[\text{CoCl}_n(\text{OH})_m(\text{H}_2\text{O})_l]^{2-n-m}$, where $n=1-3$, $m=1-(4-n)$ and $l=0-(6-n-m)$, calculated at the HF/6-31+G* level. 91
- Figure 4-4:** Co-Cl (+) and Co-O (l) bond lengths (left) and vibrational stretching frequencies (right) for $[\text{CoCl}_n(\text{OH})_m(\text{H}_2\text{O})_l]^{2-n-m}$, where $n=1-3$, $m=1-(4-n)$ and $l=0-(6-n-m)$, calculated at the MP2/6-31+G* level. 92
- Figure 4-5:** Co-Cl (+) and Co-O (l) bond lengths (left) and vibrational stretching frequencies (right) for $[\text{CoCl}_n(\text{OH})_m(\text{H}_2\text{O})_l]^{2-n-m}$, where $n=1-3$, $m=1-(4-n)$ and $l=0-(6-n-m)$, calculated at the B3LYP/6-31+G* level. 93
- Figure 4-6:** Optimized MP2 and B3LYP geometries for $[\text{CoCl}(\text{NH}_3)_m(\text{H}_2\text{O})_l]^+$, where $m=1-5$, $l=0-(5-m)$. “*” indicates only stable at MP2, “^a” indicates only stable at B3LYP. 97
- Figure 4-7:** Optimized MP2 and B3LYP geometries for $[\text{CoCl}_2(\text{NH}_3)_m(\text{H}_2\text{O})_l]$, where $m=1-4$, $l=0-(4-m)$. “*” indicates only stable at MP2, “^a” indicates only stable at B3LYP. 98
- Figure 4-8:** Optimized MP2 and B3LYP geometries for $[\text{CoCl}_n(\text{NH}_3)_m(\text{H}_2\text{O})_l]$, where $n=3-4$, $m=1-(6-n)$, $l=0-(6-n-m)$. “*” indicates only stable at MP2, “^a” indicates only stable at B3LYP. 99
- Figure 4-9:** Co-Cl (+), Co-N (x) and Co-O (l) bond lengths (left) and vibrational stretching frequencies (right) for $[\text{CoCl}_n(\text{NH}_3)_m(\text{H}_2\text{O})_l]^{2-n-m}$, where $n=1-4$, $m=1-(6-n)$ and $l=0-(6-n-m)$, calculated at the HF/6-31+G* level. 101
- Figure 4-10:** Co-Cl (+), Co-N (x) and Co-O (l) bond lengths (left) and vibrational stretching frequencies (right) for $[\text{CoCl}_n(\text{NH}_3)_m(\text{H}_2\text{O})_l]^{2-n-m}$, where $n=1-4$, $m=1-(6-n)$ and $l=0-(6-n-m)$, calculated at the MP2/6-31+G* level. 102

- Figure 4-11:** Co-Cl (+), Co-N (x) and Co-O (|) bond lengths (left) and vibrational stretching frequencies (right) for $[\text{CoCl}_n(\text{NH}_3)_m(\text{H}_2\text{O})_l]^{2-n-m}$, where $n=1-4$, $m=1-(6-n)$ and $l=0-(6-n-m)$, calculated at the B3LYP/6-31+G* level. 103
- Figure 4-12:** Optimized MP2 and B3LYP geometries for $[\text{Co}(\text{NH}_3)(\text{OH})_m(\text{H}_2\text{O})_l]^{2-m}$, where $m=1-4$, $l=0-(5-m)$. “*” indicates only stable at MP2, “a” indicates only stable at B3LYP. 106
- Figure 4-13:** Optimized MP2 and B3LYP geometries for $[\text{Co}(\text{NH}_3)_2(\text{OH})_m(\text{H}_2\text{O})_l]^{2-m}$, where $m=1-4$, $l=0-(4-m)$. “*” indicates only stable at MP2, “a” indicates only stable at B3LYP. 107
- Figure 4-14:** Optimized MP2 and B3LYP geometries for $[\text{Co}(\text{NH}_3)_n(\text{OH})_m(\text{H}_2\text{O})_l]^{2-m}$, where $n=3-5$, $m=1-(6-n)$, $l=0-(6-n-m)$. “*” indicates only stable at MP2, “a” indicates only stable at B3LYP. 108
- Figure 4-15:** Co-N (+) and Co-O (|) bond lengths (left) and vibrational stretching frequencies (right) for $[\text{Co}(\text{NH}_3)_n(\text{OH})_m(\text{H}_2\text{O})_l]^{2-m}$, where $n=1-5$, $m=1-(5-n)$ and $l=0-(6-n-m)$, calculated at the HF/6-31+G* level. 111
- Figure 4-16:** Co-N (+) and Co-O (|) bond lengths (left) and vibrational stretching frequencies (right) for $[\text{Co}(\text{NH}_3)_n(\text{OH})_m(\text{H}_2\text{O})_l]^{2-m}$, where $n=1-5$, $m=1-(5-n)$ and $l=0-(6-n-m)$, calculated at the MP2/6-31+G* level. 112
- Figure 4-17:** Co-N (+) and Co-O (|) bond lengths (left) and vibrational stretching frequencies (right) for $[\text{Co}(\text{NH}_3)_n(\text{OH})_m(\text{H}_2\text{O})_l]^{2-m}$, where $n=1-5$, $m=1-(5-n)$ and $l=0-(6-n-m)$, calculated at the B3LYP/6-31+G* level. 114

LIST OF TABLES

<u>Table 3.1</u> : Geometry comparison of hexacoordinate ammine complexes with results reported by Schmiedekamp et al. ⁵⁴ and Varadwaj and Marques ⁵⁷ . All bond lengths are averages where appropriate.	76
<u>Table 4.1</u> : Stable Geometries of $[\text{CoCl}_n(\text{OH})_m(\text{H}_2\text{O})_l]^{2-n-m}$, with lowest energy symmetries highlighted in yellow.	89
<u>Table 4.2</u> : Stable Geometries of $[\text{CoCl}_n(\text{NH}_3)_m(\text{H}_2\text{O})_l]^{2-n}$, with lowest energy point group symmetries highlighted in yellow.	95
<u>Table 4.3</u> : Stable Geometries of $[\text{Co}(\text{NH}_3)_n(\text{OH})_m(\text{H}_2\text{O})_l]^{2-m}$, with point group of the lowest energy geometry highlighted in yellow.	105

1.1 Supercritical Water-cooled Reactor (SCWR)

Atomic Energy of Canada Limited (AECL) and CANDU are currently developing concepts for Generation IV nuclear reactors¹. One of the most promising concepts is the Supercritical Water-cooled Reactor (SCWR), expected to come online by 2025, which offers advantages in the areas of sustainability, safety and an increase in thermal efficiency of ~50% vs. 33% in current Light Water Reactors (LWRs)². The SCWR will employ a single phase coolant with high enthalpy and will eliminate components such as steam generators and steam separators².

The SCWR will operate at extreme temperatures and pressures that are expected to be in the region of 650°C and 25 MPa respectively, leaving the operating conditions well beyond the critical point of water (374°C and 22.1 MPa). Because of the extreme operating conditions it becomes very important to understand the water chemistry at these extreme temperatures and pressures, with the most important region possibly being from 300-450°C where there is a considerable change in the properties of water. The long-term viability of the SCWR will largely depend on the ability to predict and control the water chemistry in the reactor environment.

Due to the existence of supercritical water inside this reactor, some of the basic properties of a supercritical fluid should be mentioned. Some of these properties are: (i) it is a single-phase fluid whose density can vary significantly when temperature and

pressure are changed, but does not undergo any phase changes; (ii) the fluid is highly compressible and generally has vapor-like properties (at the SCWR conditions); and (iii) the fluid is limited as ionic solvents, that is, although they are expected to carry trace amounts of many metals, they cannot dissolve the same order of magnitude that would be expected of a proper subcritical liquid-like solution. As water approaches its critical point (as temperature increases) the properties of the water will change significantly. There will be no distinct liquid and gas phases, the fluid will be able to effuse through solids like a gas, but be able to dissolve materials like a liquid and right around the critical point the density will change significantly with small changes in temperature and pressure.

One major issue affecting the development of the SCWR is the possibility of corrosion occurring in the pipes and valves of the water loop of the reactor. Corrosion of the pipes and valves could lead to weak spots and/or cracks in the construction material and ultimately leakage of radioactive byproducts. One type of corrosion may be caused by transition metals, existing in the construction material, dissolving and forming aqua ions which could then combine with surrounding anions that are present inside the water loop to create neutral complexes. These corrosion products may then be transported throughout the loop and settle in low-lying areas (i.e. connections between pipes) or reprecipitate in the pumps or valves thereby corroding these areas and altering the water chemistry.

1.2 Cobalt

Cobalt is a group IX transition metal with atomic number 27 and symbol Co. Cobalt compounds have been known since about 2600 BC, being found as the blue glaze

on pottery in Egyptian tombs³. The source of the blue color was recognized in 1735 by the Swedish chemist G. Brandt, who isolated a very impure metal, or “regulus”, which he named “cobalt rex”⁴. In 1780 T. O. Bergman showed this to be a new element⁴. The name of the element is derived from the German word Kobald which means goblin, a name possibly assigned because of the stench in roasting its arsenic-containing ores³. Cobalt is a hard lustrous bluish-white metal which acquires a somewhat inert coat of Co_3O_4 in air³. Cobalt makes up approximately 0.0029% of the earth’s crust and though widely distributed, stands only thirteenth in order of abundance and is less common than all other elements of the first transition series except scandium⁴. Cobalt occurs in rocks, sea waters, mineral waters, coal, soils, plants and animals⁵. A low level of cobalt, chiefly in the vitamin B_{12} complex, is necessary for human health³. The distribution of Co is influenced by the solubility in natural waters and its precipitation with changes in pH and other conditions⁵.

Prior to 1914 very little cobalt metal was produced with the oxide being the marketable form of the element⁶. Around this time however, there were two factors responsible for the development of methods designed to produce the metal⁶. Firstly, there was a war that demanded research into ferrous alloying metals, and secondly there was support from the Canadian government for comprehensive investigation into the properties and uses of Co to aid in the rapidly growing Canadian industry⁶. Before the war most of the production of cobalt went to the ceramic industry (oxide form) to serve as a glaze coloring on china, porcelain, pottery and glass, and after this period it was used to make tools (steel alloys), permanent magnets and other alloys. The major deposits of

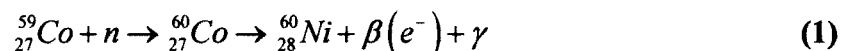
cobalt are found in Africa (Democratic Republic of the Congo, Zimbabwe and Morocco), Canada, United States, Finland and Russia⁵.

Cobalt exists in oxidation states of -1, 0, +1, +2 and +3. Cobalt is more stable in the +2 oxidation state than in the +3 oxidation state except in hydroxides, where the stability is reversed⁷. These two oxidation states are also the most important in aqueous chemistry. Cobalt(II) complexes involving chloride, hydroxide, ammonia, and water along with their importance in the development of SCWRs are the focus of this thesis and will be discussed individually in the sections to follow.

1.2.1 The Importance of Studying Cobalt in Relation to SCWRs

The operating conditions of the SCWR make cobalt an appealing metal for development of construction materials for the reactor. Cobalt metal by itself is not very useful but when alloyed with other metals it can provide many benefits. Cobalt-based alloys can provide wear resistance, resistance to aqueous corrosion and can be used for high-temperature environments⁸. Cobalt alloys were developed in the early 1900s for resisting corrosive environments and for high-temperature strength and hardness⁸. The alloys are used in cutting tools operating in aggressive chemical media, steam valves and valve seats, pressure gauges, bushings, nozzles, pressure seats and implant materials for the human body⁸. The properties of corrosion resistance and high-temperature and pressure strength make these alloys a possible candidate for construction materials for the SCWR. In fact, many of the metal alloys being considered for the construction materials of the SCWR do contain a small amount of cobalt^{9,10}.

There are two issues with using cobalt which provide reasons for wanting to investigate cobalt complexes. The first issue is that transition metals, in which cobalt is included, may dissolve and contaminate the reactor environment due to the operating conditions. At low temperatures the transition metals tend to form aqua ions (e.g. $[\text{Co}(\text{H}_2\text{O})_6]^{2+}$). At high temperatures, due to the much lower dielectric constant of water (~ 8 vs ~ 80 at room temperature), transition metals tend to form neutral complexes with surrounding anions and water and/or ammonia, which may be added into the reactor for pH adjustment. The anions may be introduced via leaking through the cooling system (i.e. Cl^- ions in river water) or from the addition of water itself (OH^- ions). This leads to the second issue and reason why cobalt may be more important to study than other transition metals commonly found in metal alloys, such as nickel, iron and chromium. There is a possibility of the highly radioactive isotope ^{60}Co being produced¹¹ when the naturally occurring isotope ^{59}Co is bombarded by neutrons emitted from the reactor core as in the following schematic:



Therefore it is important to understand and predict the possible complexes cobalt will form under the conditions of the SCWR so that corrosion due to cobalt complex formation and transportation throughout the reactor can be controlled. All of the complexes were studied up to and including the six-coordinate species.

1.3 Quantum Mechanics

Classical mechanics was developed in part due to Newton's laws of motion, but is somewhat restricted to only describing the motion of macroscopic objects that have associated speeds which are not approaching the speed of light. The theory of quantum mechanics was developed after a series of observations were made that could not be explained by classical mechanics. These observations include blackbody radiation, the photoelectric effect, heat capacity properties, atomic spectra and de Broglie waves.

Blackbody radiation refers to the radiation emitted by a blackbody, an ideal body which absorbs and emits radiation at all frequencies¹². The failure of classical mechanics in this realm was first recognized clearly by Planck in 1901, when he assumed that the blackbody was composed of harmonic oscillators and found that the absorption or emission of radiation was not continuous as thought by classical mechanics¹³. The ejection of electrons from the surface of a metal by radiation is called the photoelectric effect¹². As explained by Einstein, if the kinetic energy of the emitted electrons is plotted against the frequency of incident light, you get a straight line, which is independent of the intensity of incident light at constant frequency¹³. Classical mechanics predicts that the kinetic energy of the electrons should increase with increasing intensity of incident radiation.

A heat capacity is defined as the amount of heat required to change a substance's temperature by a given amount. The classical result says that the molar heat capacity at constant volume, C_v , is equal to $3R$, where R is the molar gas constant¹². However, according to experimental findings, the classical result is only true at high temperatures

and C_v decreases and goes to zero as the temperature is lowered and approaches zero Kelvin¹². Bohr's development in the theory of the hydrogen spectrum, in which a pattern was found in the wavelengths or frequencies of the spectral lines combined with de Broglie's postulate that electrons and other particles have waves associated with them¹⁴ both contribute to the wave nature of particles. Quantum mechanics, differing from classical mechanics, suggests that matter has both particle-like and wave-like properties and has therefore led to what is known as wave-particle duality.

Accounting for wave character in mechanical systems leads to the concept of a wavefunction, denoted by the Greek letter ψ . The wavefunction serves an important role in quantum mechanics. The most fundamental equation in quantum mechanics, the Schrödinger equation, was first proposed by an Austrian physicist, Erwin Schrödinger, in 1926¹⁵ and in its condensed version can be written as:

$$\hat{H}\psi = E\psi \quad (2)$$

The solutions to the Schrödinger equation are wavefunctions¹². A wavefunction gives a complete quantum-mechanical description of any system¹². The wavefunction is considered to be an eigenfunction of the Hamiltonian operator, \hat{H} , because when the Hamiltonian is applied to the wavefunction you get the wavefunction back along with the constant, E , which is an eigenvalue of the wavefunction. The Hamiltonian,

$$-\frac{\hbar}{2m} \frac{d^2}{dx^2} + V(x) \quad (3)$$

is a specific operator which contains both potential and kinetic energy parts¹², where \hbar is equal to $\frac{h}{2\pi}$, where h is Planck's constant; m is equal to the particle mass; $V(x)$ is the potential energy of the particle at position x .

The above Schrödinger equation is time-independent and it therefore gives solutions called stationary-state wavefunctions, which provides sufficient information to solve many problems chemists are interested in. The equation is also one-dimensional, as indicated by the single x variable, and is often used to describe the simple, yet very instructive particle-in-a-box problem. The problem applies the Schrödinger equation to a free particle of mass m that is restricted to lie along a one-dimensional interval of length a , and is used to introduce the probabilistic interpretation of wave functions which can then be applied to the Heisenberg uncertainty principle¹². The Heisenberg uncertainty principle says that you cannot know both the position and momentum of the particle of interest simultaneously due to the wavelike properties of the particle and therefore there are lower limits to the uncertainty (4) of a given measurable observable¹⁶.

$$\Delta x \Delta p \geq \frac{\hbar}{2} \quad (4)$$

The one-dimensional Schrödinger equation can be extended to include three dimensions, x , y and z giving a new equation:

$$-\frac{\hbar^2}{2m} \left(\frac{\partial^2 \psi}{\partial x^2} + \frac{\partial^2 \psi}{\partial y^2} + \frac{\partial^2 \psi}{\partial z^2} \right) = E\psi(x, y, z) \quad (5)$$

This equation can be condensed to give:

$$-\frac{\hbar^2}{2m}\nabla^2\psi(x, y, z) = E\psi(x, y, z) \quad (6)$$

The difference between (5) and (6) is the operator with the symbol ∇^2 , which is referred to as the Laplacian operator and is equivalent to:

$$\nabla^2 = \left(\frac{\partial^2\psi}{\partial x^2} + \frac{\partial^2\psi}{\partial y^2} + \frac{\partial^2\psi}{\partial z^2} \right) \quad (7)$$

These few equations are the basis of all atomic and molecular computational chemistry calculations and solving the Schrödinger equation is central to solving all quantum mechanical problems¹⁶.

1.4 Computational Chemistry

1.4.1 Born-Oppenheimer Approximation

The Schrödinger equation for the hydrogen atom can be solved exactly¹². Without approximations the Schrödinger equation for all atoms after hydrogen (two-body system) and molecules cannot be solved exactly. This is due to the fact that there is more than one electron which introduces an interelectronic repulsion term into the Schrödinger equation. Even the simplest molecule, H_2^+ consists of three particles and its Schrödinger equation cannot be solved analytically¹⁷. To overcome this issue the Born-Oppenheimer approximation is adopted. The Born-Oppenheimer approximation, proposed by Max Born and J. Robert Oppenheimer in 1927¹⁸, simplifies the Schrödinger equation for molecules. The approximation takes note of the great differences in masses of electrons

and nuclei and because of this difference the electron can respond almost instantaneously to the displacement of the nuclei⁸. Therefore you can make an approximate separation of a molecular Schrödinger equation into one for electronic motion and one for nuclear (vibrational and rotational) motion¹² by adjusting the wavefunction to:

$$\Psi_{molecule} \approx \Psi_{electronic} \times \Psi_{nuclear} \quad (8)$$

Therefore instead of trying to solve the Schrödinger equation for all the particles simultaneously, it is possible to regard the nuclei as fixed in position and to solve the equation for the electrons in the static electric potential arising from the nuclei in that particular arrangement⁸. The nuclei arrangements can then be changed and the calculation repeated, ultimately resulting in a molecular potential energy curve for the given species which will contain a minimum corresponding to the equilibrium conformation of the molecule. Even with the use of the Born-Oppenheimer approximation the only molecule that has an exact solution to the Schrödinger equation is the hydrogen ion, H_2^+ . A restriction to the Born-Oppenheimer approximation is that it is very reliable for ground electronic states, but is less reliable for excited states⁸.

1.4.2 Basis Sets

Basis sets are an essential part to performing a successful computational chemistry calculation on any molecule. A basis set is a set of mathematical functions (basis functions), linear combinations of which yield molecular orbitals¹⁹. The linear combination of atomic orbitals (LCAO) approach is used to approximately represent the

molecular orbitals (MO). The atomic orbitals associated with each nucleus are like the hydrogen-like orbitals¹⁴ which are of the form:

$$\psi_{nlm_l}(r, \theta, \phi) = R_{nl}(r) Y_l^{m_l}(\theta, \phi) \quad (9)$$

Here the n , l and m_l are quantum numbers corresponding to the energy level, subshell (s, p, d, etc.) and the specific orbital within the subshell respectively; r , θ and ϕ are spherical coordinate system parameters; $R_{nl}(r)$ is the hydrogen-like radial wave function that depends on the quantum numbers n and l and $Y_l^{m_l}(\theta, \phi)$ refers to spherical harmonics. The problem with the hydrogen atom wavefunctions is that they are not a good choice as a starting point for systems with more than one electron due to electron shielding effects¹⁶. The most commonly used basis sets for molecular systems are composed of either Slater-type orbitals (STOs) or Gaussian-type orbitals (GTOs).

Slater-type orbitals were introduced in the 1930s by John Slater¹² and are of the form:

$$S_{nlm_l}(r, \theta, \phi) = N_{nl} r^{n-1} e^{-\zeta r} Y_l^{m_l}(\theta, \phi) \quad (10)$$

Gaussian-type orbitals are of the form,

$$G_{lm_l}(r, \theta, \phi) = N_l r^l e^{-\alpha r^2} Y_l^{m_l}(\theta, \phi). \quad (11)$$

In equation (10) N_{nl} is the normalization constant, r is the distance between the nucleus and the electron, ζ (zeta) is the effective charge at the nucleus and $Y_l^{m_l}(\theta, \phi)$ are the spherical harmonics. In equation (11) there is a shielding constant α . Slater-type orbitals

and Gaussian-type orbitals differ primarily and most importantly in the exponential term. Slater-type orbitals are ideal in describing atomic orbitals as they have a proper cusp at the nucleus ($r = 0$), as indicated by the dependence on r in equation (10). The problem with using STOs in molecular calculations is that there is a high computational cost due to the cusp, or discontinuity, at the nucleus. Because of the extra computational cost, STOs are primarily used for calculations of small atomic and diatomic systems¹⁹. Gaussian-type orbitals differ from STOs at small values of r , where GTOs are lower and have a slope of zero at $r = 0$ (r^2 dependence) and also at large values of r , where GTOs are smaller than STOs. The discrepancy between a Slater orbital and a Gaussian orbital turns out to be significant in molecular calculations¹². To overcome this difficulty, linear combinations of Gaussian functions are used to curve-fit one Slater orbital, the fit improving with the number of Gaussian functions used¹². This results in an increase in the number of integrals that must be solved in a computation; however, the computational time is less for GTOs than for STOs¹⁶. The reason for the decreased computational time is because the product of two Gaussian functions centered at two different nuclei are equal to a single Gaussian centered at a third point¹⁶.

The number of Gaussian functions used in the LCAO approach needs to be determined. The individual Gaussian functions are called primitive Gaussians and when a linear combination of Gaussian functions is taken to represent the Slater orbital it is called a contracted Gaussian function. This contracted Gaussian is treated as a single fixed function in subsequent calculations. In order to produce a precise molecular orbital, an infinite basis set should be used¹⁶. In reality only finite basis sets can be used. When

the smallest number of functions is used it is referred to as a minimal basis set. A minimal basis set is comprised of the minimum number of atomic orbitals needed to hold all of the electrons in a given atom¹⁶. There are two shortcomings with using a minimal basis set for molecular systems. One shortcoming is that all basis functions are either themselves spherical (s functions) or come in sets that describe a sphere (p functions)¹⁶. The other is that the basis functions are atom centered, which restricts the flexibility of the functions to describe electron distribution between the nuclei to form chemical bonds¹⁶. The net effect of these limitations is to make molecules too ionic and bonds too long¹⁶. The easy way to overcome these problems is to use a basis set that is composed of more functions. This will allow for more adjustable parameters in the optimization, but will come at a computational cost. The solution to the problem of the minimal basis function being too spherical is to introduce a split-valence basis set. In a split-valence basis set the valence atomic orbitals are split into two parts: an inner compact orbital, and an outer more diffuse one¹⁶. A commonly used split-valence basis set is 3-21G. This nomenclature indicates that the core orbitals (represented by the first number) are made up of 3 Gaussian functions¹⁶. The inner valence orbitals are made up of 2 Gaussian functions and the outer valence orbitals are made up of 1 Gaussian function¹⁶, as indicated by the last two numbers. To overcome the problem of the basis functions being atom centered, polarization functions can be added to the basis set. The result of adding polarization functions is that *d* character can be added to the valence electrons in a *p* orbital. The addition of polarization functions is denoted by adding a "*" at the end of the basis set. An example of a polarization basis set is 6-31G*, which indicates that *d* orbitals

have been added to the p orbitals of the 6-31G basis set. Polarization can also be used to add p orbitals to hydrogen atoms. This is done by adding an additional “*” to the end of the basis set, with an example being 6-31G**.

In addition to adding polarization it is sometimes desirable to add what are called diffuse functions¹². Diffuse functions are Gaussian functions with fairly small orbital exponents, which cause the Gaussian functions to be large in extent¹². Diffuse functions are particularly useful for describing electrons that are relatively far from the nucleus, such as lone-pair electrons or electrons in anions¹². One diffuse function, composed of a single Gaussian function, is added to each valence orbital of the atoms beyond helium¹². Diffuse functions are indicated in a basis set by the addition of a “+” before the G, such as 6-31+G*. Diffuse functions can also be added to hydrogen atoms by inserting an additional “+” before the G in the basis set.

1.4.3 Hartree-Fock Method

The Hartree-Fock approximation is the standard first approximation for all atomic and molecular calculations in modern quantum chemistry¹². This approximation gives the optimal molecular orbital representation of the electronic structure of a molecule¹². The Hartree-Fock method is used to solve the wavefunctions of molecules and gives molecular information such as geometries and bond lengths which gives an indication of reactivity. This is considered an approximation method because the very concept of molecular orbitals, or atomic orbitals in the case of atoms, assumes that the electrons interact in some average potential¹². The Hartree-Fock method obeys the Pauli exclusion principle by stating that all electronic wavefunctions must be antisymmetric under the

interchange of any two electrons¹². The Pauli exclusion principle is most commonly known to state that no two electrons in an atom can have the same values for all four quantum numbers, n , l , m_l and m_s . Antisymmetric wavefunctions can be represented by Slater determinants which are of the form:

$$\Psi(1,2,\dots,2N) = \frac{1}{\sqrt{(2N)!}} \begin{vmatrix} \psi_1\alpha(1) & \psi_1\beta(1) & \cdots & \psi_N\alpha(1) & \psi_N\beta(1) \\ \psi_1\alpha(2) & \psi_1\beta(2) & \cdots & \psi_N\alpha(2) & \psi_N\beta(2) \\ \vdots & \vdots & \ddots & \vdots & \vdots \\ \psi_1\alpha(2N) & \psi_1\beta(2N) & \cdots & \psi_N\alpha(2N) & \psi_N\beta(2N) \end{vmatrix} \quad (12)$$

for a closed-shell system containing $2N$ electrons, in which the wavefunctions are represented by N doubly occupied spatial orbitals¹². The $2N$ represents the number of electrons, each of which has a spin of α or β . The equation is normalized with the normalization constant being the fraction in front of the determinant. The wavefunctions in the determinant are antisymmetric because of two important properties of determinants. The first is that the value of a determinant changes sign when any two rows or any two columns of the determinant are interchanged (i.e. interchange two electrons) and the second is that a determinant is equal to zero if any two rows or any two columns are the same¹² (i.e. two electrons occupy the same spin orbital). The Hamiltonian operator for a $2N$ electron molecule with M nuclei is given by:

$$\hat{H} = -\frac{1}{2} \sum_{i=1}^{2N} \nabla_i^2 - \sum_{i=1}^{2N} \sum_{A=1}^M \frac{Z_A}{r_{iA}} + \sum_{i=1}^{2N} \sum_{j>i}^{2N} \frac{1}{r_{ij}} + \sum_A^M \sum_{B<A}^M \frac{Z_A Z_B}{R_{AB}} \quad (13)$$

The first term represents the kinetic energy of the electrons, the second term is the interaction of each electron with each nucleus, the third term is the electron-electron

interactions and the fourth term represents the internuclear repulsion. The internuclear repulsion terms can be ignored initially because they are constants for a given molecular geometry. The energy, in bra-ket notation is given by:

$$E = \langle \Psi(1,2,\dots,2N) | \widehat{H} | \Psi(1,2,\dots,2N) \rangle \quad (14)$$

which can be written as:

$$E = 2 \sum_{i=1}^N I_j + \sum_{i=1}^N \sum_{j=1}^N (2J_{ij} - K_{ij}) \quad (15)$$

In equation (15) I_j , J_{ij} and K_{ij} are represented by:

$$I_j = \int dr_j \psi_j^*(r_j) \left(-\frac{1}{2} \nabla_j^2 - \sum_A^M \frac{Z_A}{r_{jA}} \right) \psi_j(r_j) \quad (16)$$

$$J_{ij} = \iint dr_1 dr_2 \psi_i^*(r_1) \psi_j^*(r_2) \frac{1}{r_{12}} \psi_i(r_1) \psi_j(r_2) \quad (17)$$

$$K_{ij} = \iint dr_1 dr_2 \psi_i^*(r_1) \psi_j^*(r_2) \frac{1}{r_{12}} \psi_i(r_2) \psi_j(r_1) \quad (18)$$

J_{ij} integrals are called Coulomb integrals and the K_{ij} integrals are called exchange integrals. The spatial orbitals ψ_i are determined by applying the variational principle to equation (15). The variational principle states that if any trial wavefunction that is not the ground-state wavefunction is used, it will produce an energy that is greater than the ground-state energy. If the trial wavefunction depends on some arbitrary parameters called variational parameters, the energy will also depend on these parameters. This

allows the energy to be minimized with respect to each of the variational parameters and therefore approach the ground-state energy. When the variational principle is applied, the result is:

$$\hat{F}(r_1)\psi_i(r_1) = \varepsilon_i\psi_i(r_1) \quad (19)$$

The eigenvalue of equation (19) is called the Hartree-Fock orbital energy, $\hat{F}(r_1)$ is the Fock operator and is represented by:

$$\hat{F}(r_1) = -\frac{1}{2}\nabla_1^2 - \frac{Z}{r_1} + \sum_j^N [2\hat{J}_j(r_1) - \hat{K}_j(r_1)] \quad (20)$$

where $\hat{J}_j(r_1)$ is the Coulomb operator given by:

$$\hat{J}_j(r_1)\psi_i(r_1) = \psi_i(r_1) \int dr_2 \psi_j^*(r_2) \frac{1}{r_{12}} \psi_j(r_2) \quad (21)$$

and $\hat{K}_j(r_1)$ is the exchange operator given by:

$$\hat{K}_j(r_1)\psi_i(r_1) = \psi_j(r_1) \int dr_2 \psi_j^*(r_2) \frac{1}{r_{12}} \psi_i(r_2) \quad (22)$$

The Hartree-Fock equations must be solved by a self-consistent procedure, which is described in the next section.

The Hartree-Fock approximation yields the best energy that can be obtained using a determinantal wavefunction consisting of spin orbitals¹². The HF method does have some limitations though. One of the limitations of HF calculations is that they do not

include electron correlation²⁰. This means that HF takes into account the average effect of electron repulsion, but not the explicit electron-electron interaction²⁰. The correlation energy can be defined as the exact energy minus the Hartree-Fock energy as in:

$$E_{corr} = E_{exact} - E_{HF} \quad (23)$$

This difference turns out to be very small for small atoms and diatomic molecules. The correlation energy increases with the number of electrons, so the inclusion of correlation is an important goal in quantum chemistry¹². Correlation in quantum chemical calculations is important for many reasons. Including correlation generally improves the accuracy of computed energies and molecular geometries²⁰. For organic molecules, correlation is an extra correction for very-high-accuracy work, but is not generally needed to obtain quantitative results, where transition metal systems often require correlation in order to obtain results that are qualitatively correct²⁰. Two types of calculations that begin with HF energies and then correct for correlation, Møller-Plesset perturbation theory and B3LYP hybrid density functional theory, will be discussed in later sections.

1.4.4 Self-Consistent Field

As mentioned, the Hartree-Fock equations must be solved by using a self-consistent procedure. In particular the equation of interest is (19). Initially, a set of orbitals $\psi_i(r_i)$ are assumed. Then the coulomb operator, $\hat{J}_j(r)$, and the exchange operator, $\hat{K}_j(r)$, can be evaluated which are used to evaluate the Fock operator, $\hat{F}(r)$. The Fock operator can then be used with equation (19) to calculate a new set of

wavefunctions. This new set of wavefunctions can then be used to calculate the new coulomb and exchange operators, which are used to calculate the new Fock operator and subsequently a newer set of wavefunctions. This iterative process is continued until the energies and wavefunctions (molecular orbitals) have converged, or are self-consistent. Convergence has occurred when the new wavefunctions are the same, or sufficiently close. The procedure is referred to as the self-consistent field method (SCF).

1.4.5 Møller-Plesset Perturbation Theory

Correlation can be added as a perturbation from the Hartree-Fock wavefunction²⁰. This method is called Møller-Plesset perturbation theory and is considered a post Hartree-Fock method. Its main idea was first published in 1934 by Christian Møller and Milton S. Plesset²¹. The basic idea of Møller-Plesset perturbation theory is to start with the Hartree-Fock wavefunction as the unperturbed wavefunction and then to improve it systematically by perturbation theory¹². This allows for a correction to be made for the electron correlation in a many-electron system. It turns out that the Møller-Plesset (MP) perturbation theory energy through first order is equal to the Hartree-Fock energy and second-order MP perturbation theory is the first correction to Hartree-Fock results and is designated by MP2¹². The problem that needs to be solved is still the Schrödinger equation, but now there is a correction being made to the Hamiltonian operator as in:

$$\hat{H} = \hat{H}^{(0)} + \lambda \hat{H}^{(1)} \quad (24)$$

In this equation $\hat{H}^{(0)}$ is the unperturbed Hamiltonian operator, $\hat{H}^{(1)}$ is the perturbed Hamiltonian operator and λ is an arbitrary parameter used to keep track of the order of

perturbation (where terms in λ give first-order corrections, terms in λ^2 give second-order corrections and so on). There are also corrections made to the wavefunction and energy terms represented by:

$$\psi_n = \psi_n^{(0)} + \lambda \psi_n^{(1)} + \lambda^2 \psi_n^{(2)} + \dots \quad (25)$$

$$E_n = E_n^{(0)} + \lambda E_n^{(1)} + \lambda^2 E_n^{(2)} + \dots \quad (26)$$

The first-order correction to $E_n^{(0)}$ is $E_n^{(1)}$ and through first-order the energy is given by:

$$E_n = E_n^{(1)} + E_n^{(2)} \quad (27)$$

where $E_n^{(1)}$ is given by:

$$E_n^{(1)} = \int \psi_n^{(0)*} \widehat{H}^{(1)} \psi_n^{(0)} d\tau \quad (28)$$

The “*” in the superscript of the wavefunction in (28) indicates that it is the complex conjugate of the wavefunction. The first-order MP correction to the energy is the Hartree-Fock energy and therefore the first correction to the HF energy, resulting from electron correlation, is given by second-order Møller-Plesset perturbation theory (MP2). The second-order correction to the wavefunction gives the energy through second-order as:

$$E_n = E_n^{(0)} + E_n^{(1)} + E_n^{(2)} \quad (29)$$

with an energy correction of $E_n^{(2)}$ which is given as:

$$E_n^{(2)} = \sum_{j \neq n} \frac{|\int \psi_n^{(0)*} \widehat{H}^{(1)} \psi_j^{(0)} d\tau|^2}{E_n^{(0)} - E_j^{(0)}} \quad (30)$$

Successive terms in their series grow progressively less important, and good results can be obtained with just a few terms¹². In general, bond lengths based on MP2 are in excellent agreement with experimental bonds involving hydrogen⁸. However the same cannot be said in general for multiple bonds⁸. The most significant advantage of using correlated models is to obtain reliable thermodynamic information¹⁶. The biggest disadvantage of Møller-Plesset calculations is that they are not variational as in Hartree-Fock calculations. This means that the result of the energy calculation is not an upper bound to the exact energy. In fact, it is not uncommon to find MP2 calculations that give total energies below the exact total energy²⁰. Another disadvantage of Møller-Plesset perturbation theory, although becoming less of a disadvantage as computing technology improves, is that it is more computationally expensive than Hartree-Fock calculations.

1.4.6 Density Functional Theory

Density functional theory (DFT) was developed in the 1960s by Pierre Hohenberg and Walter Kohn²² and Walter Kohn and Lu Jeu Sham²³, and is largely used today by the quantum chemical community in calculations on complex molecular systems²⁴. Density functional theory begins with the concept of electron probability density. Not only is the electron density simpler than the wavefunction, it can be determined experimentally by X-ray diffraction or electron diffraction techniques¹². Thus it would appear desirable to formulate quantum chemistry in terms of the electron density,

$\rho(x_1) = N \int dx_2 \cdots dx_N \Psi \Psi^*$ instead of the much more detailed many-electron wavefunction $\psi(x_1, \dots, x_n)$ ¹². Hohenberg and Kohn published two remarkable results. The first was that they showed it was indeed possible to express the ground-state energy, as well as all other ground-state molecular properties, as an integral involving the electron density¹² as indicated in:

$$E = E[\rho] \quad (31)$$

The square bracket denotes an integral, in this case involving the electron density ρ . In equation (31), the electronic energy E is said to be a functional of the electron density, denoted by $E[\rho]$, in the sense that for a given function $\rho(r)$, there is a single corresponding energy¹⁷. The problem with the first theorem is that it does not give the form of the functional dependence of energy on the density: it confirms only that such a functional exists¹⁷. The second thing that Hohenberg-Kohn showed was that (31) is variational in the sense that if E_0 and ρ_0 are exact quantities, then the following is true:

$$E_0 = E[\rho_0] \leq E[\rho] \quad (32)$$

where ρ is any trial electron density. These two Hohenberg-Kohn theorems opened up an entirely different approach to quantum chemistry, bypassing wavefunctions in favor of electron densities¹². The next major step in the development of DFT came with the derivation of a set of one-electron equations from which in theory the electron density ρ could be obtained²³. The functional derivative of the electronic energy is nothing but the effective one-electron Kohn-Sham Hamiltonian \hat{H}^{KS} as given by:

$$\frac{\partial E[\rho]}{\partial \rho(r)} = \widehat{H}^{KS}(r) = -\frac{\hbar^2}{2m_e} \nabla^2 + V_{eff}(r) \quad (33)$$

where $V_{eff}(r)$ is the effective potential given by:

$$V_{eff}(r) = V_{nuc}(r) + V_{Coul}(r) + V_{XC}(r) \quad (34)$$

In this equation $V_{nuc}(r)$ is the attractive potential arising from the nuclei, $V_{Coul}(r)$ is the Coulomb potential arising from the total electronic density that is sometimes referred to as a “screening” potential and $V_{XC}(r)$ is the exchange-correlation potential which is also a functional of the electron density and takes into account all non-classical electron-electron interactions. The mathematical representation of $V_{nuc}(r)$ and $V_{Coul}(r)$ are given by:

$$V_{nuc}(r) = -\sum_{I=1}^N \frac{Z_I e^2}{4\pi\epsilon_0 r_{I1}} \rho(r_1) dr_1 \quad (35)$$

$$V_{Coul}(r) = \frac{1}{2} \int \frac{\rho(r_1)\rho(r_2)e^2}{4\pi\epsilon_0 r_{12}} dr_1 dr_2 \quad (36)$$

The exchange-correlation is not known exactly and therefore approximations have to be used. The most used functional to describe the exchange and correlation components is B3LYP, which will be discussed shortly. The Kohn-Sham orbitals are then obtained from the iterative SCF solution of the corresponding Kohn-Sham eigenvalue equations,

$$\widehat{H}^{KS}(r)\psi_i(r) = \epsilon_i\psi_i(r) \quad (37)$$

much as is done for the HF calculations seen previously²⁴. Here $\psi_i(r)$ are the one-electron Kohn-Sham orbitals. First there is an initial guess for the charge density ρ which is used to compute the exchange-correlation potential as a function of r . Then the equation is solved for an initial set of Kohn-Sham orbitals which are used to compute an improved density and the process is repeated until the density and exchange-correlation energy have converged to within some accepted value. The electronic energy can then be computed.

Much of the research in DFT has involved the development of various approximations for $E[\rho]$. One successful commonly used approximation is due to work completed by Becke, Lee, Yang, and Parr and is called the BLYP functional. This functional is referred to as a gradient-corrected functional and involves both the values of the electron spin densities and their gradients²⁵. The functional used in this thesis is a hybrid functional. Hybrid functionals define the exchange functional as a linear combination of Hartree-Fock, local, and gradient-corrected exchange terms; this exchange functional is then combined with a local and/or gradient-corrected correlation functional²⁵. The best known of these hybrid functionals is Becke's three-parameter exchange²⁶ formulation that is combined with Lee, Yang and Parr's correlation functional²⁷ known as B3LYP. The B3LYP method is defined by²⁸:

$$E_{XC}^{B3LYP} = (1-a) E_X^{LSDA} + aE_X^{exact} + b\Delta E_X^{B88} + (1-c) E_C^{LSDA} + cE_C^{LYP} \quad (38)$$

In this equation a , b and c are semiempirical coefficients determined by an appropriate fit to experimental data. Becke suggested that the coefficients have values of $a = 0.2$,

$b = 0.72$ and $c = 0.81$ based on fitting to heats of formation of small molecules²⁹. In equation (38) E_X^{LSDA} and E_C^{LSDA} are the local-spin-density approximations for the exchange and correlation energies respectively, E_X^{exact} is the exact Hartree-Fock exchange energy, ΔE_X^{B88} is Becke's gradient correction to the exchange functional and E_C^{LYP} is the correlation functional suggested by Lee, Yang and Parr. The B3LYP hybrid functional will be used throughout this thesis.

Much of the appeal of DFT is that its results are comparable to those of post-HF methods, but the time required is comparable to that of HF calculations¹². Also, for systems involving d-block metals, DFT yields results that very frequently agree more closely with experiment than HF calculations do¹⁷. Therefore, DFT is very appealing in this work because of the involvement of cobalt as the central atom in the complexes studied. DFT does have disadvantages and perhaps the most serious deficiency is that the method cannot be improved in a systematic manner. Other electron correlation methods can sometimes achieve better results by including more terms in their expansions (i.e. Møller-Plesset perturbation theory). Improvements in DFT depend upon the construction of better functionals¹².

1.5 Conductor-like Screening Model (COSMO)

The Conductor-like Screening Model, or COSMO, is a dielectric continuum model developed by Klamt and Schüürmann³⁰. These models are used to determine the electrostatic interactions between the molecule of interest and a solvent. In these models the solute molecule is embedded in a dielectric continuum of permittivity ϵ ²⁶. Thus the

solute forms a cavity within the dielectric²⁶. The COSMO model assumes that the surrounding medium is well modeled as a conductor which simplifies the electrostatics computations, and corrections are made for dielectric behavior³¹. The cavity surface, i.e. the interface between the cavity and the dielectric is usually called the ‘solvent accessible surface’ (SAS)²⁶. The response of a homogeneous dielectric continuum to any charge distribution of the solute consists of a surface charge distribution on the interface arising from the polarization of the dielectric medium²⁶. COSMO is used to calculate the energy of the interaction between the solute molecule and the solvent. COSMO is part of a group of methods referred to as polarizable continuum models (PCM). Specifically, this research will incorporate the conductor-like PCM (C-PCM) model to calculate the total free energy in solution of stable molecules. This method is applicable to the work completed in this thesis because the molecules that are investigated will be found inside the SCWR environment which will consist of supercritical water. Although the dielectric constant of the water inside the reactor will be considerably lower than water under standard conditions, these calculations will provide a good starting point for the COSMO study.

1.6.0 Research Objectives

The primary objective of this thesis is to perform a comprehensive *ab initio* computational study of cobalt(II) complexes involving water, chloride, hydroxide and ammonia ligands. These series of complexes will be studied up to and including the hexacoordinate species. The studies will include geometry optimizations and bond length and frequency analysis. Single-point C-PCM calculations will be performed on the

optimized B3LYP/6-31+G* Structures. Calculated polarized Raman spectra will be plotted for the optimized HF/6-31+G* complexes. Although this research will not include data at high temperature and pressure, it will provide a good starting point for the experimental Raman work that will be performed at the University of Guelph by the Peter Tremaine research group. Even with our Raman data being calculated at zero Kelvin and in the gas phase it will still be applicable to the high temperature, high pressure experiments because the frequencies will not actually deviate that much due to anharmonicity and weaker molecular bonds at high temperatures. There could be interference due to fluorescence (windows of sample chamber or the solution itself) as well as the peaks may broaden and become less intense, but they will occur at approximately the same wavenumbers.

2.1 Computational Methods

The calculations were performed using the Gaussian03³² software package through the Atlantic Computational Excellence Network (ACEnet). ACEnet is a pan-Atlantic network of world-class, High-Performance Computing (HPC) clusters³³. The specific cluster used is located at Memorial University in Newfoundland and is named 'placentia'. The levels of theory used were Hartree-Fock (HF), second-order Møller-Plesset perturbation theory (MP2) and B3LYP hybrid density functional theory. All of these theories were combined with the 6-31+G* basis set. The molecular geometries were fully optimized using a stepping stone approach, in which the geometries at the HF, MP2 and B3LYP levels were optimized sequentially. When this approach failed, due to ligand dissociation, the problematic level was skipped. Default optimization specifications were normally used. After geometry convergence of each level a frequency calculation was performed and the resulting Hessian was used in the subsequent optimization (geom=allcheck). Z-matrix coordinates were used to speed up the optimization process, as required, to constrain the complexes to an appropriate symmetry. Since frequency calculations were performed at each level, any problems with the z-matrix coordinates would be indicated with the appearance of imaginary (negative) frequencies. Generally, the molecule would initially be constrained to the highest possible symmetry. In the cases where there were imaginary frequencies, the symmetry would be reduced based on the mode of the imaginary frequencies and the optimizations would be performed again for

the given level of theory. The Hessian was evaluated at the first geometry (Opt=CalcFC) for the first level in the sequence in order to aid geometry convergence. All of the optimizations were completed using a self-consistent field procedure (SCF) and in the cases where the geometry optimization ran out of steps before convergence the input was altered to Opt=Calcall. This alteration would perform a frequency calculation after each step to check for convergence. Optimizations were carried out to completion for all levels in the sequence even if one or more of the levels proved not to be local minima. This ensured that no minimum energy structures were missed during the stepping stone approach to optimization. Frequency analysis and pictures of the molecular geometries were completed using MOLDEN³⁴.

The polarized Raman spectra were plotted using a code created by my supervisor, Dr. Cory C. Pye. These spectra were created from the frequency data obtained in the output file of the HF/6-31+G* calculation primarily because Raman intensity calculations are standard in Hartree-Fock frequency calculations. Conductor-like polarizable continuum model (C-PCM) calculations were performed only on the stable, optimized B3LYP/6-31+G* structures. These calculations were single-point, room temperature calculations and were completed by inserting SCRF=CPCM in the input line of the calculation along with the level of theory and basis set. Water was used as the default solvent, with a dielectric constant equal to 78.39 (value at 25°C).

CHAPTER THREE

HYDRATED COBALT(II) AND SINGLE-LIGAND COMPLEXES

The *ab initio* investigations of cobalt(II) complexes throughout this thesis involve four ligands and the complexes that they make with the cobalt(II) ion. These ligands are chloride (Cl^-), hydroxide (OH^-), ammonia (NH_3) and water (H_2O). These ligands, and the cobalt complexes of them, are all important with respect to the development of the Supercritical Water-cooled Reactor (SCWR). The formation of these complexes and their transportation throughout the reactor environment may lead to corrosion of the pipes and valves and, ultimately, a nuclear leakage.

This chapter includes the computational results and discussion/literature comparison of the single-ligand cobalt(II) complexes. These aqua complexes were studied up to and including the six-coordinate species. The chloro, hydroxo and ammine complexes were studied up to six-coordinate with and without water molecules. The water molecules were added to investigate how hydration affects the stability of the given species. All of the results regarding total energies, bond lengths and vibrational frequencies are from the HF, MP2 and B3LYP calculations utilizing the 6-31+G* basis set. These calculations are all zero Kelvin, gas-phase calculations. Molecular geometries are presented for the MP2/6-31+G* and B3LYP/6-31+G* calculations. The aqueous C-PCM results are all from single-point calculations using the fully optimized B3LYP/6-31+G* geometry. All simulated Raman spectra are from the vibrational frequency data calculated at HF/6-31+G* because Raman intensities are standard for HF calculations.

All structures shown will only be those of the absolute energy minima, unless other local minima were found that had noticeably different geometries.

3.1 Water, Chloride, Hydroxide and Ammonia Ligands

Ab initio calculations were performed on the ligands involved with the cobalt(II) complexes for reasons of stability comparison. Table 3A.1, found in the supplementary materials section, gives the total energies of the ligands with the given levels of theory (the basis set will be excluded in all energy tables because only results utilizing the 6-31+G* basis set will be reported). Also included in Table 3A.1 is the total free energy in solution, calculated using C-PCM and the optimized B3LYP geometry.

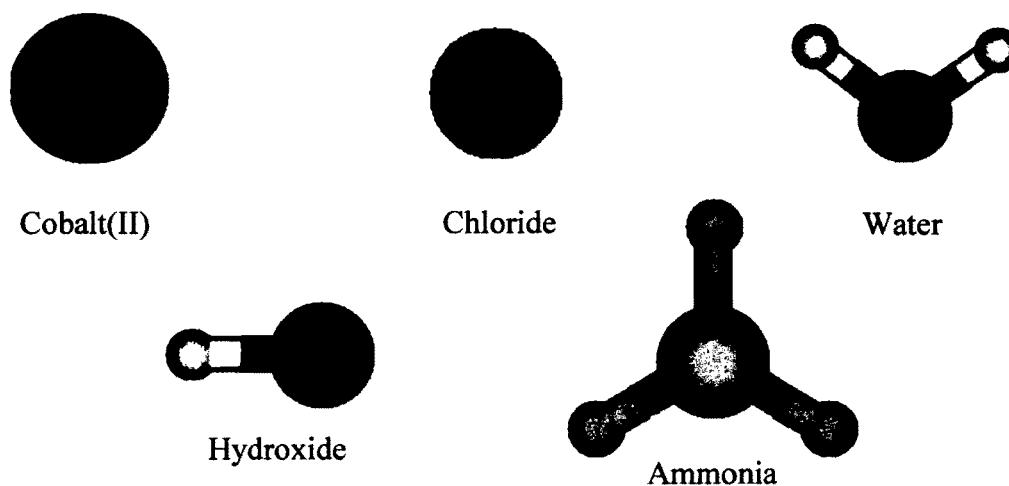


Figure 3-1: The cobalt(II) and chloride ions as well as optimized MP2 and B3LYP geometries for the remaining ligands used in the calculations of cobalt(II) complexes.

3.2 Aquacobalt(II) Complexes, $[\text{Co}(\text{H}_2\text{O})_n]^{2+}$, where $n=1 - 6$

The Co(II) ion is known to form both octahedral and tetrahedral complexes⁷. Therefore it would seem that the aqua ion would be either $[\text{Co}(\text{H}_2\text{O})_6]^{2+}$ with octahedral symmetry or $[\text{Co}(\text{H}_2\text{O})_4]^{2+}$ with tetrahedral symmetry. Swift showed evidence³⁵ that both of these ions exist in equilibrium with each other, which was later confirmed with high temperature experiments by Swaddle and Fabes.³⁶ The hexaaquacobalt(II) ion is the most recognized of the aquacobalt(II) complexes. Oxygen-17 NMR studies by Chmelnick and Fiat³⁷ and ¹H NMR studies by Matwiyoff and Darley³⁸ have given evidence for the existence of the hexaaquacobalt(II) ion. X-ray crystallography studies have also shown the hexaaquacobalt(II) ion to exist with anions of nitrate³⁹, bromate⁴⁰, hydrogen phthalate⁴¹ and hydroxysulfate⁴², with the ion also existing in Tutton salts.⁴³ The hexaaquacobalt(II) (as well as penta- and tetraaquacobalt) ion was also studied in photodissociation experiments by Faherty et al⁴⁴ and spectrophotometry experiments by Beaver et al⁴⁵. There have been numerous *ab initio* studies involving the hexaaquacobalt(II) ion. Åkesson et al. studied the theoretical binding energies and Co-O distances of the hexaaquacobalt(II) ion using SCF calculations with Huzinaga basis sets and the MOLECULE-SWEDEN system of programs⁴⁶. Åkesson et al. also reported a theoretical study involving water-exchange reactions involving the hexaaquacobalt(II) ion as well as two geometries of the pentaquacobalt(II) ion⁴⁷. A similar study of water exchange for hexaaqua ions was reported by Rotzinger⁴⁸. In a series of reports by Gilson and Krauss on the reinterpretation of the absorption spectra of hydrated Co^{2+} , they found optimized geometries for the hexahydrate as well as the hydroxopentahydrate,

pentahydrate, hydroxotetrahydrate and the hydroxotrihydrate using CAS-MCSCF and MCQDPT calculations with the GAMESS code^{49,50,51}. Mendoza-Huizar et al. reported a study on the electrochemical reduction of $[\text{Co}(\text{H}_2\text{O})_6]^{2+}$, involving electronic charge transfer and desolvation mechanisms, using semiempirical PM3, Hartree-Fock pseudopotential *ab initio* and density functional theory⁵². Deeth and Randell investigated ligand field stabilization and activation energies of the hexaaquacobalt(II) ion using density functional theory with the Amsterdam density functional program⁵³. The spin-state stability of the $[\text{Co}(\text{H}_2\text{O})_6]^{2+}$ ion was studied by Schmiedekamp et al. using the Jaguar 3.5 and 4.0 software with the B3LYP functional coupled with both the LACVP** and 6-31G** basis sets⁵⁴. Garmer and Krauss studied metal substitution and the active site of carbonic anhydrase using HF/CEP-31G with both the GAMESS and Gaussian software⁵⁵. Rulišek and Havlas studied the hexaaquacobalt(II) ion using various computational methods (CASSCF(7,5) and CASPT2(7,5) with GAMESS and Gaussian) to critically evaluate the accuracy of these methods⁵⁶. Varadwaj and Marques used DFT-X3LYP/6-311++G(d,p) with Gaussian software to investigate the structure, energetics and topological properties of the electron density of the hexaaqua ion⁵⁷. A study of binding patterns in single-ligand complexes of first series transition metals by Magnusson and Moriarty gives geometry information for the monoaquacobalt(II) ion⁵⁸.

3.2.1 Results

Stable structures were found for all aquacobalt(II) complexes up to and including the hexaaquacobalt(II) ion. The total energies, including the aqueous C-PCM energy, for all aqua complexes studied are given in Table 3A.2 in the supplementary materials. The

lowest energy optimized MP2 and B3LYP structures of these complexes are given in Figure 3-2 along with their respective symmetries.

The monohydrate and dihydrate did not cause any symmetry issues as the highest possible symmetry proved to be stable for both levels of theory. The monohydrate has C_{2v} symmetry and the dihydrate has D_{2h} symmetry. The trihydrate has a preferred symmetry dependent on the level of theory. For MP2 the most stable geometry is C_1 (unconstrained), which appears to be a slightly distorted D_3 geometry. The B3LYP structure was most stable with D_3 symmetry although a slightly higher energy C_1 structure was also found. For the tetrahydrate there was ultimately an agreement among both levels of theory that the most stable geometry exists as an S_4 structure. The pentrahydrate was found to be most stable in a C_2 geometry at both levels although C_1

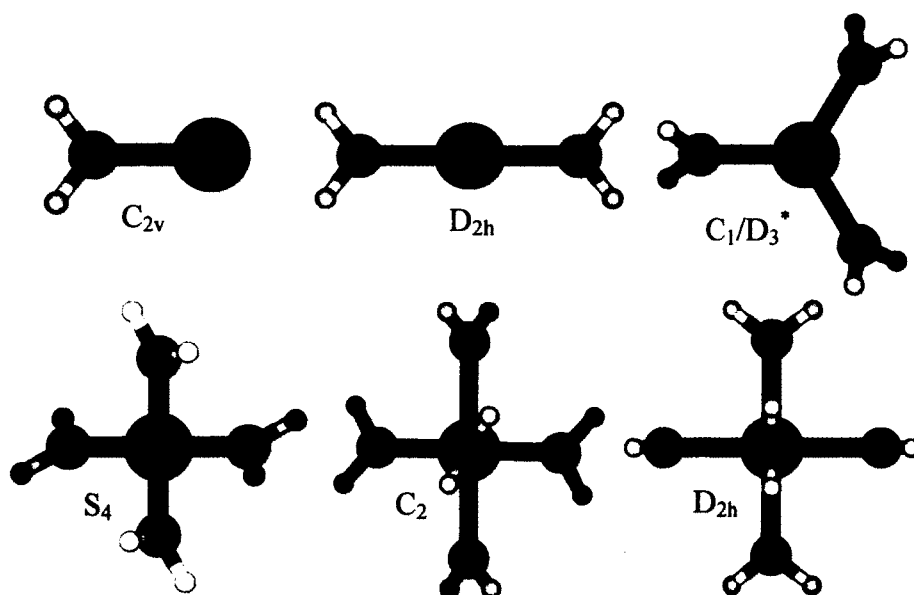


Figure 3-2: Optimized MP2 and B3LYP geometries for $[Co(H_2O)_n]^{2+}$, where $n=1 - 6$. All structures are similar with the exception of the trihydrate which is C_1 at MP2 and D_3 at B3LYP (indicated by “*”).

structures were found for both at slightly higher energies. Finally, the hexahydrate has a preferred D_{2h} geometry at both levels, with T_h structures being slightly higher in energy.

Plots were constructed of the Co-O bond lengths and vibrational stretching frequencies and are shown in Figure 3-3, Figure 3-4 and Figure 3-5 for HF, MP2 and B3LYP respectively. The simulated polarized Raman spectrum for the hexaaquacobalt(II) species can be found in Figure 3-6.

3.2.2 Discussion/Literature Comparison

The structure we found for the monohydrate complex is consistent with the computational study by Magnusson and Moriarty⁵⁸ who found the Co-O bond length to be 1.932Å, which is consistent with our MP2 and B3LYP results of 1.930Å and 1.915Å respectively. Our HF result is slightly longer at 1.974Å. This difference can be attributed to the overestimating nature of HF calculations as well as the fact that Magnusson and Moriarty used MP2 theory with a slightly larger basis set, 6-311+G**. No experimental data was found regarding the monohydrate complex.

The Co-O bond lengths for the dihydrate are 1.953, 1.912 and 1.888Å for HF, MP2 and B3LYP respectively. Overall the Co-O bond has decreased slightly when compared to the monohydrate. No experimental or computational data was found to compare with these results.

The most stable trihydrate complexes we found to have Co-O bond lengths of 2.007, 1.964 and 1.943Å for HF, MP2 and B3LYP respectively. Although the HF and MP2 geometries proved only to be stable at C_1 symmetry, they are very close to being D_3

structures which becomes evident when comparing bond lengths and geometries. These bond lengths are longer when compared to the mono and dihydrate values. This result can be attributed to there being an increased number of ligands which would have the effect of repulsion forcing the bonds to be longer. Again, no experimental or computational data was available for comparison.

The most stable geometry for the tetrahydrate complex proved to be S_4 for all levels of theory. The Co-O bond lengths for these structures were found to be 2.050, 2.010 and 2.003 Å for HF, MP2 and B3LYP respectively. Gilson and Krauss⁴⁹ reported Co-O bond lengths of 2.050, 2.048(x2) and 2.044 Å in their computational study of the unconstrained tetrahydrate complex. These results are in very good agreement with our HF results. Because Gilson and Krauss used HF based calculations with a different basis set, therefore our MP2 and B3LYP results cannot be compared. Their optimized geometry was unconstrained whereas ours is highly symmetrical. Other than this study, no others were found regarding molecular structure of tetrahydrate species.

The pentahydrate species that proved to be most stable has C_2 symmetry. The average Co-O bond lengths are 2.120, 2.059 and 2.056 Å for HF, MP2 and B3LYP respectively. In the same study as the tetrahydrate, Gilson and Krauss⁴⁹ also reported an unconstrained pentahydrate complex. The average Co-O bond length for the complex they optimized was 2.114 Å, which is in very good agreement with the results that we found. Akesson et al.⁴⁷ reported two different structures of the pentahydrate of cobalt(II), based on CASSCF calculations using Huzinaga basis sets. They reported a trigonal

bipyramidal structure and a square pyramidal structure, both having a mean Co-O distance of 2.100Å. These results are also in good agreement with what we have found.

The hexaaquacobalt(II) ion is the most reported of the cobalt(II) aqua ions in the literature. We found the most stable geometry of this ion to be either D_{2h} or T_h depending on the level of theory used. The Co-O bond distances that we found are 2.206 (avg), 2.109 and 2.114Å for HF, MP2 and B3LYP respectively. There have been many computational studies on the hexaaquacobalt(II) ion. Akesson et al.⁴⁶ reported a mean Co-O bond distance of 2.143Å from SCF calculations using Huzinaga basis sets. Gilson and Krauss⁴⁹ reported a T_h constrained geometry with a Co-O distance of 2.229Å and an unconstrained geometry with a mean Co-O distance of 2.156Å based on CAS-MCSCF and MCQDPT calculations. Rulišek and Havlas⁵⁶ also reported a T_h constrained structure with a Co-O bond length of 2.155Å calculated using CASSCF(7,5) and CASPT2(7,5) methods. Deeth and Randell⁵³ found a Co-O distance of 2.105Å for a BLYP calculation of D_{2h} symmetry. Varadwaj and Marques⁵⁷ performed calculations on the hexahydrate, using B3LYP/6-311+G**, and found stable geometries with C_i and C_1 (unconstrained) symmetry. The average Co-O bond lengths were 2.1265Å for both symmetries. Finally, Schmiedekamp et al.⁵⁴ performed a B3LYP/LACVP** calculation and found an average Co-O bond length of 2.12Å. These computational results are all in good agreement with the results that we have found. The subtle differences could be a result of the varying software, theories used and basis sets. Experimental studies, primarily X-ray crystallography, have also been reported on the hexaaquacobalt(II) ion existing as the cation in a specific compound. Prelesnik et al.³⁹ reported a crystal structure containing the

nitrate anion which has an average Co-O bond distance of 2.077Å, Blackburn et al.⁴⁰ investigated a bromate complex and found the mean Co-O distance to be 2.095Å, Kariuki and Jones⁴¹ studied a hydrogen phthalate complex which had an average Co-O bond length of 2.091Å, Yotnoi et al.⁴² found a mean Co-O bond length of 2.065Å in a hydroxysulfate compound and finally Cotton et al.⁴³ report on Tutton salts containing hexaaquacobalt(II) that have a Co-O mean distance of 2.092Å. These crystal structures all showed very similar Co-O bond distances and contain the hexaaqua ion in an approximate octahedral geometry. These experimental results are all very consistent with our computational findings and suggest that the MP2 and B3LYP results may be more reliable than the HF results based on closeness to the experimental values, which are all just below the 2.100Å value. Both the MP2 and B3LYP methods include electron correlation and therefore generally provide closer results when dealing with transition metals.

Vibrational stretching frequencies were also calculated for this set of hydrated cobalt(II) complexes as seen in Figures 3-3 to 3-5. One of the reasons for calculating these frequencies is so that they can be compared to experimental Raman studies that have or will be completed. They can be used to confirm or refute any experimental Raman findings that cannot be unambiguously assigned to a specific complex. The only solution Raman data that could be found regarding these complexes was for the hexaaqua ion, in aqueous solution, and was reported by Irish and Brooker⁵⁹. The observed symmetric Co-O stretch was reported at 380 cm⁻¹ which was assigned based on an octahedral cation. Our results include calculated Raman intensity data for the HF level of

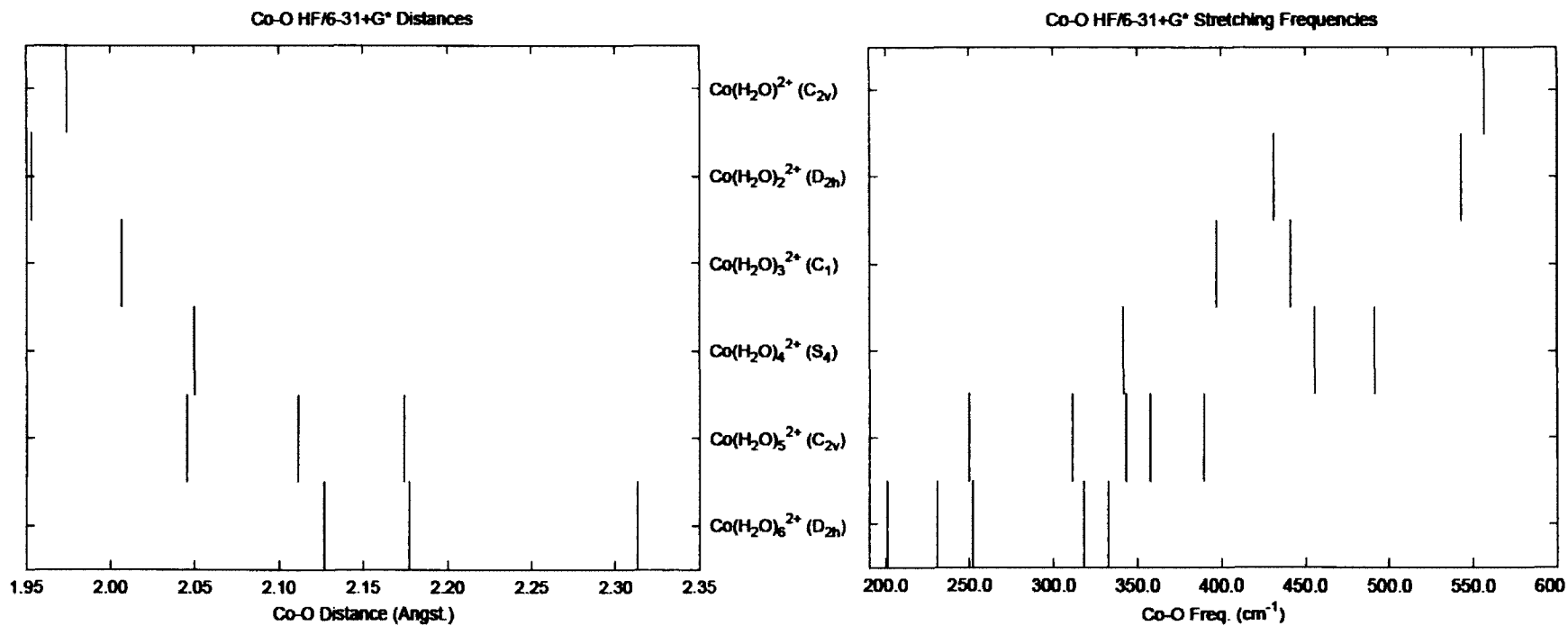


Figure 3-3: Co-O bond lengths (left) and vibrational stretching frequencies (right) for $[\text{Co}(\text{H}_2\text{O})_n]^{2+}$, where $n=1 - 6$, calculated at the HF/6-31+G* level.

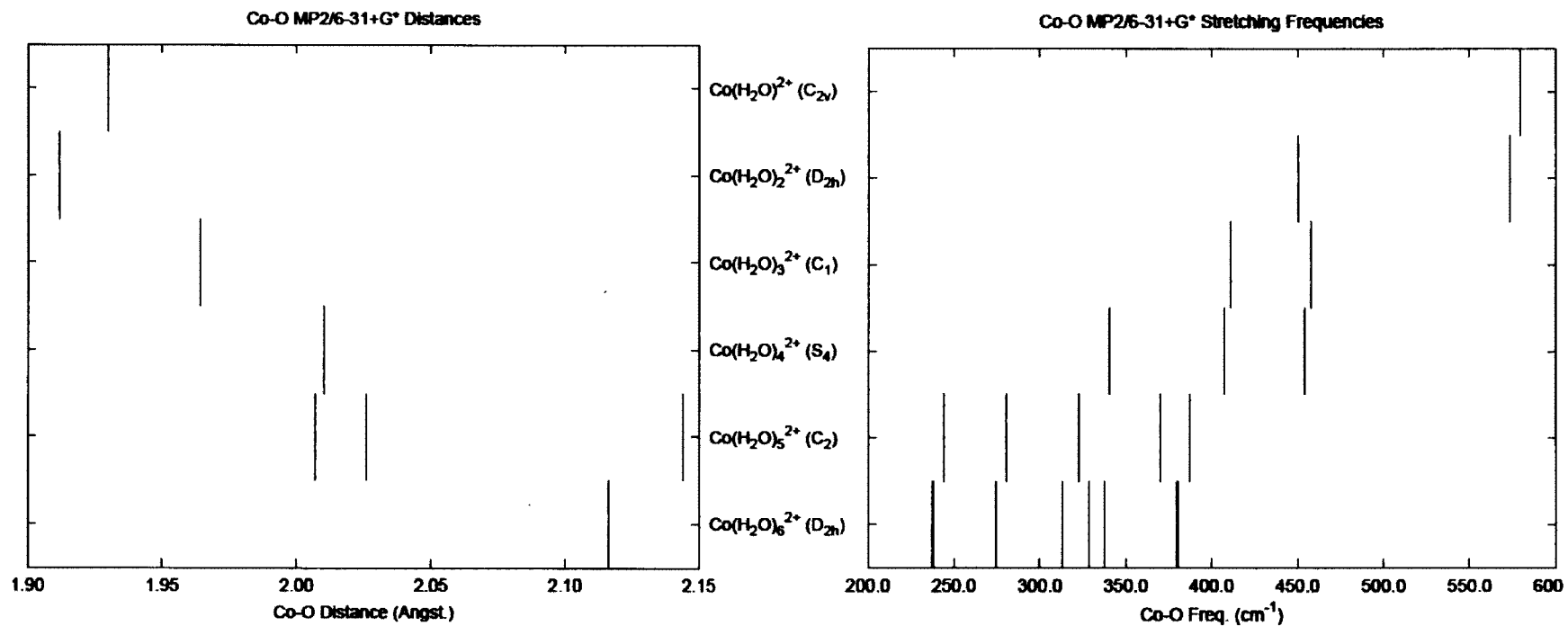


Figure 3-4: Co-O bond lengths (left) and vibrational stretching frequencies (right) for $[\text{Co}(\text{H}_2\text{O})_n]^{2+}$, where $n=1-6$, calculated at the MP2/6-31+G* level.

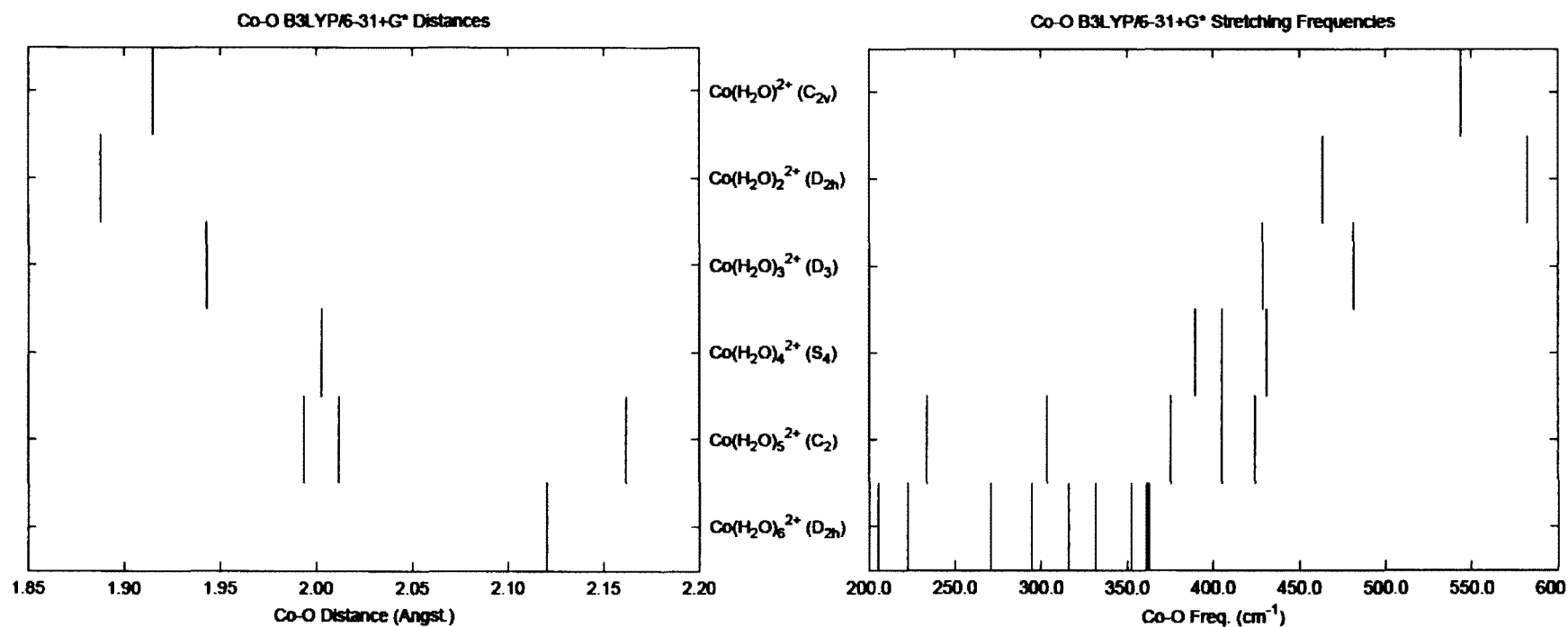


Figure 3-5: Co-O bond lengths (left) and vibrational stretching frequencies (right) for $[\text{Co}(\text{H}_2\text{O})_n]^{2+}$, where $n=1 - 6$, calculated at the B3LYP/6-31+G* level.

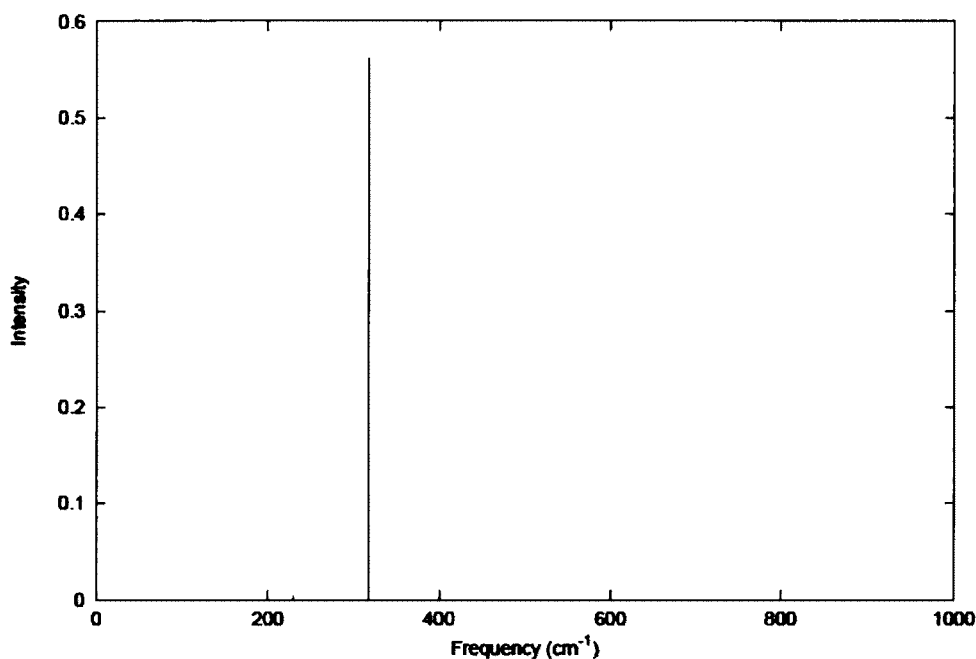


Figure 3-6: Simulated Raman plot of the hexaaqua complex based on our HF/6-31+G* frequency calculation.

theory only, but the symmetric stretches can still be found for MP2 and B3LYP. The symmetric stretches calculated in our work are 316, 344 and 340 cm^{-1} for HF, MP2 and B3LYP. A polarized Raman plot of the hexaaqua complex, based on our HF results can be seen in Figure 3-6. Our values underestimate the experimental band by 40 to 64 cm^{-1} depending on the level of theory. This result is expected due to neglect of additional hydration spheres when performing the calculations. These underestimations are consistent with similar studies completed previously on scandium chloro complexes⁶⁰ and zinc chloro complexes⁶¹. We have performed calculations on hexaaquacobalt(II) with a second hydration sphere consisting of twelve water molecules in a T geometry. This molecule proved to be stable at the HF level. The totally symmetric stretch of this further

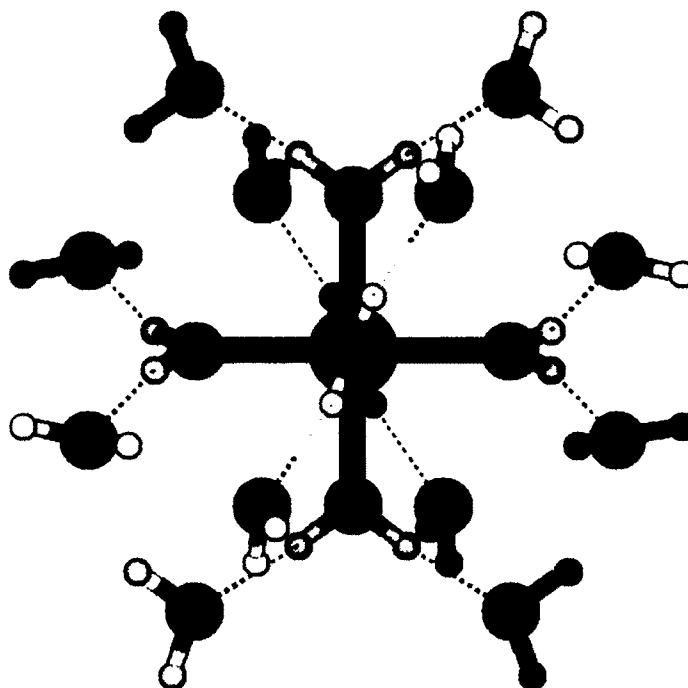


Figure 3-7: Hexaaquacobalt(II) dodecahydrate optimized at HF/6-31+G* with T (chiral tetrahedral) symmetry.

hydrated cobalt(II) ion is at 354 cm^{-1} , which is an improvement of 38 cm^{-1} and now only 26 wavenumbers lower than experimental. Addition of a second hydration sphere caused the Co-O bond distances to decrease (2.138 vs. 2.205Å), thereby increasing the amount of energy required for the vibration resulting in an increased wavenumber. Therefore, further addition of water molecules would probably bring this stretch very close to the experimental value. The B3LYP calculation on this molecule yielded an even closer approximation of 367 cm^{-1} , but due to three imaginary frequencies at this level we cannot make any definitive statements regarding the accuracy of the B3LYP calculation, since time restrictions kept us from desymmetrizing to find a stable geometry at the B3LYP level.

An interesting result regarding the C-PCM calculations is that in the zero Kelvin gas phase B3LYP calculation on the hexaaquacobalt(II) ion the D_{2h} symmetry was preferred over T_h , but the T_h geometry was preferred in the conductor-like PCM model. The reason for this switch in stability is most likely due to the spherical symmetry of the T_h point group versus the D_{2h} point group. The T_h geometry is more spherically symmetric and is therefore more easily incorporated into the dielectric continuum and energetically favored.

Some general trends can be drawn from our plots of bond lengths and stretching frequencies in Figures 3-3 to 3-5. Concerning the bond lengths, as more water ligands are added to the cobalt, the Co-O bond distances show a general increasing trend. This is caused by overcrowding of the cobalt resulting in electronic repulsion between the water ligands. The opposite trend is seen in the Co-O vibrational stretching frequencies. As the Co-O bond lengths increase the vibrational stretching frequencies decrease. This trend makes sense because if a bond is longer it will take less energy to cause it to vibrate and therefore have a corresponding frequency that is lower.

3.3 Chlorocobalt(II) Complexes, $[\text{CoCl}_n(\text{H}_2\text{O})_m]^{2-n}$, where $n=1 - 4$, $m=0 - (6-n)$

If cobalt metal or compounds of cobalt, such as the oxide, hydroxide or carbonate, are dissolved in hydrochloric acid, crystals are obtained of cobalt(II) chloride hexahydrate after evaporation⁶. This complex can be regarded as that of an octahedral complex containing four waters with the other two waters being located close to the chlorides⁵. Neutral cobalt(II) chloride is soluble in water and gives a pink color when under the conditions of a dilute solution, with water as the solvent and at low temperatures⁵. The pink color can be associated with the hydrated Co^{2+} ion being present. When the temperature is raised or excess hydrochloric acid is added, the solution turns blue in color, which is due to the presence of the tetrachloro cobalt(II) ion⁵. Crystallographic methods have been used to study the neutral cobalt(II) chloride anhydrate⁶², dihydrate^{62,63,64}, the tetrahydrate⁶⁵ and the hexahydrate^{64,66}, which can be seen as the tetrahydrate with two water molecules in the outer hydration sphere. Crystal structures have also been reported for the pentahydrated monochloro species⁶⁵, the trichloro species as part of medicinal molecules^{67,68}, the tetrachloro species^{65,69,70,71} and the monohydrated pentachloro species^{72,73}. The pentachloro crystal does have five chlorides surrounding the central Co atom, but only four of them are close enough to be directly bound to the cobalt. Structure analysis by Waizumi also suggests that there may be a monohydrated trichloro cobalt(II) species⁶⁵. The mono-^{45,74,75,76}, di-^{45,75,76,77,78}, tri-^{45,75,76,78,79,80} and tetrachloro^{45,80,74-79} cobalt(II) complexes have been studied by using UV/Vis spectroscopy. Infrared spectroscopy has also been used to characterize many of the hydrated dichloro complexes^{62,64,81,82} as well as the hydrated tetrachloro complex⁶².

Thermodynamic studies of dehydration⁸³, conductance⁸⁴ and heats of solution⁸⁵ have been completed on the dichloro complexes as well as stability⁸⁶, ³⁵Cl NMR⁸⁷ and activity⁸⁸ investigations.

3.3.1 Results

Stable structures were found for all anhydrous chlorocobalt(II) complexes up to and including those with four chloride ligands. These chlorocobalt complexes were hydrated and studied further up to a hexacoordinate species. The penta and hexachloro complexes were also studied but these structures underwent dissociation of one or more chloride ligands. Hence, stable structures for these complexes were not found. The total energies for the stable geometries, as well as the others that were attempted, can be found in Table 3A.7 of the supplementary materials section. The geometries of the lowest energy structures can be found in Figure 3-8 for the mono- and dichloro complexes and Figure 3-9 for the tri- and tetrachloro complexes.

The anhydrous monochloro complex did not cause any symmetry problems as all levels showed a preferred C_{3v} symmetry. The monohydrate has C_{2v} symmetry with the exception of B3LYP, which preferred a planar C_s symmetry instead. There was disagreement among levels as to which symmetry the dihydrate prefers. The MP2 level predicts the highest symmetry at C_{2v} , B3LYP predicts a C_2 structure and HF indicates that the stable geometry is without symmetry at C_1 . The trihydrate has stable C_3 structures at all levels but these do not prove to be the most stable. Higher stability structures were found for HF and MP2 with C_s symmetry and B3LYP ultimately prefers C_1 symmetry that is very close to the C_s structure. The most stable tetrahydrate has no

symmetry at all the levels, but a slightly higher energy C_{2v} structure was found for the HF level. Both C_2 and C_1 structures were found for the pentahydrate. The C_1 geometry was preferred for all levels except MP2, where C_2 was slightly lower in energy.

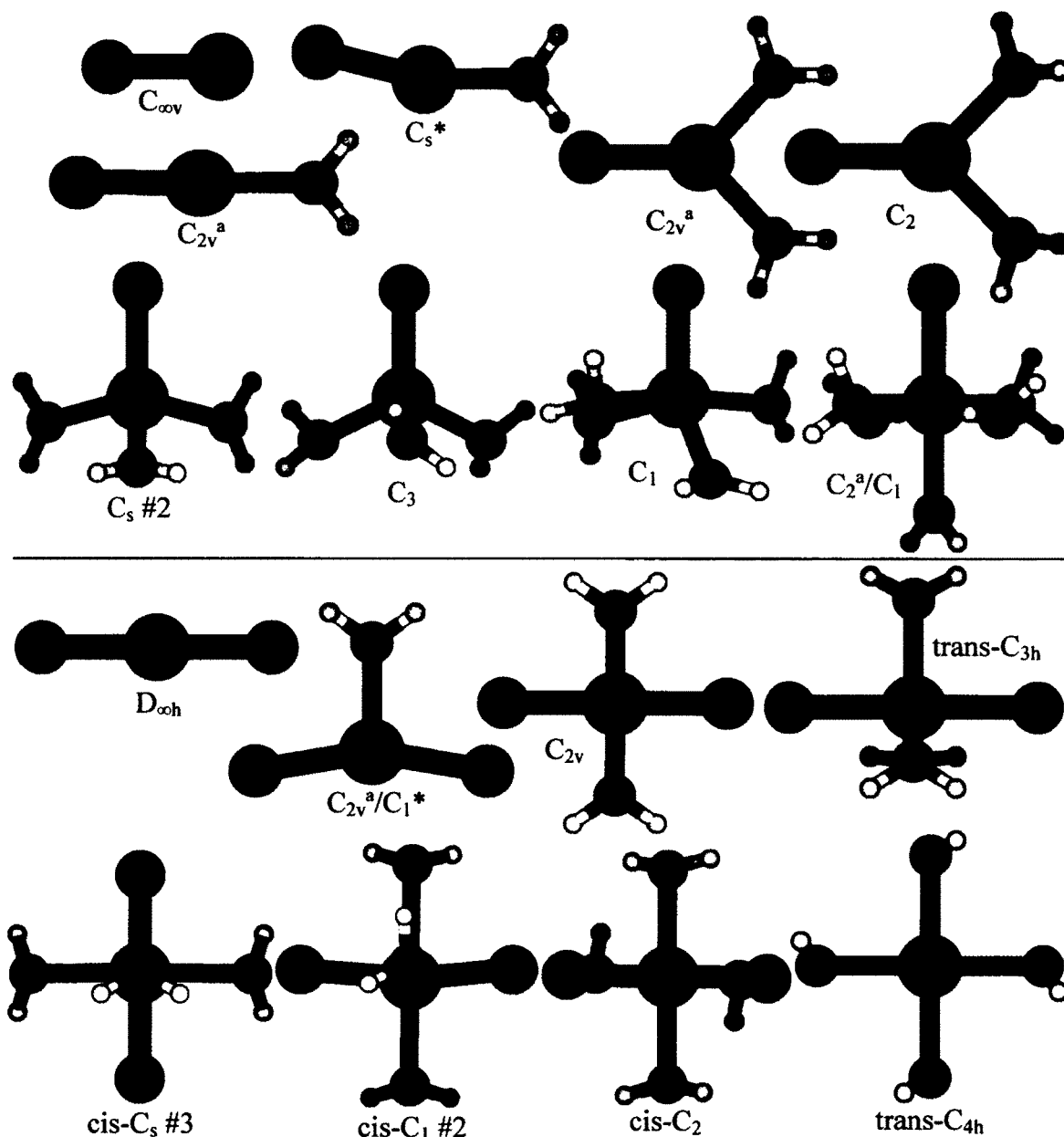


Figure 3-8: Optimized MP2 and B3LYP geometries for $[\text{CoCl}_n(\text{H}_2\text{O})_m]^{2-n}$, where $n=1-2$ and $m=0-(6-n)$. All symmetries marked with “*” indicates B3LYP, “a” indicates MP2, otherwise all MP2 and B3LYP structures are similar.

The anhydrous dichloro complex proved to be stable at its highest possible symmetry of $D_{\infty h}$ for all levels. The monohydrate is most stable in a C_{2v} geometry for HF and MP2, whereas C_1 is preferred for B3LYP. There is agreement among levels that the dihydrate has C_{2v} symmetry. Stable geometries were found for the trihydrate in cis and trans conformations, with respect to the chloride ligands. A trans- C_{3h} geometry was found to be stable at all levels, but was not as low in energy as the cis- C_s #3 or cis- C_1 #2 structures. Ultimately the most stable geometry proved to be cis- C_1 at all levels. All levels showed a preferred cis- C_2 structure for the tetrahydrate although a stable trans- C_{4h} structure was also found.

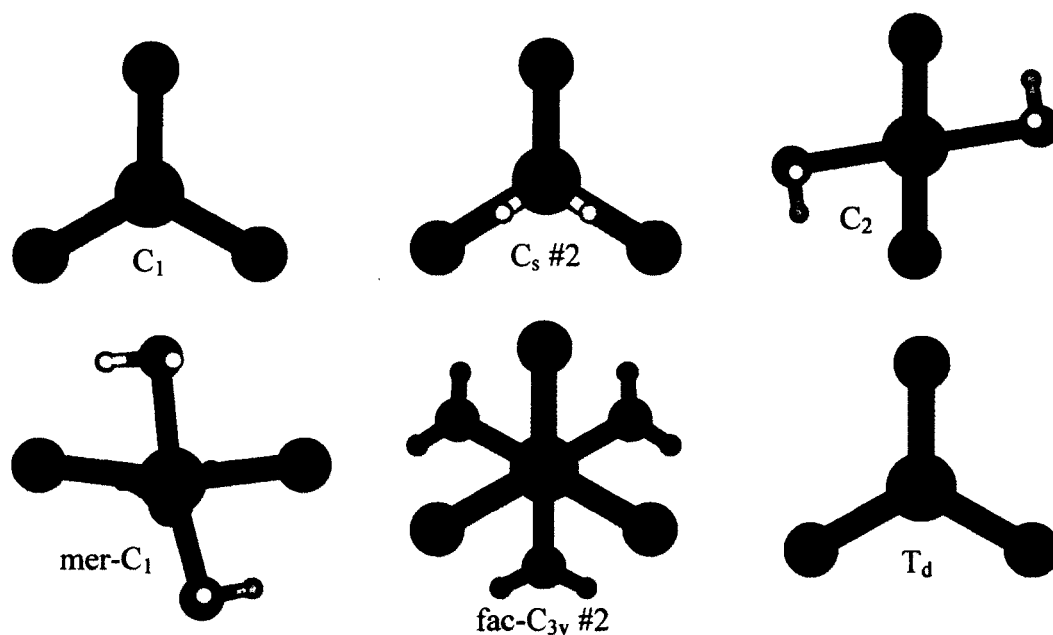


Figure 3-9: Optimized MP2 and B3LYP geometries for $[\text{CoCl}_n(\text{H}_2\text{O})_m]^{2-n}$, where $n=3-4$ and $m=0-(6-n)$. There was no distinction between structures for MP2 and B3LYP.

The anhydrous trichloro species initially caused a slight issue due to some of the optimized geometries that did not have any imaginary frequencies being higher in energy

than those that did have imaginary frequencies. This problem was eventually solved by attempting a C_1 geometry, which was distorted from D_{3h} , which turned out to be the energy minimum at all levels. The monohydrate was found to have C_s symmetry at all levels. There were three different stable geometries found for the dihydrate (only two for the HF level). There is a C_{2v} structure for MP2 and B3LYP with both water molecules hydrogen bonded to the central chloride species, but this geometry is less stable than the other two. Of the other two geometries, C_2 and C_1 , the C_2 geometry was most stable at the MP2 level whereas HF and B3LYP showed energetic preference for the C_1 structure (which looks very similar to the C_2 structure). The trihydrate was found to be stable in a completely bound facial (fac) C_{3v} geometry at all levels, with a meridional (mer) C_1 geometry being stable, but higher in energy.

The anhydrous tetrachloro complex preferred a tetrahedral, T_d , symmetry at all levels. No stable structures were found for the tetrachloro complexes when water was added. All of these structures showed either a chloride or water molecule dissociating from the rest of the molecule and ultimately went to a four coordinate species.

No stable structures were found for the penta and hexachlorocobalt(II) complexes. All of the geometries attempted showed dissociation of chloride ligands. Since stable structures were not found for these complexes, they will not be discussed.

Plots of the Co-O and Co-Cl bond lengths and vibrational stretching frequencies were constructed and can be seen in Figure 3-10, Figure 3-11 and Figure 3-12 for HF, MP2 and B3LYP respectively. Within these plots, the lines highlighted in red indicate

which bond lengths and stretches involve chloride ligands. Simulated polarized Raman spectra were also created for the stable HF structures and can be found in Figure 3A-2 of the supplementary materials section.

3.3.2 Discussion/Literature Comparison

Structural comparisons made between our results and the literature found on these complexes will be done primarily through bond length data. The Co-O and Co-Cl bond distances resulting from our investigations have been tabulated and can be found in Table 3A.8 of the supplementary materials section. When attempting to find structural data in the literature to compare our computational results with, the dichlorocobalt(II) complexes were most abundant. Morosin and Graeber⁶³ reported a crystal structure of the dichlorocobalt(II) dihydrate which had average Co-O and Co-Cl bond lengths of 2.040 and 2.454Å respectively. Gamo⁶⁴ reported an average Co-O bond length of 1.93Å for the same complex using electron diffraction. The Co-O and Co-Cl bond distances that we calculated for the dihydrate are 2.083 and 2.212Å for MP2 and 2.095 and 2.218Å for B3LYP. Our Co-O values are in very good agreement with the experimental results, but the Co-Cl values that we calculated seem to be short in comparison. Gamo also reported a hexahydrated dichloro species, which essentially is octahedral with respect to four of the water molecules with the two remaining waters being located in the second hydration sphere. This complex was reported by Gamo to have an average Co-O bond length of 2.21Å⁶⁴. In their X-ray diffraction study, Waizumi et al.⁶⁵ reported a similar octahedral dichloro species in solution that had average Co-O and Co-Cl bond lengths of 2.11 and

2.40Å respectively. These two results confirm the geometry that we have calculated for the tetraqua dichloro species.

The CoCl_3^- ion has been found to exist as part of drug molecules. Tesarowicz et al.⁶⁷ and Skórska et al.⁶⁸ reported various crystal structures of these CoCl_3^- containing molecules which have an average Co-Cl bond length of 2.24 to 2.28Å. Depending on the level of theory, we found the Co-Cl bond length of the trichloro ion to be in the range of 2.23 to 2.31Å, which is in excellent agreement with the experimental results.

The tetrachloro cobalt(II) ion was found to exist in crystal structures reported by Waizumi et al.⁶⁵ and Girma et al.⁶⁹. Waizumi et al. reported an average Co-Cl bond distance of 2.28Å, while Girma et al. reported an average Co-Cl distance of 2.267Å in a $[\text{Co}(\text{O-acrylamide})_6][\text{CoCl}_4]$ complex. We found a stable tetrahedral geometry for the anhydrous tetrachloro species which had a Co-Cl bond length of 2.36Å for MP2 and B3LYP and 2.45Å for HF. The MP2 and B3LYP results are in good agreement with experiment, with HF overestimating due to lack of electron correlation in the calculation. A couple of crystal structures were found in the literature containing CoCl_5^{3-} , which is perceived as containing a CoCl_4^{2-} group with an additional Cl^- contained elsewhere in the structure. Therefore these bond lengths can be compared to our tetrachloro results. The crystal structure of Cs_3CoCl_5 was reported on by both Powell et al.⁷² and Figgis et al.⁷³. Powell et al. reported the average Co-Cl bond length of the tetrachloro group to be 2.34Å, while Figgis et al. reported it to be 2.252Å.

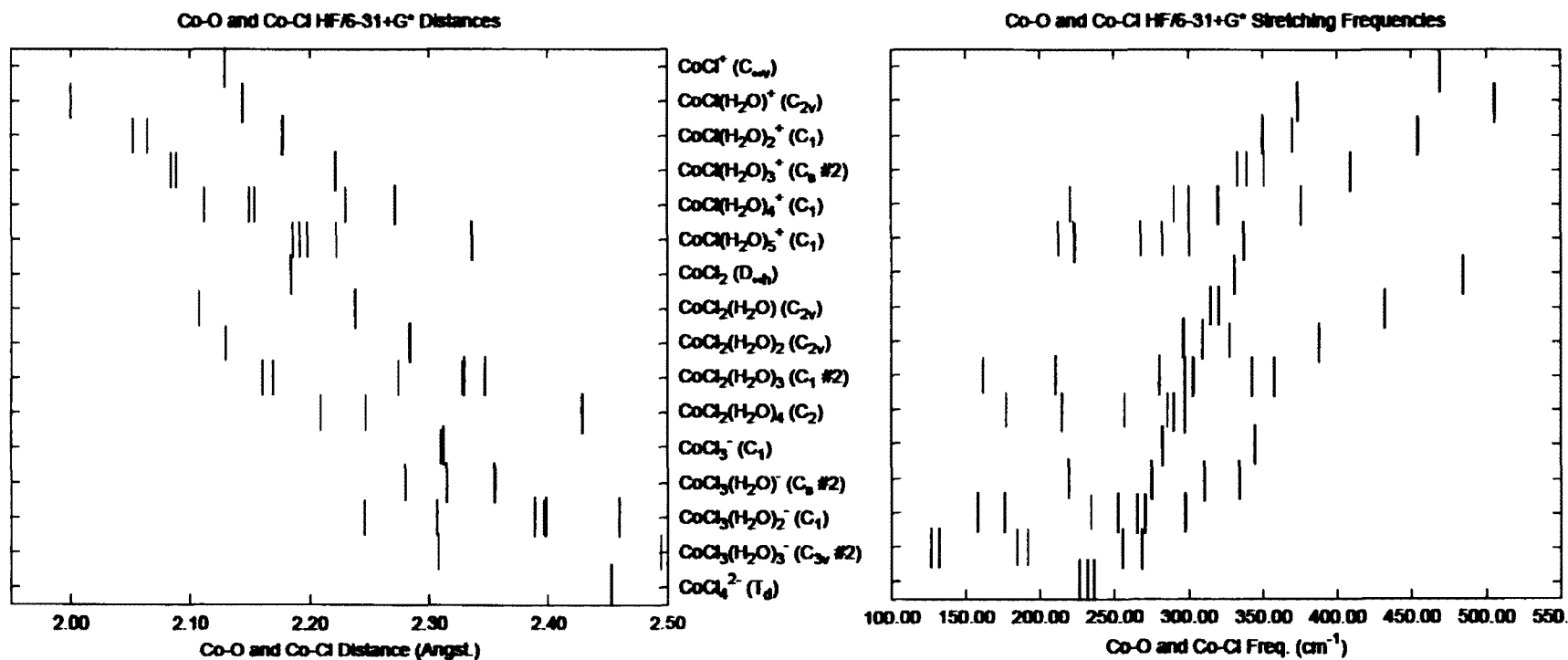


Figure 3-10: Co-O and Co-Cl (highlighted in red) bond lengths (left) and vibrational stretching frequencies (right) for $[\text{CoCl}_n(\text{H}_2\text{O})_m]^{2-n}$, where $n=1 - 4$ and $m=0 - (6-n)$, calculated at the HF/6-31+G* level.

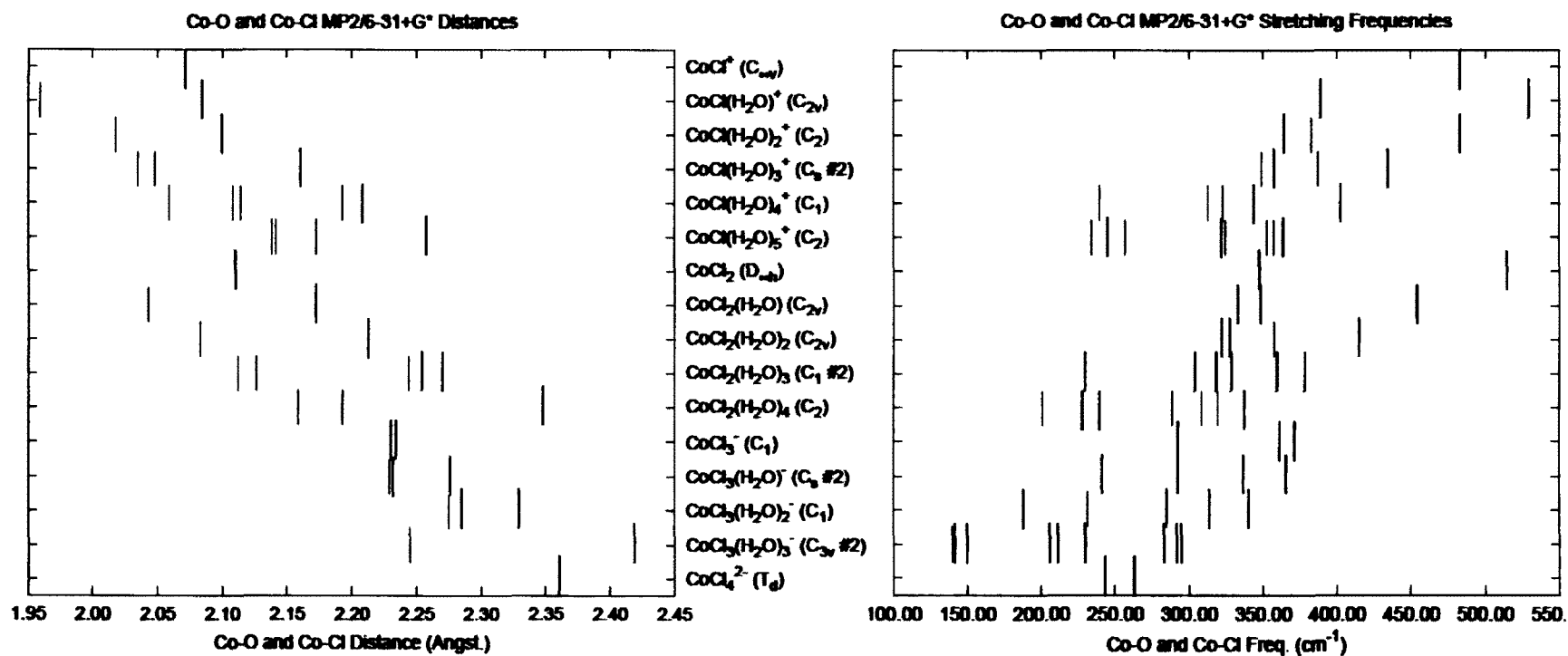


Figure 3-11: Co-O and Co-Cl (highlighted in red) bond lengths (left) and vibrational stretching frequencies (right) for $[\text{CoCl}_m(\text{H}_2\text{O})_m]^{2-n}$, where $n=1-4$ and $m=0-(6-n)$, calculated at the MP2/6-31+G* level.

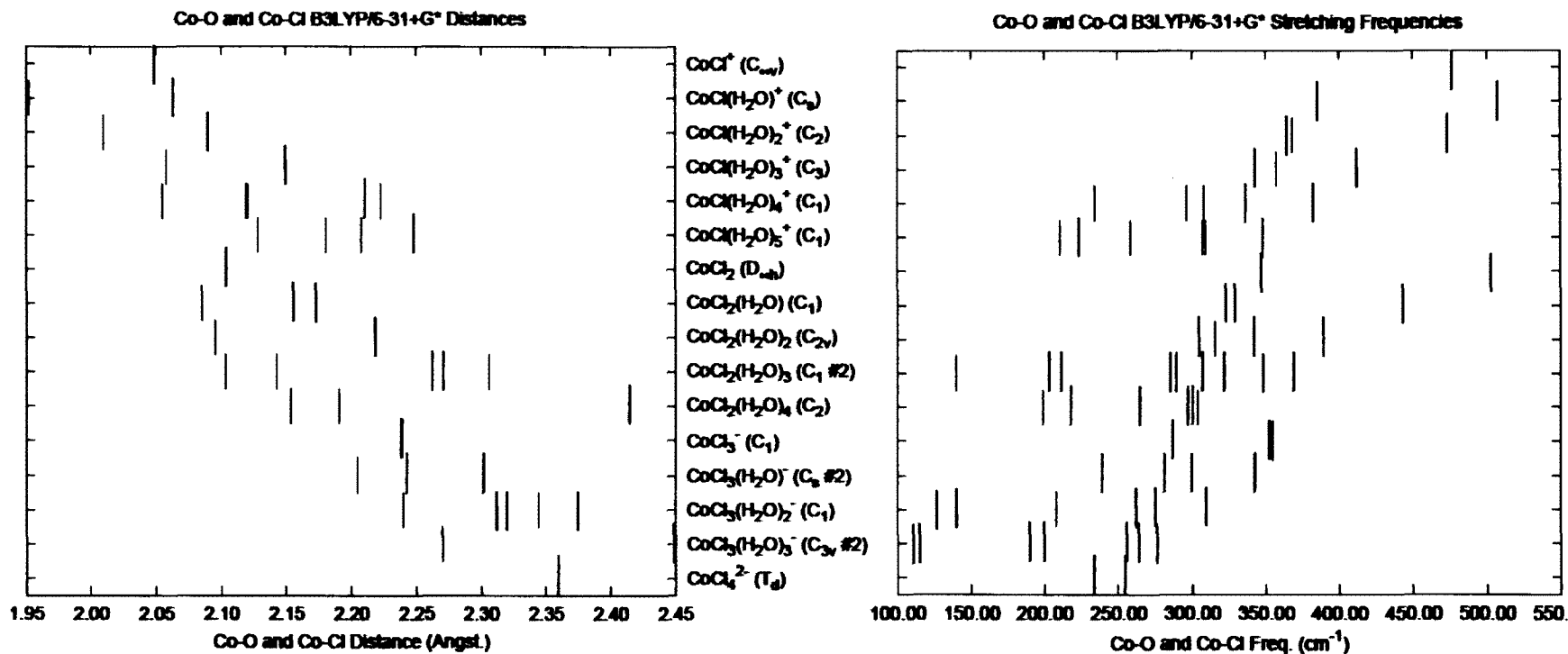


Figure 3-12: Co-O and Co-Cl (highlighted in red) bond lengths (left) and vibrational stretching frequencies (right) for $[\text{CoCl}_n(\text{H}_2\text{O})_m]^{2-n}$, where $n=1-4$ and $m=0-(6-n)$, calculated at the B3LYP/6-31+G* level.

Plots of Co-O and Co-Cl bond lengths can be found in Figures 3-10 to 3-12. These plots were constructed so that trends could be discovered with respect to lengthening and shortening of bonds depending on the hydration number. From these plots we can see that as more water molecules are added to the system there is a general increase in the distance of the Co-O and Co-Cl bond lengths. This trend can be understood through increased electron-electron repulsion, due to the addition of more water ligands.

Vibrational stretching frequency plots are accompanying the bond length plots in each of the figures. The trends seen here are opposite of the bond lengths. As more waters are added to the system there is a decrease in the vibrational stretching frequency value. This is due to the increase in bond distance, causing the bond to be weaker and therefore less energy is required to stretch the bond resulting in a lower frequency of vibration. These results show the inverse relationship between the bond length and the magnitude of the vibrational frequencies associated with it. The Raman active frequencies are important to us for comparison with experiment. Simulated polarized Raman plots are located in Figure 3A-2 the supplementary materials section. These plots are based on Raman intensities calculated at the HF level of theory. Unfortunately no experimental Raman data was found to compare our results with.

3.4 Hydroxycobalt(II) Complexes, $[\text{Co}(\text{OH})_n(\text{H}_2\text{O})_m]^{2-n}$, where $n=1 - 4$, $m=0 - (6-n)$

The neutral complex of cobalt(II) hydroxide can be precipitated by strong bases as either a blue or a pink solid, depending on the conditions, but only the pink form is permanently stable⁷. The stable, pink, form is known as β - $\text{Co}(\text{OH})_2$ with the unstable, blue, form being α - $\text{Co}(\text{OH})_2$. The stable form (β) will then dissolve in very concentrated alkali to give a deep blue solution of $[\text{Co}(\text{OH})_4]^{2-}$ ions⁷. There have been many reports on neutral cobalt(II) hydroxide, including; solubility in acidic and basic solutions⁸⁹, synthesis of the α -^{90,91,92} and β -^{90,92} forms, the crystal structure of the β -form⁹³ and the interconversion of the two phases⁹⁴. With the exception of the anhydrous neutral cobalt(II) hydroxide complexes a small number of the other complexes have been studied using either *ab initio* computational methods or experimentation. Binding energies for the single ligand monohydroxo species have been calculated^{58,95}. Absorption spectra have also been studied, by way of *ab initio* calculations, for hydrated four-, five- and six-coordinate monohydroxo cobalt(II) species⁴⁹⁻⁵¹. A computational study of the structure, vibrational frequencies and bonding energies of $\text{Co}(\text{OH})^+$ has also been reported⁹⁶. Photodissociation methods have been used to determine bond energies of the anhydrous monohydroxo species⁹⁷ as well as generate the monohydrate monohydroxo species⁴⁴. Hydrolysis studies of cobalt^{98,99,100} have shown the existence of the monohydroxo species as a reaction product. The monohydroxo species, as well as $\text{Co}(\text{OH})_2$, has also been reported as minor inorganic cobalt species in seawater¹⁰¹. Evidence was found for the existence of the tetrahydroxo cobalt(II) species in NMR-relaxation studies¹⁰² and the deep blue color of the tetrahydroxo cobalt(II) ion has been used as a qualitative test for

cobalt¹⁰³. Spectral studies by Cotton et al.⁸⁰ show evidence of the tetrahydroxo ion as well as suggest the possibility of the monohydrated trihydroxo species.

3.4.1 Results

Stable structures were found for all hydroxide complexes up to and including hexacoordinate tetrahydroxo species with the additional ligands being water. Calculations were also completed on the penta and hexahydroxo complexes, but these species showed dissociation of one or more hydroxide ligand and preferred to exist as ion pairs. Stable structures of these ion pair complexes were not found. Total energies, as well as C-PCM energies, for all hydroxide complexes studied can be found in Table 3A.12 of the supplementary materials section. Optimized geometries of the stable complexes are located in Figure 3-13 for the mono and dihydroxo complexes and in Figure 3-14 for the tri and tetrahydroxo complexes.

The anhydrous monohydroxo complex preferred to be in a linear $C_{\infty v}$ structure for all levels except B3LYP where the Co-O-H angle is bent, resulting in a stable C_s geometry. The most stable geometry for the monohydrate depended on the level of theory. For HF there were two stable C_s geometries found, with the non-planar geometry being lower in energy. A C_{2v} structure, with a linear hydroxide, was preferred for the MP2 level, while B3LYP preferred the planar C_s geometry. The dihydrate was only stable in a C_1 geometry due to the preferentially bent nature of the hydroxide. The trihydrate was also found to have C_1 symmetry at all levels, with two different C_1 structures for the HF level. One was slightly preferred over the other, but both are very similar. The tetrahydrate and pentahydrate geometries were both found to be C_1 for all levels.

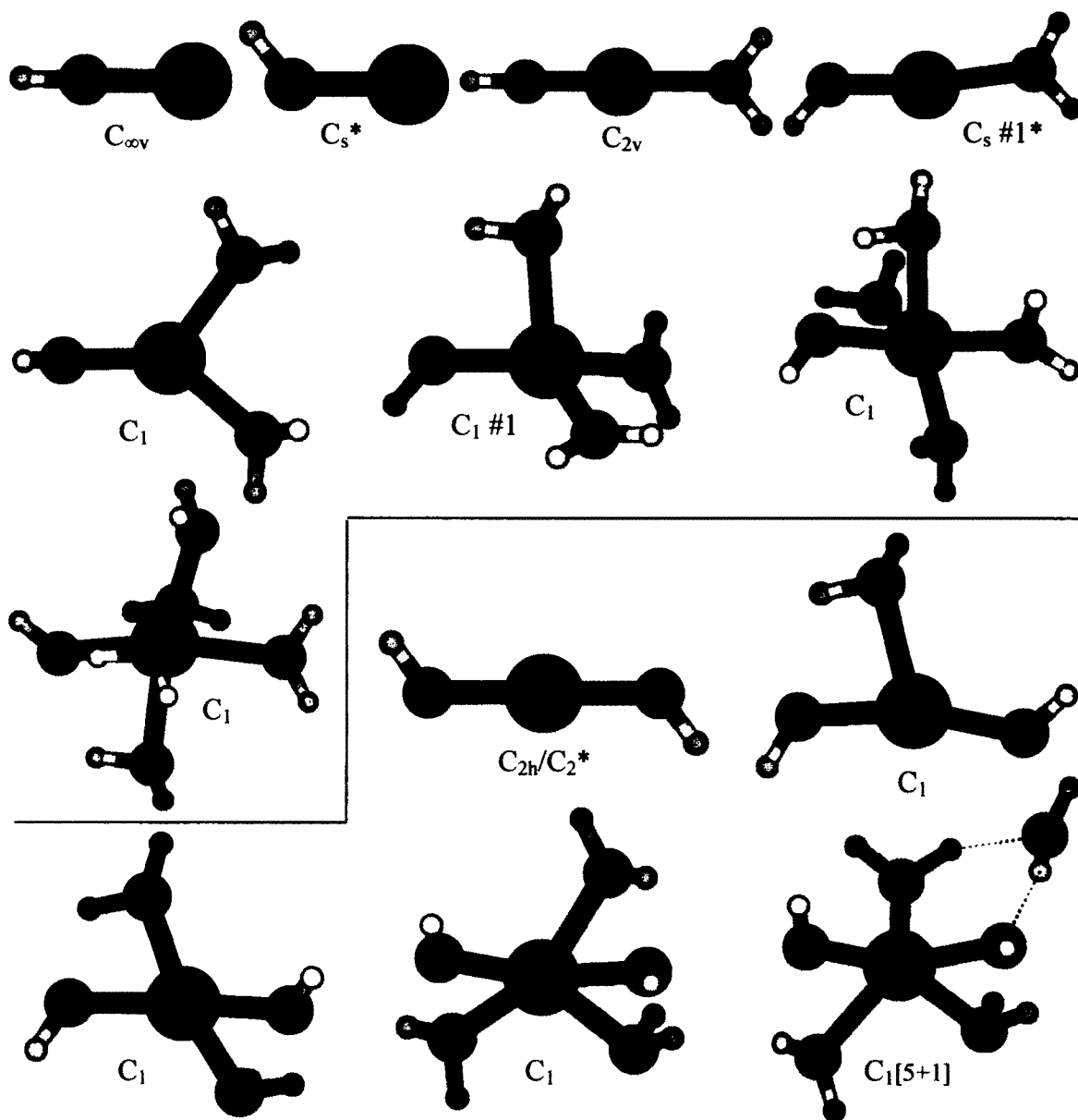


Figure 3-13: Optimized MP2 and B3LYP geometries for $[\text{Co}(\text{OH})(\text{H}_2\text{O})_m]^+$ (top) and $[\text{Co}(\text{OH})_2(\text{H}_2\text{O})_m]$ (bottom). "*" indicates B3LYP geometry is different than MP2.

For the anhydrous dihydroxo species the hydroxide ligands preferred to be bent with all levels having a stable C_{2h} geometry. The B3LYP level had a slight energetic

preference for a C_2 structure over C_{2h} , but the geometry looks very similar. There were two stable geometries found for the monohydrate complex with C_s and C_1 symmetry. The C_1 symmetry is energetically preferred for all levels. The only stable geometry found for the dihydrate and trihydrate at all levels has C_1 symmetry. The tetrahydrate was also most stable with a C_1 geometry, except this structure does not have all ligands completely bound, one of the water molecules has dissociated and is in the second hydration sphere hydrogen bonded in a donor-acceptor fashion to a hydroxide and water molecule respectively.

Many stable geometries were found for the anhydrous trihydroxo cobalt complexes, with symmetry as high as C_3 (HF) and as low as C_1 (MP2 and B3LYP). Two different C_s structures were also found but were less energetically favored when compared to the C_3 and C_1 geometries. The energy minimum for the monohydrate was a C_1 structure that had the water molecule hydrogen bonded in a donor-donor fashion to two hydroxide ligands. No stable structure was found where the water molecule stayed bound to the central cobalt atom. The dihydrate was similar in that the energy minimum geometry preferred to have at least one water molecule in the second hydration sphere hydrogen bonded. For HF and B3LYP there are two water molecules hydrogen bonded, both in donor-donor manners to two hydroxide ligands. The MP2 geometry only has one water molecule in the second hydration sphere being hydrogen bonded in a donor-donor manner to two hydroxides. In all cases of the trihydrate, the C_1 geometry is preferred with two water molecules being located in the second hydration sphere. These two water molecules show hydrogen bonds to the central molecule.

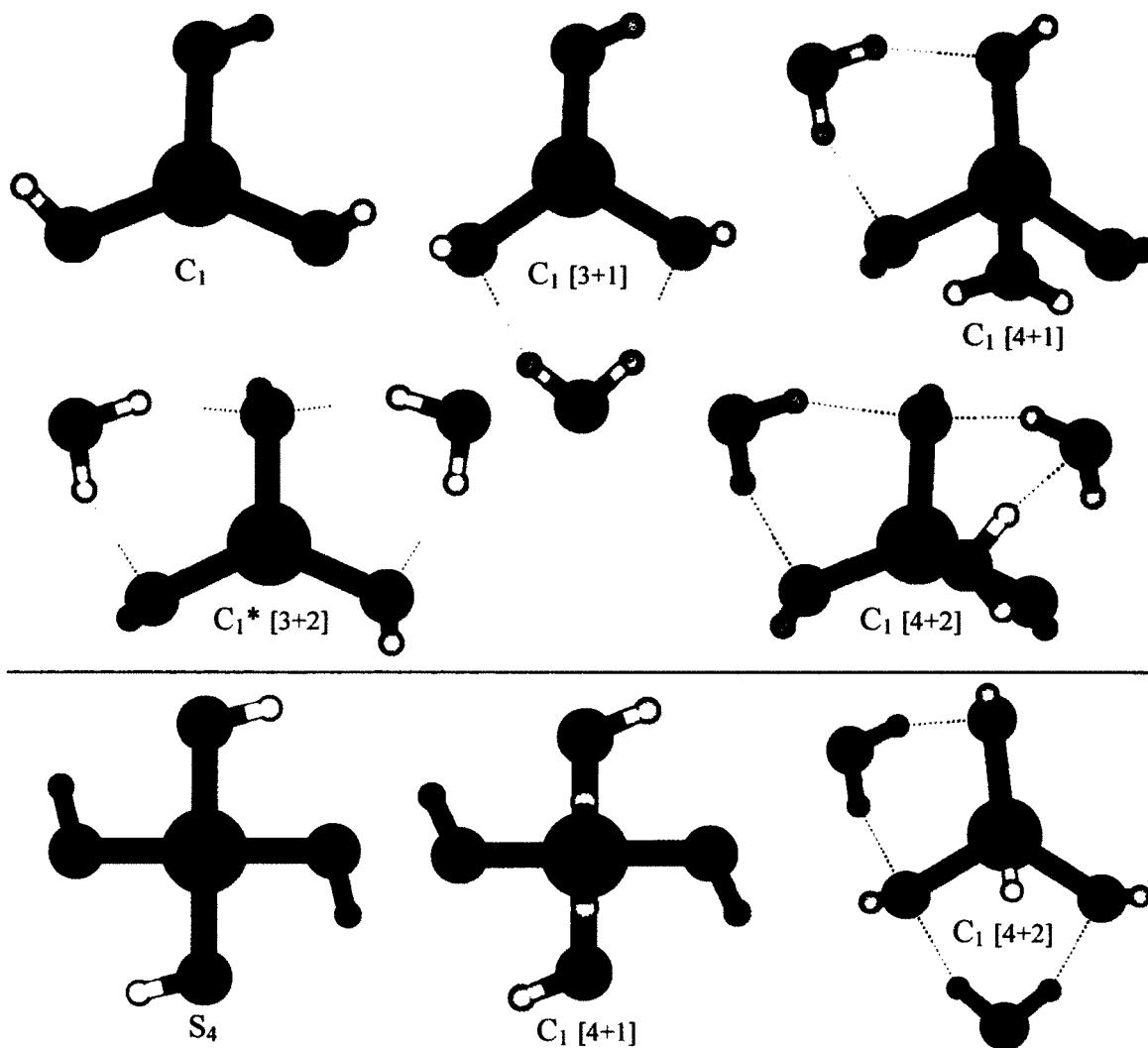


Figure 3-14: Optimized MP2 and B3LYP geometries for $[\text{Co}(\text{OH})_3(\text{H}_2\text{O})_m]^-$ (top) and $[\text{Co}(\text{OH})_4(\text{H}_2\text{O})_m]^{2-}$ (bottom). “*” indicates B3LYP geometry if different than MP2.

Three stable geometries were found for the tetrahydroxo species with no water molecules. These three geometries have symmetries of S_4 , C_2 and C_1 , with S_4 being energetically preferred at all levels. The monohydrate was also found to be stable in both C_2 (B3LYP was not stable in this geometry) and C_1 geometries, with C_1 being

energetically favored at all levels. Both of the structures have the water molecule being hydrogen bonded in a donor-donor fashion to two hydroxide ligands. The C_1 geometries appear to be very close to a C_2 structure. There was agreement among levels that the dihydrate was only stable with C_1 symmetry having both water molecules in the second hydration sphere and being hydrogen bond in donor-donor fashions to hydroxide ligands.

As mentioned previously, no stable structures were found for complexes with more than four hydroxide ligands. These complexes showed preference for ion pairs and therefore the calculations were not taken to completion. Since we do not have any concrete data for these complexes, they will not be discussed in the following section.

Bond length and vibrational frequency data was also tabulated for the stable hydroxo complexes and can be found in the supplementary materials section. Plots of the Co-O bond lengths and vibrational stretching frequencies can be found in Figure 3-15, Figure 3-16 and Figure 3-17 for HF, MP2 and B3LYP respectively. Simulated polarized Raman spectra can be found in Figure 3A-3 of the supplementary materials section.

3.4.2 Discussion/Literature Comparison

The geometries that we have found can primarily be confirmed by comparison with available data from crystal structures found in the literature, or other computational studies that have been completed on similar complexes. Something that is interesting to note about the energy minimum structures of the monohydroxo complexes is that the anhydrate was most stable with a linear Co-O-H for HF and MP2 calculations. This was

also true for the monohydrate at the MP2 level. However, when more water molecules are added, the linear hydroxyl group is no longer preferred at any level of theory.

Some previous computational work has been completed related to the anhydrous monohydroxo species by Magnusson and Moriarty⁵⁸, Ricca and Bauschlicher⁹⁵ and Trachtman et al.⁹⁶. The values that we have calculated for the Co-O bond length are 1.721, 1.686 and 1.721 Å for the HF, MP2 and B3LYP levels respectively. Magnusson and Moriarty calculated a Co-O bond length of 1.744 Å at the MP2/6-311+G** level which is very comparable to the values that we have found using a smaller basis set. Ricca and Bauschlicher found the same bond length to be 1.723 Å using B3LYP with a different basis set than ours, but the result is very close to our HF and B3LYP results and only slightly higher than our MP2 value. Trachtman et al. found the Co-O bond length to be 1.718 Å using MP2 with the 6-311++G** basis set. This value is also in good agreement with our findings. Gilson and Krauss⁴⁹ have reported a computational study containing results for the tri-, tetra- and pentahydrate species using CAS-MCSCF and MCQDPT calculations. The single hydroxide trihydrate complex that they calculated contained Co-O bond lengths of 1.835 (OH) and 2.098 Å (avg H₂O)⁴⁹. These results are in agreement with what we have found for HF as 1.832 (OH) and 2.101 Å (avg H₂O), MP2 as 1.815 (OH) and 2.062 Å (avg H₂O) and B3LYP as 1.794 (OH) and 2.071 Å (avg H₂O). The results Gilson and Krauss⁴⁹ reported for the tetrahydrate (1.874 OH and 2.178 Å H₂O) and pentahydrate (1.938 OH and 2.198 Å H₂O) are also in similar agreement with what we have found, which can be viewed in Table 3A.13 of the supplementary materials section.

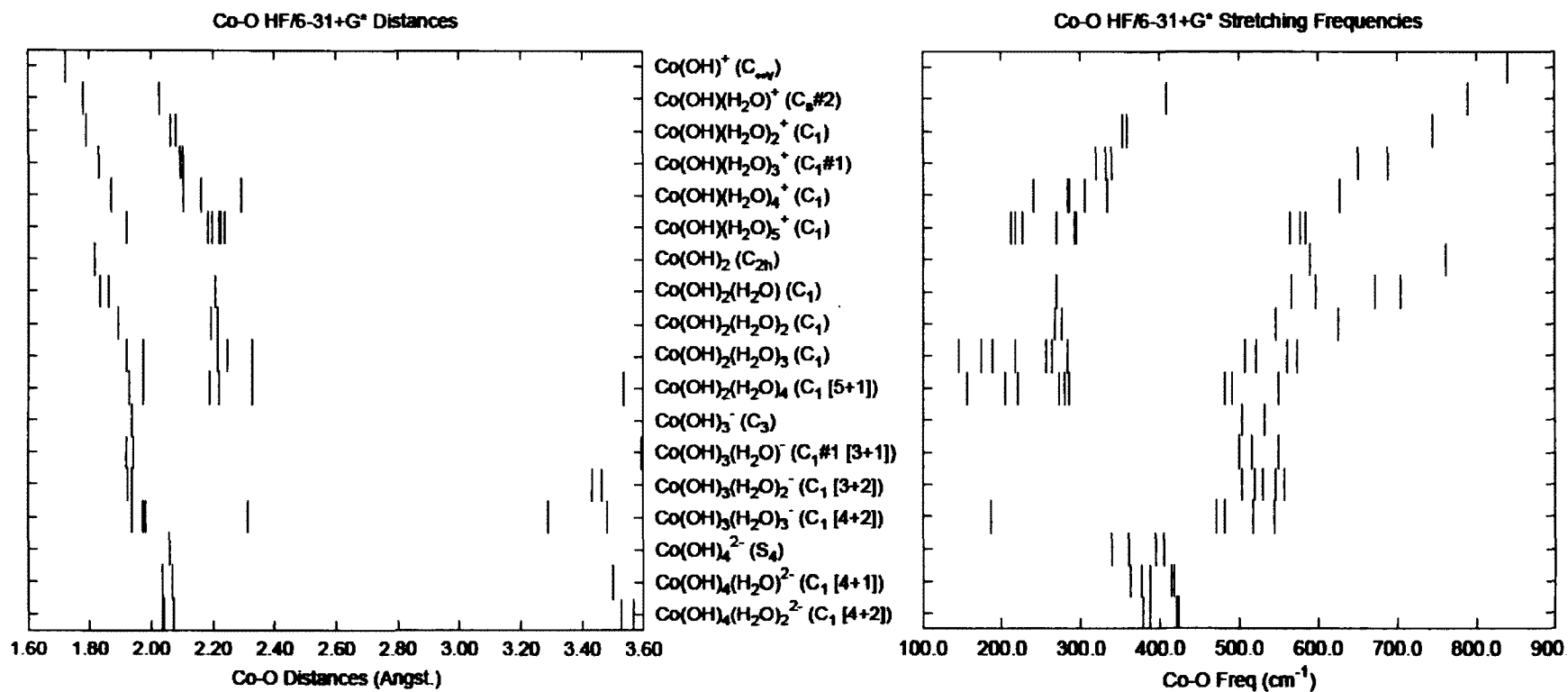


Figure 3-15: Co-O bond lengths (left) and vibrational stretching frequencies (right) for $[\text{Co}(\text{OH})_n(\text{H}_2\text{O})_m]^{2-n}$, where $n=1-4$ and $m=0-(6-n)$, calculated at the HF/6-31+G* level.

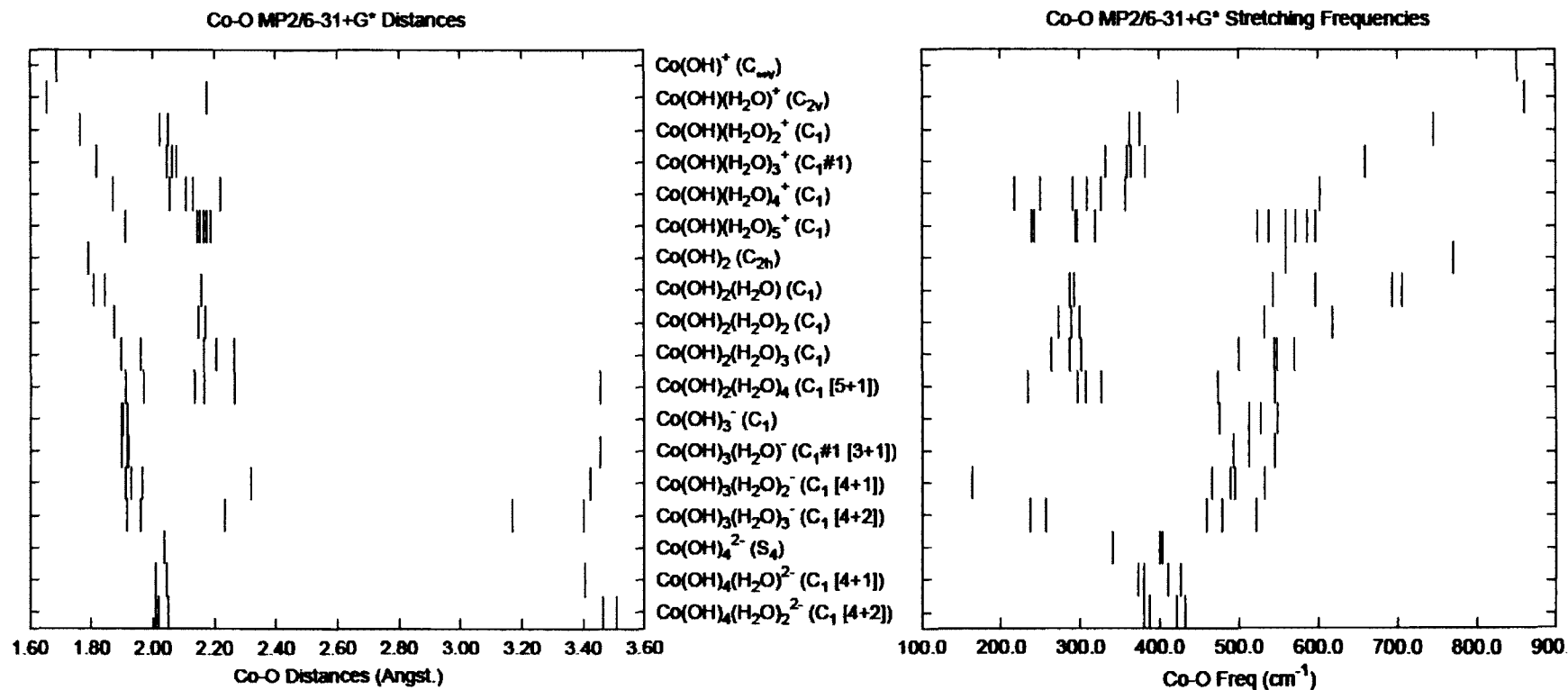


Figure 3-16: Co-O bond lengths (left) and vibrational stretching frequencies (right) for $[\text{Co}(\text{OH})_n(\text{H}_2\text{O})_m]^{2-n}$, where $n=1-4$ and $m=0-(6-n)$, calculated at the MP2/6-31+G* level.

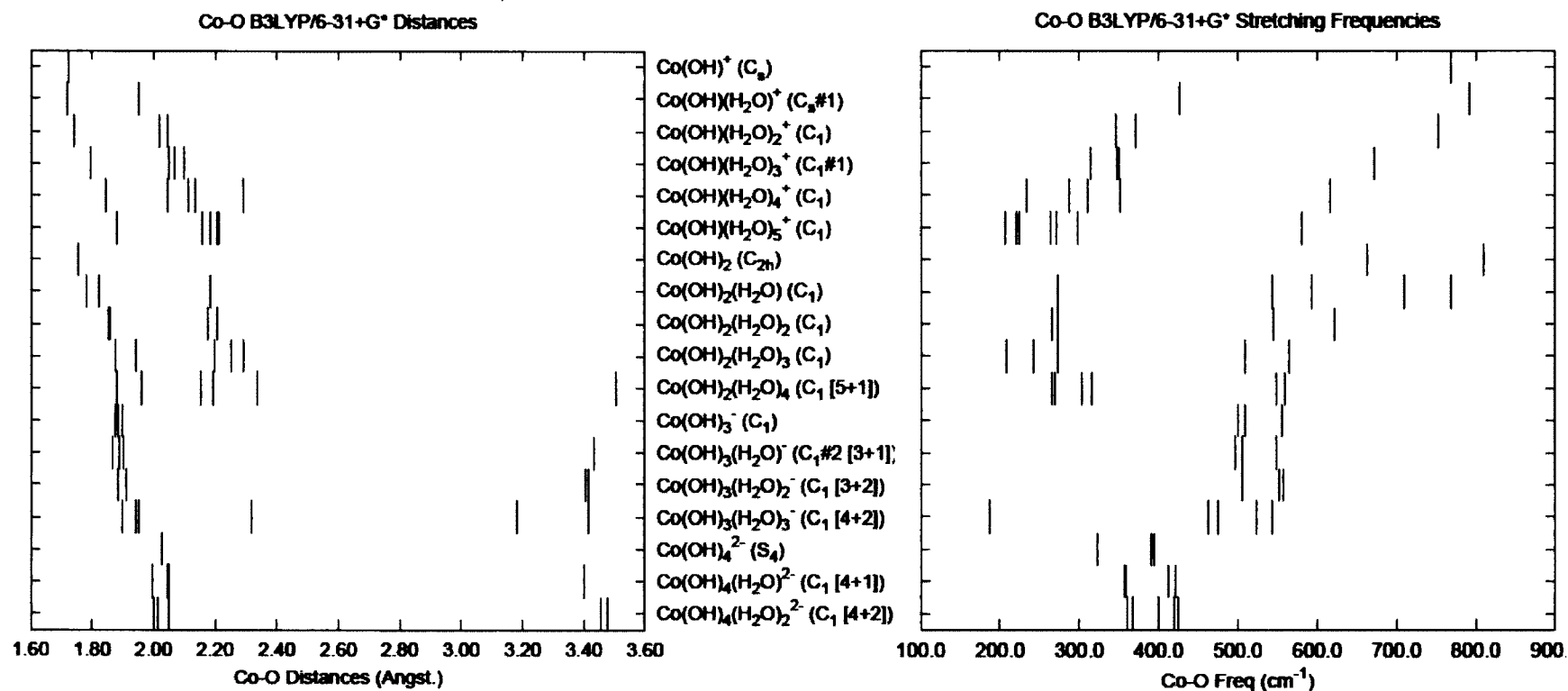


Figure 3-17: Co-O bond lengths (left) and vibrational stretching frequencies (right) for $[\text{Co}(\text{OH})_n(\text{H}_2\text{O})_m]^{2-n}$, where $n=1 - 4$ and $m=0 - (6-n)$, calculated at the B3LYP/6-31+G* level.

Our optimized structures for the anhydrous form of Co(OH)_2 contained a Co-O bond length of 1.816, 1.790 and 1.752Å for HF, MP2 and B3LYP respectively. These results can be compared to the crystal structure of $\beta\text{-Co(OH)}_2$ reported by Mockenhaupt et al.⁹³. They reported Co-O bond distance values of 2.083Å for the deuterated form and 2.10Å for the non-deuterated form. These experimental values are higher than our computational results. This could be explained by the nature of their crystal structure versus the gas-phase molecule that we calculated. Our cobalt center is surrounded by only two hydroxide ligands whereas in the crystal structure the cobalt atom is surrounded by six oxygen atoms. Having more oxygen atoms surrounding the cobalt center would cause the Co-O bond distance to be longer due to repulsion. There were no other literature reports found regarding the remaining cobalt complexes we have investigated in this study and therefore we have nothing to compare our optimized geometries with.

Plots were constructed of the Co-O bond lengths and vibrational stretching frequencies and can be found in Figures 3-15 to 3-17. Within each of these plots a trend can be seen of increasing Co-O bond length with addition of water ligands. Consequently there is a decrease in Co-O vibrational stretching frequencies due to longer bond lengths as water molecules are added. Within each of the bond distance plots there is a small cluster of bond lengths above 3.0Å which correspond to those water molecules that have dissociated from the Co(II) center and are hydrogen bonded to the central molecule.

Raman spectroscopy will be the primary experimental technique used to identify these compounds at high temperatures and pressures, based on the Raman active bands that we have calculated. This experimental work has not been completed yet and no

Raman data was found in the literature related to this set of cobalt(II) hydroxide complexes. However, predicted polarized Raman spectra have been constructed based on intensities calculated at the HF level of theory and can be found in Figure 3A-3 of the supplementary materials section.

3.5 Ammincobalt(II) Complexes, $[\text{Co}(\text{NH}_3)_n(\text{H}_2\text{O})_m]^{2+}$, where $n=1 - 6$, $m=0 - (6-n)$

As mentioned previously, Co(II) complexes tend to exist in either tetrahedral or octahedral forms. The same is true here with the ammine ions with a tetrahedral $[\text{Co}(\text{NH}_3)_4]^{2+}$ ion in $[\text{Co}(\text{NH}_3)_4](\text{ReO}_4)_2$ although in other cases the hexammine ion $[\text{Co}(\text{NH}_3)_6]^{2+}$ is formed⁷. The hexammine cobalt(II) ion is the most known aminocobalt(II) complex. The cation has been studied by using crystallographic methods^{104,105,106} as well as *ab initio* computational chemistry methods^{54,56,57}. The *ab initio* studies have included the electrochemical reduction of the $[\text{Co}(\text{NH}_3)_5(\text{H}_2\text{O})]^{2+}$ ion⁵², high versus low spin-state stability⁵⁴ and structure, energetics and electron density of the six-coordinate species⁵⁷, metal substitution in carbonic anhydrase including the triammine complex⁵⁵, binding patterns in single-ligand complexes⁵⁸ and also has been used in a test of various computational methods⁵⁶. There have also been some kinetic studies of ligand detachment in the hexammine ion^{107,108} as well as reports on UV/Vis absorption spectra¹⁰⁹, energies of electronic transitions¹¹⁰, heat of formation¹¹¹, ¹⁴N NMR based exchange studies^{112,113} of the amine ligands and also an IR absorption study of hexamminecobalt(II) halides¹¹⁴. The hexammine and pentammine complexes have also been used as models for oxygen uptake¹¹⁵. Most of the studies completed only include six-coordinate species whereas this thesis includes all of the complexes with a coordination number from 1 to 6.

3.5.1 Results

The cobalt(II) ammine complexes were studied up to and including hexacoordinate species with and without water molecules. Stable geometries were found for all of the complexes studied. Total molecular energies as well as C-PCM energies of all the geometries studied can be found in Table 3A.16 of the supplementary materials section. The optimized geometries of the stable species can be found in Figure 3-18 for the mono and diammine complexes and in Figure 3-19 for the tri, tetra, penta and hexammine complexes.

The anhydrous monoammine was stable in its highest possible symmetry of C_{3v} at all levels of theory. There were no symmetry problems with the monohydrate either as it was C_s at all levels. Initially two different C_s structures were attempted for the dihydrate, but neither was stable so the symmetry was reduced to a C_1 structure which turned out to be stable at all levels, except the MP2 energy was higher than both unstable C_s structures. The geometry was altered slightly and a different C_1 structure was found to be stable at MP2. The trihydrate preferred C_3 symmetry over C_{3v} (unstable) at all levels. A stable C_s geometry was found for the tetrahydrate, while the pentahydrate preferred a C_1 geometry.

The anhydrous diammine was initially tried as D_{3d} and D_{3h} , but ultimately preferred to have C_{2v} symmetry. A C_s symmetry was also attempted, but the structure seemed to revert back to the C_{2v} form although the C-PCM energy was marginally lower for the C_s geometry. Four different C_{2v} structures were attempted for the monohydrate, but all contained imaginary frequencies and the most stable structure ended up having C_s symmetry. The dihydrate was stable with C_2 symmetry after finding imaginary

frequencies and desymmetrizing the two different C_{2v} geometries. The trihydrate was attempted as a D_{3h} structure, but after reducing symmetry based on an imaginary frequency the structure became stable with D_3 symmetry. Four stable geometries were found for the tetrahydrate, C_i , C_2 , C_s and C_1 . The only stable geometries for B3LYP were C_i and C_1 , whereas HF was stable in all configurations and MP2 was stable with C_i , C_2 and C_1 symmetries. All levels had energetic preference for the C_i (inversion center) geometry.

The triammine with no water molecules showed agreement among levels that the most stable structure has C_3 symmetry. The monohydrate was stable with a C_s symmetry at all levels. The dihydrate had two stable geometries at the HF and MP2 levels of C_s and C_1 . The C_1 structure was more stable at both levels. At B3LYP only the C_1 geometry was stable, except at this level the C_1 structure has one of the water molecules hydrogen bonded to the central molecule, whereas the HF and MP2 structures have all the water molecules bound to the central Co atom. The trihydrate was most stable with fac- C_3 symmetry at all levels although the C-PCM energy for the mer- C_1 structure is slightly lower than that of the fac- C_3 structure.

Two stable structures of C_3 and C_1 symmetry were found for the anhydrous tetrammine. Although the C_1 geometry is energetically preferred for the HF and MP2 levels, the structures look very similar. For B3LYP, there is very little difference in energy between both geometries with the C_3 being marginally lower. The monohydrate has two stable structures at the HF and B3LYP levels with C_{2v} and C_1 symmetry. The C_1

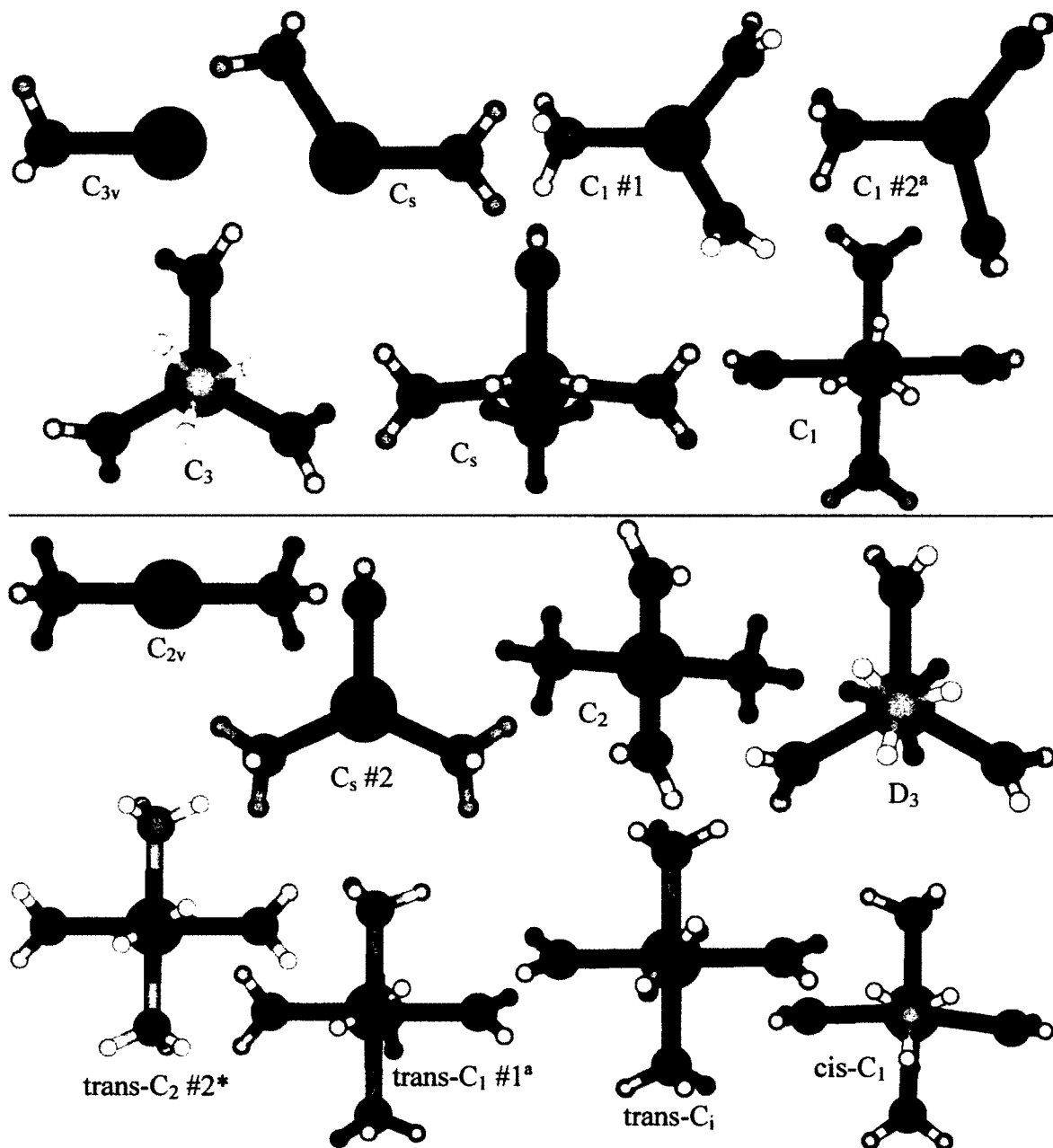


Figure 3-18: Optimized MP2 and B3LYP geometries for $[\text{Co}(\text{NH}_3)_n(\text{H}_2\text{O})_m]^{2+}$, where $n=1-2$, $m=0-(6-n)$. “*” indicates only stable at MP2, “^a” indicates only stable at B3LYP.

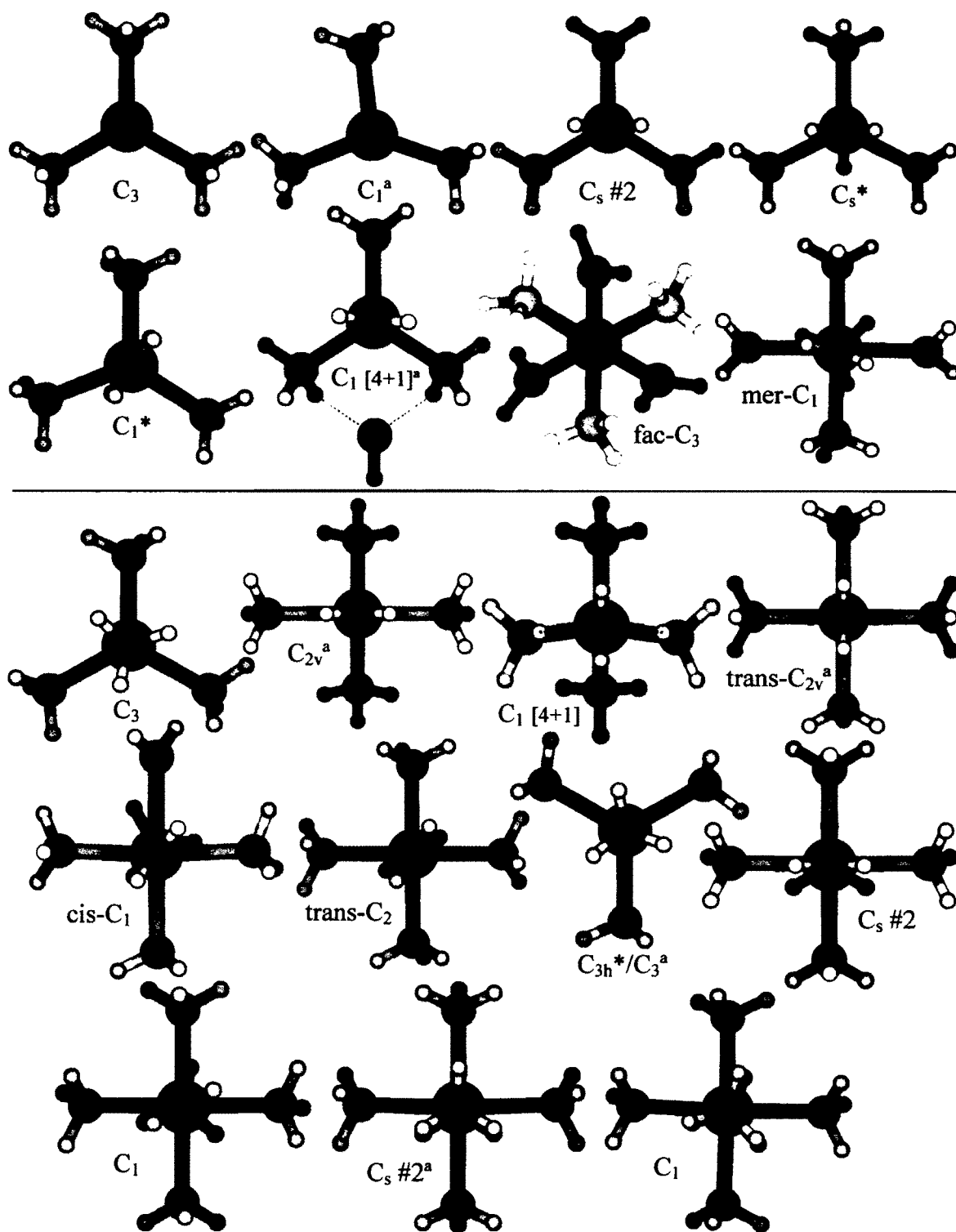


Figure 3-19: Optimized MP2 and B3LYP geometries for $[Co(NH_3)_n(H_2O)_m]^{2+}$, where $n=3-6$, $m=0-(6-n)$. “*” indicates only stable at MP2, “^a” indicates only stable at B3LYP.

geometry is energetically favored at both levels. The stable C_1 structure at B3LYP has the water molecule hydrogen bonded to the central tetrammine, whereas the HF structure has the water molecule bound to the cobalt center. Only the C_1 symmetry was stable at the MP2 level with a similar structure to B3LYP with the water molecule hydrogen bonded. The most stable geometry for the dihydrate has C_2 symmetry at all levels. A stable C_{2v} symmetrical structure was found at the HF and B3LYP levels, but is higher in energy and therefore less stable.

A stable C_1 geometry was found at all levels for the anhydrous pentammine. This was the only stable structure found for the HF level, but there was a stable C_3 structure found at the MP2 and B3LYP levels which is more stable than the C_1 structure although not by very much and in fact the C_3 and C_1 structures at these two levels look very similar. Both a C_s and a C_1 geometry were found to be stable for the monohydrate. The preference was dependent on the level of theory, with HF and B3LYP preferring the C_1 structure and MP2 preferring the C_s structure. Finally the hexammine species preferred C_1 symmetry at all levels. Only B3LYP had another stable structure with C_s symmetry, but is higher in energy than the C_1 geometry.

Bond length and vibrational stretching frequency data was collected and plots were constructed which can be seen in Figure 3-20, Figure 3-21 and Figure 3-22 for HF, MP2 and B3LYP respectively. Raman intensities were calculated at the HF level and therefore simulated polarized Raman plots were able to be created and these can be found in the supplementary materials section in Figure 3A-4.

3.5.2 Discussion/Literature Comparison

The geometries that we have found will be compared to computational and crystallography results reported in the literature. Garmer and Krauss⁵⁵ studied the active site of carbonic anhydrase and modeled the enzyme with $[\text{Co}(\text{NH}_3)_3(\text{H}_2\text{O})]^{2+}$ inserted into the active site. They reported a Co-O bond distance of 2.12Å and an average Co-N bond distance of 2.13Å based on a HF/CEP-31G calculation. These results are consistent with the bond lengths we have calculated at the HF level (Co-O = 2.098Å, Co-N = 2.132Å). Rulišek and Havlas⁵⁶ performed *ab initio* calculations on the $[\text{Co}(\text{NH}_3)_6]^{2+}$ complex and reported an average Co-N bond distance of 2.31Å at the CASSCF(7,5)/TZVP level. This result is in good agreement with our average Co-N bond distance which is in the range of 2.230-2.301Å depending on the level of theory. Magnusson and Moriarty⁵⁸ used *ab initio* methods to study binding patterns in single-ligand Co(II) complexes and reported a Co-N bond distance in $[\text{Co}(\text{NH}_3)]^{2+}$ of 2.012Å, which is inside the range of our lowest value (1.985Å – B3LYP) and our highest value (2.042Å – HF).

Works by Schmiedekamp et al.⁵⁴ and Varadwaj and Marques⁵⁷ include *ab initio* results on six-coordinate Co(II) complexes with ammonia and water ligands. Both of their calculations incorporated the B3LYP hybrid density functional, but their basis sets were different. Schmiedekamp et al. used the LACVP** basis set while Varadwaj and Marques used the 6-311++G** basis set which is very similar to the ones we have used in our calculations. We plotted their results in Table 3.1 along with our B3LYP/6-31+G* results for comparison purposes.

Table 3.1: Geometry comparison of hexacoordinate ammine complexes with results reported by Schmiedekamp et al.⁵⁴ and Varadwaj and Marques⁵⁷. All bond lengths are averages where appropriate.

Complex	Point Group	Schmiedekamp et al. ⁵⁴		Varadwaj and Marques ⁵⁷		Our Results	
		Co-N	Co-O	Co-N	Co-O	Co-N	Co-O
$\text{Co}(\text{NH}_3)(\text{H}_2\text{O})_5^{2+}$	C_1	2.156	2.143	2.135	2.161	2.123	2.148
$\text{Co}(\text{NH}_3)_2(\text{H}_2\text{O})_4^{2+}$	cis- C_1	2.186	2.151	2.154	2.182	2.156	2.184
$\text{Co}(\text{NH}_3)_2(\text{H}_2\text{O})_4^{2+}$	trans- C_1	--	--	2.201	2.145	2.125	2.184
$\text{Co}(\text{NH}_3)_2(\text{H}_2\text{O})_4^{2+}$	trans- C_1	2.167	2.174	2.142	2.199	2.156	2.184
$\text{Co}(\text{NH}_3)_2(\text{H}_2\text{O})_4^{2+}$	trans- C_2	--	--	2.137	2.212	Not Stable	
$\text{Co}(\text{NH}_3)_2(\text{H}_2\text{O})_4^{2+}$	mer- C_1	2.175	2.216	2.169	2.192	2.156	2.184
$\text{Co}(\text{NH}_3)_3(\text{H}_2\text{O})_3^{2+}$	fac- C_1	2.173	2.228	2.152	2.261	--	--
$\text{Co}(\text{NH}_3)_3(\text{H}_2\text{O})_3^{2+}$	fac- C_3	--	--	--	--	2.164	2.209
$\text{Co}(\text{NH}_3)_4(\text{H}_2\text{O})_2^{2+}$	cis- C_1	2.208	2.252	2.192	2.323	2.184	2.278
$\text{Co}(\text{NH}_3)_4(\text{H}_2\text{O})_2^{2+}$	trans- C_1	2.219	2.213	--	--	--	--
$\text{Co}(\text{NH}_3)_4(\text{H}_2\text{O})_2^{2+}$	trans- C_2	--	--	--	--	2.195	2.243
$\text{Co}(\text{NH}_3)_5(\text{H}_2\text{O})^{2+}$	C_1	2.239	2.209	2.234	2.284	2.212	2.357
$\text{Co}(\text{NH}_3)_6^{2+}$	C_1	2.264	N/A	2.259	N/A	2.247	N/A

Although attempted, we did not find a stable geometry for the trans- C_2 geometry of $[\text{Co}(\text{NH}_3)_2(\text{H}_2\text{O})_4]^{2+}$. The only significant difference is between the Co-O bond length that Schmiedekamp et al. found for their monoaquapentammine complex (2.209 Å) and what we found for ours (2.357 Å). Other than that, all of our results are very comparable to what they have found in their studies. However, Schmiedekamp et al. and Varadwaj and Marques did not study the ammine complexes that have fewer than six ligands, whereas we studied all complexes with a coordination of 1 to 6.

Two crystal structures of $[\text{Co}(\text{NH}_3)_6\text{Cl}_2]$ were found in the literature that contain the Co(II) hexammine ion. These structures were reported by Barnet et al.¹⁰⁴ and Newman et al.¹⁰⁵. Barnet et al.¹⁰⁴ reported a Co-N bond distance of 2.114Å, while Newman et al.¹⁰⁵ reported a slightly longer Co-N bond length of 2.170Å. Both of these

values are a little bit shorter than the range that we have calculated for the Co-N bond length of 2.230-2.301 Å. No other crystal structures were found in the literature for the other ammine complexes.

There is something interesting to note regarding the C-PCM results. Two of the complexes, $[\text{Co}(\text{NH}_3)_3]^{2+}$ and $[\text{Co}(\text{NH}_3)_3(\text{H}_2\text{O})_3]^{2+}$, showed lower C-PCM energies for an optimized geometry that is not the energy minimum. Firstly, the anhydrous species is most stable in a C_3 geometry, but the C-PCM result indicated that the C_1 geometry is more stable when contained in an aqueous dielectric continuum. The same result can be seen for the trihydrate species, the C_3 geometry is lowest in energy for the gas-phase calculation, whereas the C_1 geometry is preferred in the dielectric continuum calculation.

Plots were created of the Co-O and Co-N bond lengths and vibrational stretching frequencies which can be seen in Figures 3-20 to 3-22. These plots showcase the trends in the bond lengths and stretching frequencies as more ligands, either ammonia or water, are added to the system. As more water molecules are added to the cobalt center, the longer the bond distances become. Due to the closeness of the Co-O and Co-N bond lengths, all of the Co-N bond lengths have been plotted using a dark green plus sign (+) to distinguish one from the other. A couple of the lowest energy structures contained a water molecule which is hydrogen bonded to the central cobalt molecule. The Co-O bond lengths of these hydrogen bonded water molecules have been left out of the plots so that the rest of the data points could be spread out and the trends could be seen more clearly. The stretching frequency plots show the opposite trend of the bond length plots. As more

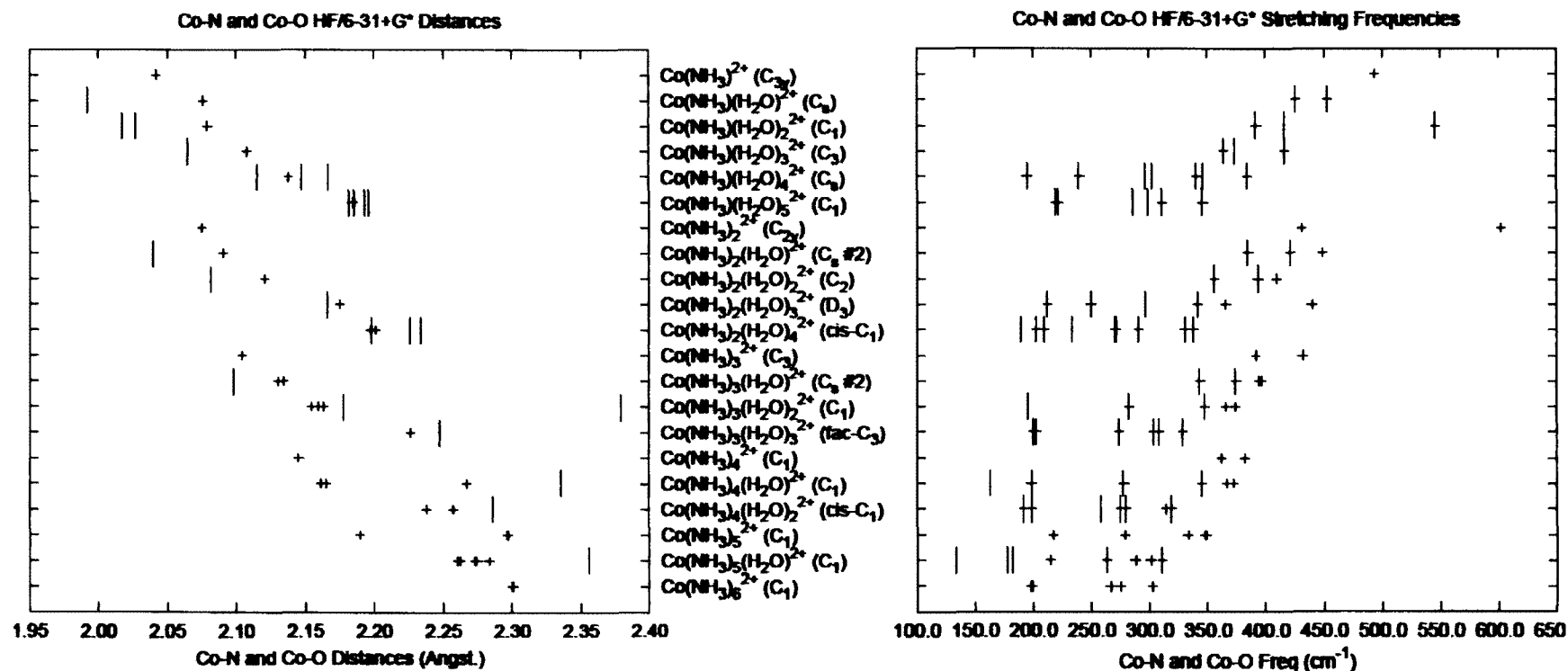


Figure 3-20: Co-N (+) and Co-O (||) bond lengths (left) and vibrational stretching frequencies (right) for $[\text{Co}(\text{NH}_3)_n(\text{H}_2\text{O})_m]^{2+}$, where $n=1-6$ and $m=0-(6-n)$, calculated at the HF/6-31+G* level.

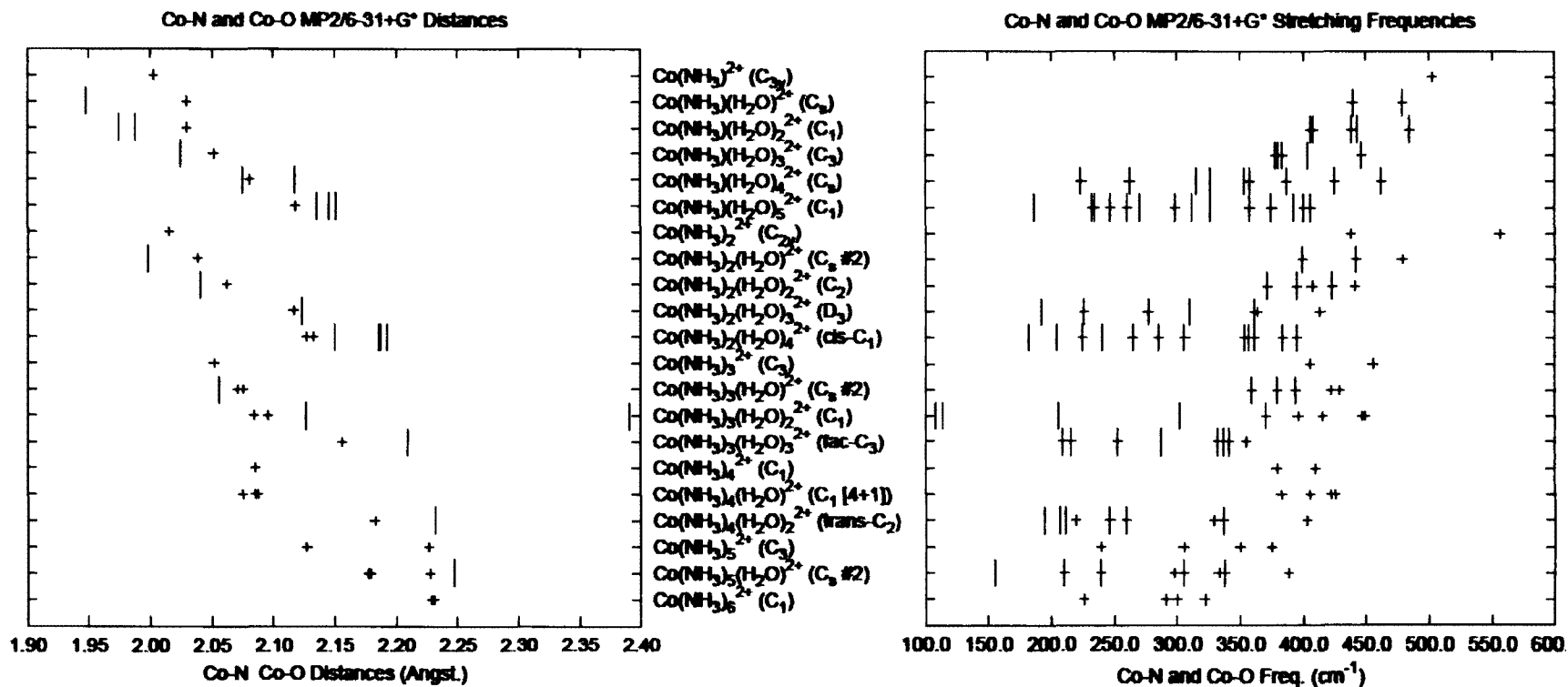


Figure 3-21: Co-N (+) and Co-O (()) bond lengths (left) and vibrational stretching frequencies (right) for $[\text{Co}(\text{NH}_3)_n(\text{H}_2\text{O})_m]^{2+}$, where $n=1-6$ and $m=0-(6-n)$, calculated at the MP2/6-31+G* level.

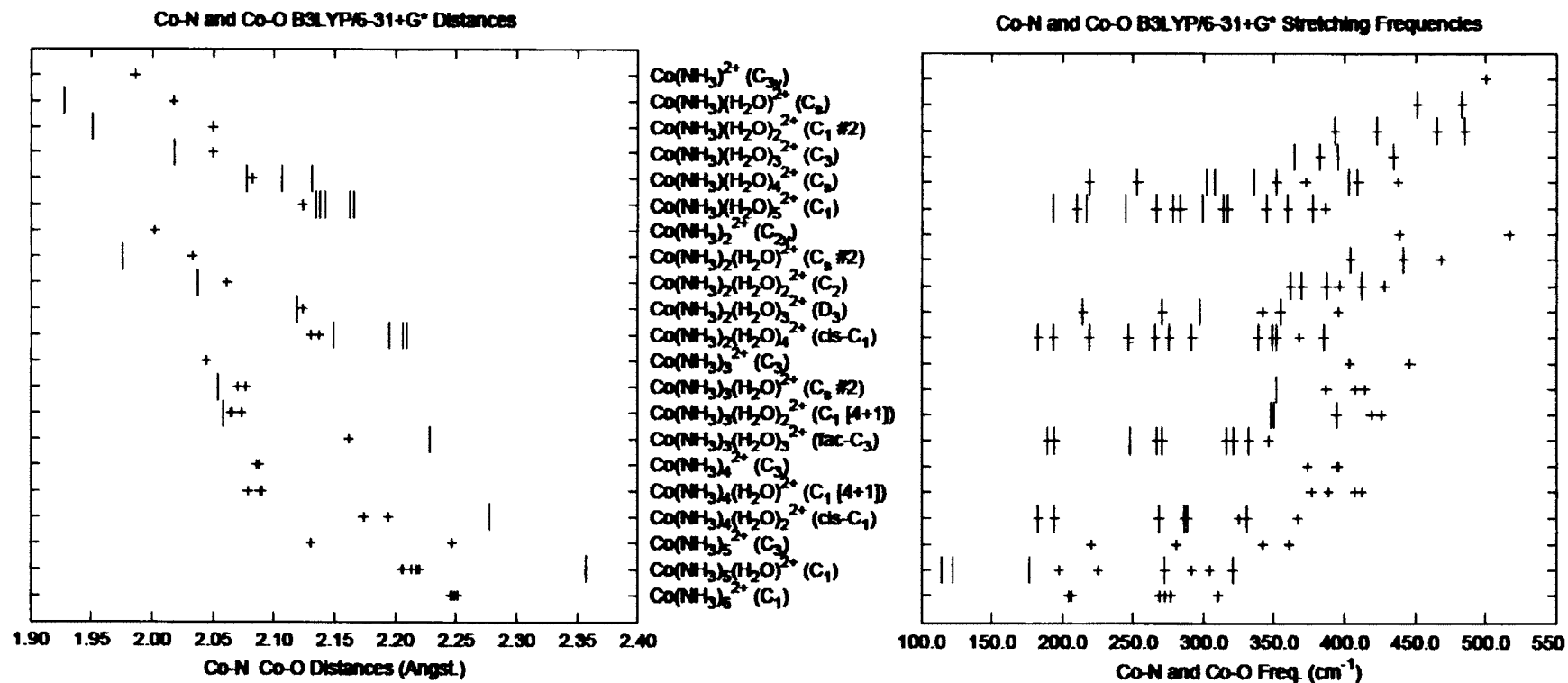


Figure 3-22: Co-N (+) and Co-O (|) bond lengths (left) and vibrational stretching frequencies (right) for $[\text{Co}(\text{NH}_3)_n(\text{H}_2\text{O})_m]^{2+}$, where $n=1-6$ and $m=0-(6-n)$, calculated at the B3LYP/6-31+G* level.

ammonia or water ligands are added to the system, the vibrational stretching frequencies associated with the given ligand are lower.

No experimental Raman data was found to compare with the polarized Raman plots that we have generated, which can be seen in Figure 3A-4 of the supplementary materials section. However, Bertin et al.¹¹⁴ have reported IR absorption frequencies of hexamminecobalt(II) complexes with halides which contain a Co-N stretch in the range of 308-318 cm^{-1} , depending on the halide. This value is very close to the values we found of 302, 322 and 310 cm^{-1} for HF, MP2 and B3LYP respectively.

4.1 Cobalt(II) Mixed-Ligand Complexes

The cobalt(II) complexes with mixed ligands were also studied. These complexes include the chlorohydroxo complexes $[\text{CoCl}_n(\text{OH})_m(\text{H}_2\text{O})_l]^{2-n-m}$, the chloroammine complexes $[\text{CoCl}_n(\text{NH}_3)_m(\text{H}_2\text{O})_l]^{2-n}$ and the hydroxoammine complexes $[\text{Co}(\text{OH})_n(\text{NH}_3)_m(\text{H}_2\text{O})_l]^{2-n}$. These sets of complexes have not been extensively studied in the literature like the single-ligand complexes. There have been specific gravity and molecular volume studies of some of the chloroammine complexes⁸⁶, specifically dichloro complexes with two, four, five and six ammonia molecules. There have also been kinetic ligand detachment studies of the monochloropentammine and dichlorotetrammine complexes¹⁰⁸. A theoretical study of metal substitution for the active site of carbonic anhydrase included a tetrahedral monohydroxotriammine complex, in which geometries and energetics were calculated⁵⁵. Two of the chlorohydroxo complexes (CoClOH and CoCl_2OH^-) were mentioned in the cobalt(II) chloride complexation study by Migdisov et al.⁷⁶ in relation to fitting the absorption spectra of the chloride complexes with these mixed-ligand complexes, but indicated that the results were not reliable. Other than the reports mentioned, the literature on mixed-ligand cobalt(II) complexes with chloride, hydroxide and ammonia seem to be scarce.

4.2 Chlorohydroxocobalt(II) Complexes, $[\text{CoCl}_n(\text{OH})_m(\text{H}_2\text{O})_l]^{2-n-m}$, where $n=1-3$, $m=1-(4-n)$, $l=0-(6-n-m)$

This set of complexes was studied up to and including the overall six-coordinate species with various combinations of chloride, hydroxide and water. All complexes have at least one chloride and one hydroxide ligand. Although they were attempted, no stable structures were found for species with a combination of chloride and hydroxide ligands greater than four. Many of these complexes tended to form ion pairs. No computational or experimental data was found in the literature therefore the discussion will be limited to comparison of the optimized structures we have found as well as bond distance and vibrational stretching frequency trends.

4.2.1 Results

Total energies have been tabulated for all successfully optimized geometries and can be seen in Table 4A.1 in the supplementary materials section for this chapter. The optimized geometries of stable structures can be seen in Figure 4-1 for chlorohydroxo and chlorodihydroxo complexes and Figure 4-2 for chlorotrihydroxo, dichlorohydroxo, dichlorodihydroxo, dichlorotrihydroxo and trichlorohydroxo complexes.

The chlorohydroxo complex, $[\text{CoCl}(\text{OH})]$, did not cause any symmetry problems as it was found to have C_s symmetry at all levels. We did not attempt a linear structure due to the realization previously, when studying hydroxide complexes, that the hydroxyl group prefers to be bent. Two different C_s structures we attempted initially for the monohydrate, $[\text{CoCl}(\text{OH})(\text{H}_2\text{O})]$, but neither were stable and the lowest energy structure ended up having C_1 symmetry at all levels. The dihydrate also ended up having C_1

symmetry at all levels. The trihydrate showed preference for a structure having one water molecule being hydrogen bonded to the rest of the molecule in a donor-acceptor fashion to a hydroxide and water ligand respectively. The tetrahydrate presented a similar result, except now two water molecules are hydrogen bonded to the central molecule.

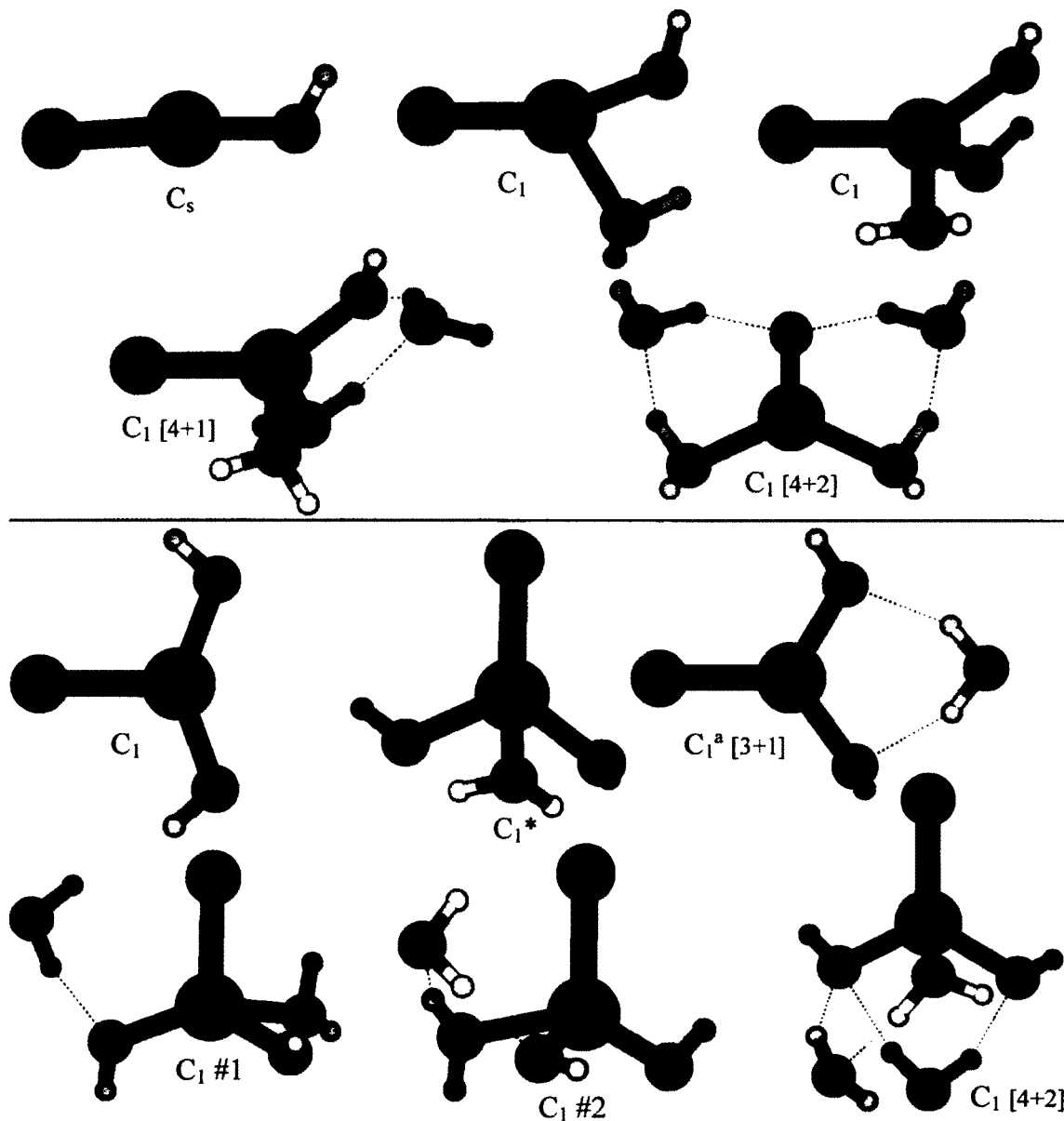


Figure 4-1: Optimized MP2 and B3LYP geometries for $[\text{CoCl}(\text{OH})_m(\text{H}_2\text{O})_l]^{1-m}$, where $m=1-2$, $l=0-(5-m)$. “*” indicates only stable at MP2, “^a” indicates only stable at B3LYP.

The next set of complexes studied were the chlorodihydroxo species, $[\text{CoCl}(\text{OH})_2]^-$. Initially two different C_{2v} structures were attempted, but neither of these structures was stable at MP2 and B3LYP. One C_{2v} structure, with the hydroxides angled towards the chloride, was stable at HF. One C_s structure, which appears to be very similar to the C_{2v} structure, was found to be stable at the MP2 level. Overall, a C_1 geometry was found (very similar to the C_{2v} geometry) that was lowest in energy at all levels. There were a few different geometries attempted for the monohydrate species, including three different C_{2v} geometries, two different C_s geometries and a C_1 geometry. One of the C_s geometries was stable at both HF and MP2. However, the C_1 geometry was found to be more stable for the MP2 level. The only stable geometry found for B3LYP was the C_1 , except, unlike the HF and MP2 levels, the B3LYP structure was found to have the water molecule dissociated from the cobalt center and hydrogen bonded, in a donor-donor fashion, to both the hydroxide ligands. There was agreement among levels that the dihydrate has C_1 symmetry, with one water molecule being hydrogen bonded. Two different C_1 structures were found, both of them having a hydrogen bonded water molecule, with the difference being the position of the hydrogen bonded water molecule. The second C_1 structure that was calculated was the lowest in energy at all levels. Five different C_s geometries were attempted for the trihydrate, but none of them were stable at any level. A C_1 geometry was attempted based on the lowest energy C_s geometry which gave a stable geometry at each level. None of the structures had all ligands completely bound to the central cobalt atom. At all levels the stable C_1 geometry has two water molecules hydrogen bonded to the central complex.

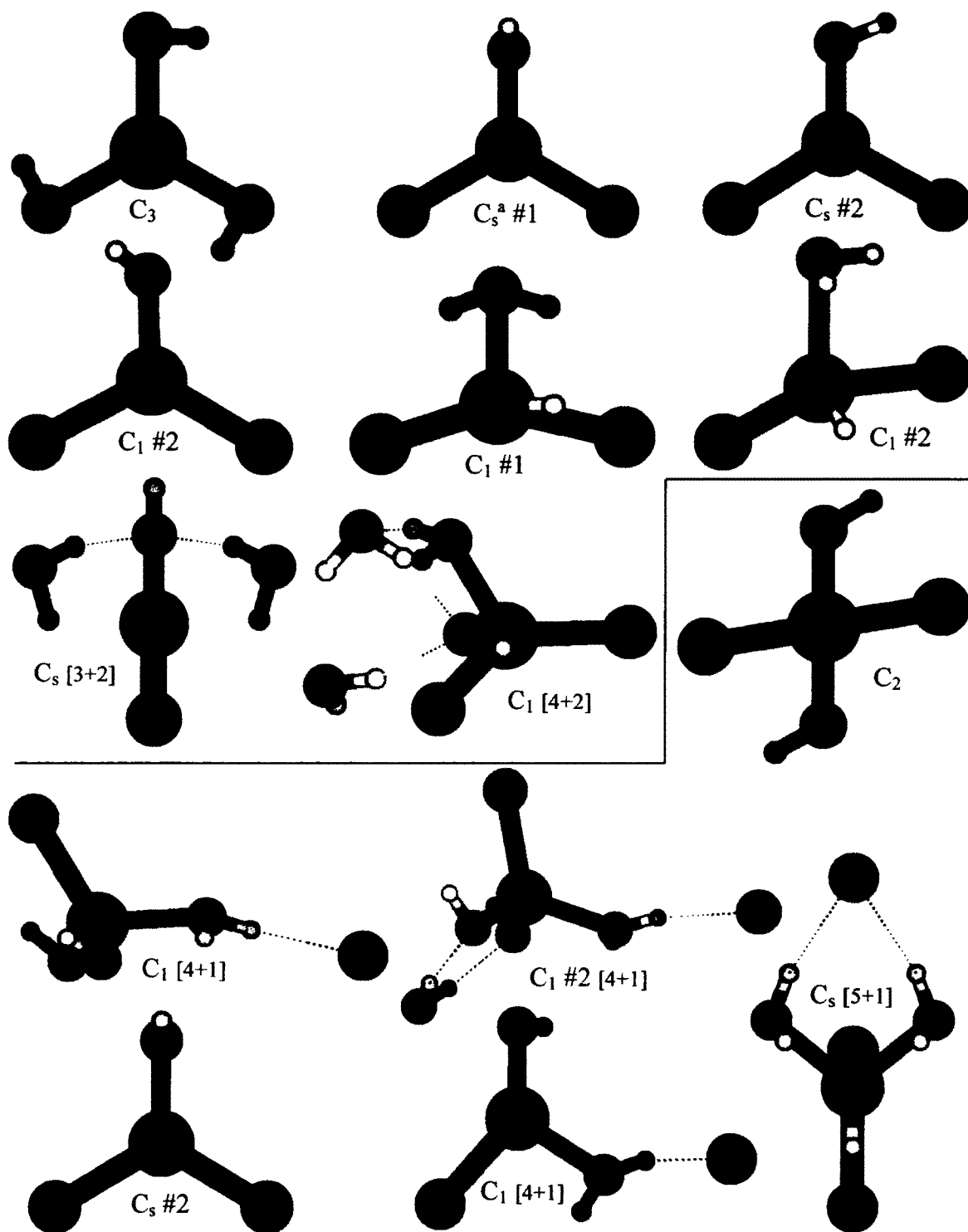


Figure 4-2: Optimized MP2 and B3LYP geometries for $[\text{CoCl}_n(\text{OH})_m(\text{H}_2\text{O})]^{1-n-m}$, where $n=1-3$, $m=1-3$, $l=0-(6-n-m)$.

The anhydrous chlorotrihydroxo complex, $[\text{CoCl}(\text{OH})_3]^{2-}$, showed its highest stability in a C_3 symmetrical geometry for all levels. When water molecules were added to this system, chloride ions dissociated and we were left with an ion pair. No optimized geometries were found for any of these hydrated species and therefore no stable geometries were available to report.

A couple of different stable geometries were found for the anhydrous dichlorohydroxo complexes, $[\text{CoCl}_2(\text{OH})]^-$. Two different C_s geometries were attempted, with both of them being stable at B3LYP and only C_s #2 (planar) being stable at HF and MP2. The most stable structure for this complex was dependent on the level of theory used. The preferred geometry for HF was a C_1 structure that is very similar to the planar C_s geometry, MP2 was most stable with the planar C_s geometry and B3LYP preferred the bisected C_s geometry. Two different C_1 (the first almost planar, the second with the hydroxide pointing outward) geometries were found for the monohydrate. Ultimately all levels preferred the second C_1 structure over the first. The dihydrate was found to be stable with C_s symmetry at all levels. The only difference among the levels for the dihydrate is that MP2 and B3LYP prefer the water molecules to be hydrogen bonded to the anhydrous center. Only a C_1 geometry, with two hydrogen bonded water molecules, was found to be stable at all levels for the trihydrate.

The anhydrous dichlorodihydroxo complex, $[\text{CoCl}_2(\text{OH})_2]^{2-}$, preferred C_2 symmetry at all levels after initially attempting two different C_{2v} structures. All geometries that were calculated for the monohydrate formed ion pairs as chloride ions dissociated from the rest of the molecule. Stable structures were found, with a C_s

structure having the lowest energy at the HF level and a C_1 structure being preferred by MP2 and B3LYP. Both of these structures have one chloride ion being hydrogen bonded to the water molecule. Similar to the monohydrate, all structures found for the dihydrate became ion pairs when optimized. A stable C_s geometry was found for MP2 with the two water molecules dissociated and hydrogen bonded to one of the hydroxide ligands and a chloride ligand also dissociated and hydrogen bonded to the two water molecules. The most stable structure found for this complex has C_1 symmetry with one water molecule and one chloride ligand dissociated and hydrogen bonded to the central molecule.

The anhydrous trichlorohydroxo complex, $[\text{CoCl}_3(\text{OH})]^{2-}$, was found to be stable with C_s symmetry at all levels. There was agreement among levels that the most stable structure for the monohydrate has C_1 symmetry (ion pair with a hydrogen bonded chloride). The dihydrate also was most stable as an ion pair (hydrogen bonded chloride) with C_1 symmetry at all levels.

These results have been summarized in Table 4.1. Only the stable geometries are included, with the energy minimum for each complex highlighted in yellow. The formation of ion pairs is indicated by the "IP" after the point group symmetry label. Coordination number of the Co(II) center is represented by the first number in the brackets. The labels without brackets indicate the coordination number is equal to the number of ligands.

Table 4.1: Stable Geometries of $[\text{CoCl}_n(\text{OH})_m(\text{H}_2\text{O})_l]^{2-n-m}$, with lowest energy symmetries highlighted in yellow.

n	m	l	Stable Geometries		
1	1	0	C_s	C_s	C_s
1	1	1	C_1	C_1	C_1
1	1	2	C_1	C_1	C_1
1	1	3	$C_1 [4+1]$	$C_1 [4+1]$	$C_1 [4+1]$
1	1	4	$C_1 [4+2]$	$C_1 [4+2]$	$C_1 [4+2]$
1	2	0	$C_{2v} \#2, C_1$	C_s, C_1	C_1
1	2	1	$C_s \#1, C_1$	$C_s \#1, C_1$	$C_1 [3+1]$
1	2	2	$C_s \#2, C_1 \#1 [4+1],$ $C_1 \#2 [4+1]$	$C_s \#1 [3+2], C_1 \#1$ $[4+1], C_1 \#2 [4+1]$	$C_1 \#1 [4+1],$ $C_1 \#2 [4+1]$
1	2	3	$C_1 [4+2]$	$C_1 [4+2]$	$C_1 [4+2]$
1	3	0	C_3, C_1	C_3, C_1	C_3, C_1
2	1	0	$C_s \#2, C_1 \#1, C_1 \#2$	$C_s \#2, C_1 \#1, C_1 \#2$	$C_s \#1, C_s \#2,$ $C_1 \#1, C_1 \#2$
2	1	1	$C_1 \#1, C_1 \#2$	$C_1 \#1, C_1 \#2$	$C_1 \#1, C_1 \#2$
2	1	2	C_s	$C_s [3+2]$	$C_s [3+2]$
2	1	3	$C_1 [4+2]$	$C_1 [4+2]$	$C_1 [4+2]$
2	2	0	C_2	C_2	C_2
2	2	1	$C_s \#2 [4+1] \text{ IP},$ $C_1 [4+1] \text{ IP}$	$C_s \#2 [4+1] \text{ IP},$ $C_1 [4+1] \text{ IP}$	$C_1 [4+1] \text{ IP}$
2	2	2	$C_1 \#2 [4+2] \text{ IP}$	$C_s \#1 [3+3] \text{ IP},$ $C_1 \#2 [4+2] \text{ IP}$	$C_1 \#2 [4+2] \text{ IP}$
3	1	0	$C_s \#2$	$C_s \#2$	$C_s \#2$
3	1	1	$C_1 [4+1] \text{ IP}$	$C_1 [4+1] \text{ IP}$	$C_1 [4+1] \text{ IP}$
3	1	2	$C_s [5+1] \text{ IP}$	$C_s [5+1] \text{ IP}$	$C_s [5+1] \text{ IP}$

4.2.2 Discussion/Literature Comparison

No data was found in the literature to compare our stable geometries with. Therefore we can neither confirm nor deny that our structures are viable with respect to experimentation or other computational methods. We can however comment on the trends observed within the bond length and vibrational stretching frequency plots constructed at each of the three levels of theory. Within the bond length figures there is a general trend of increasing Co-O and Co-Cl bond distance as more water molecules are

added to the system. However, when there are ion pairs, shown by the small cluster of Co-Cl bond lengths greater than 4Å, the trend is reversed. This could be caused by the dissociated chloride anion hydrogen bonding to the central complex, thereby stabilizing the structure, resulting in shorter bond distances. There is also a cluster of Co-O bond distances at approximately 3.5Å, which is a result of water molecules dissociating and forming hydrogen bonds to the central complex. These trends are found with all three levels of theory. As mentioned in previous sections, when the bond lengths increase, the vibrational stretching frequencies associated with those bonds decrease. As the bond length trend reverses, the stretching frequency trend also changes. This trend with respect to the frequencies is also found with all levels of theory.

Since our results are going to be primarily used to compare with experimental Raman data gathered by our colleagues at the University of Guelph, we have constructed Raman spectra based on the Raman intensities calculated at the HF/6-31+G* level of theory. These plots will be beneficial in the assignment of the experimental Raman bands. These plots are located in Figure 4A-1 of the appendix for Chapter 4.

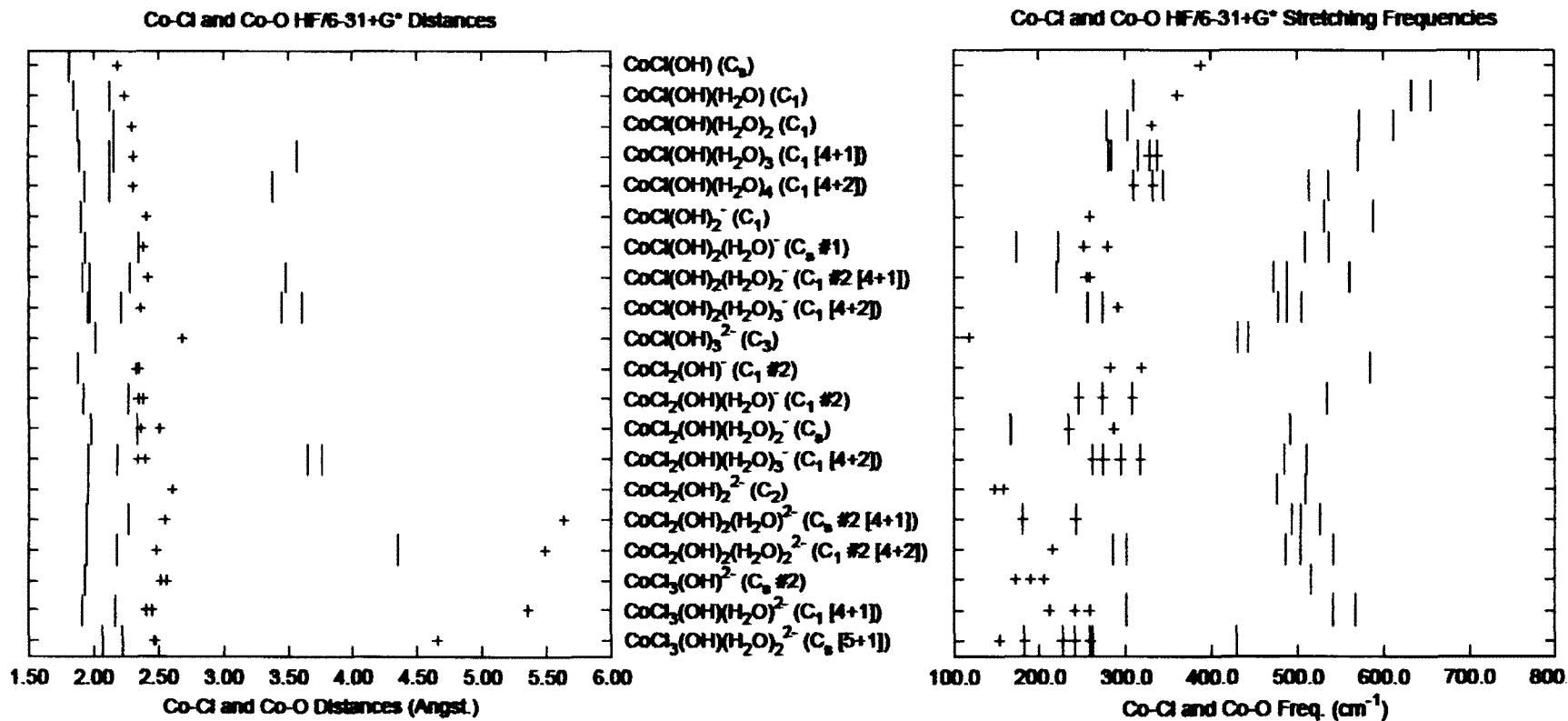


Figure 4-3: Co-Cl (+) and Co-O (l) bond lengths (left) and vibrational stretching frequencies (right) for $[\text{CoCl}_n(\text{OH})_m(\text{H}_2\text{O})_l]^{2-n-m}$, where $n=1-3$, $m=1-(4-n)$ and $l=0-(6-n-m)$, calculated at the HF/6-31+G* level.

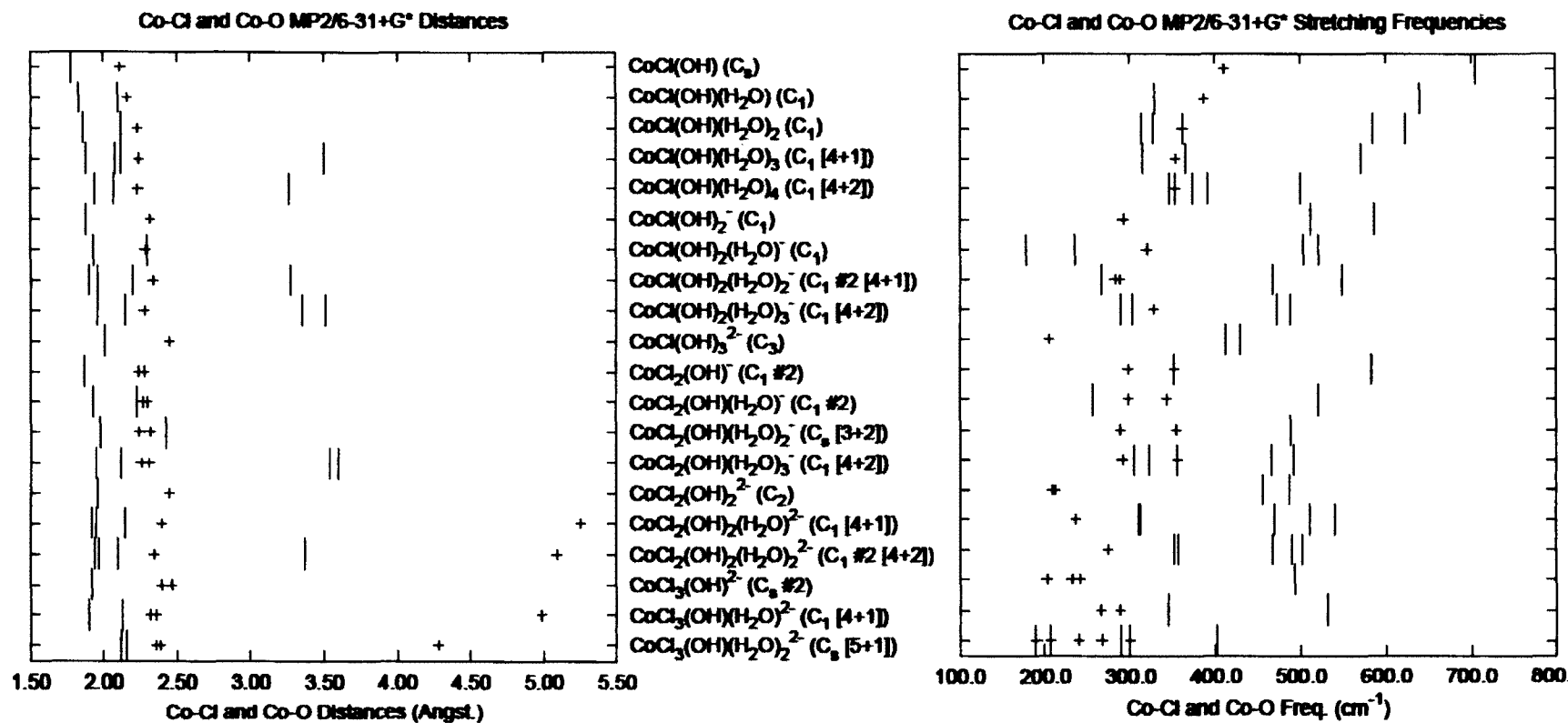


Figure 4-4: Co-Cl (+) and Co-O (l) bond lengths (left) and vibrational stretching frequencies (right) for $[\text{CoCl}_n(\text{OH})_m(\text{H}_2\text{O})_l]^{2-n-m}$, where $n=1-3$, $m=1-(4-n)$ and $l=0-(6-n-m)$, calculated at the MP2/6-31+G* level.

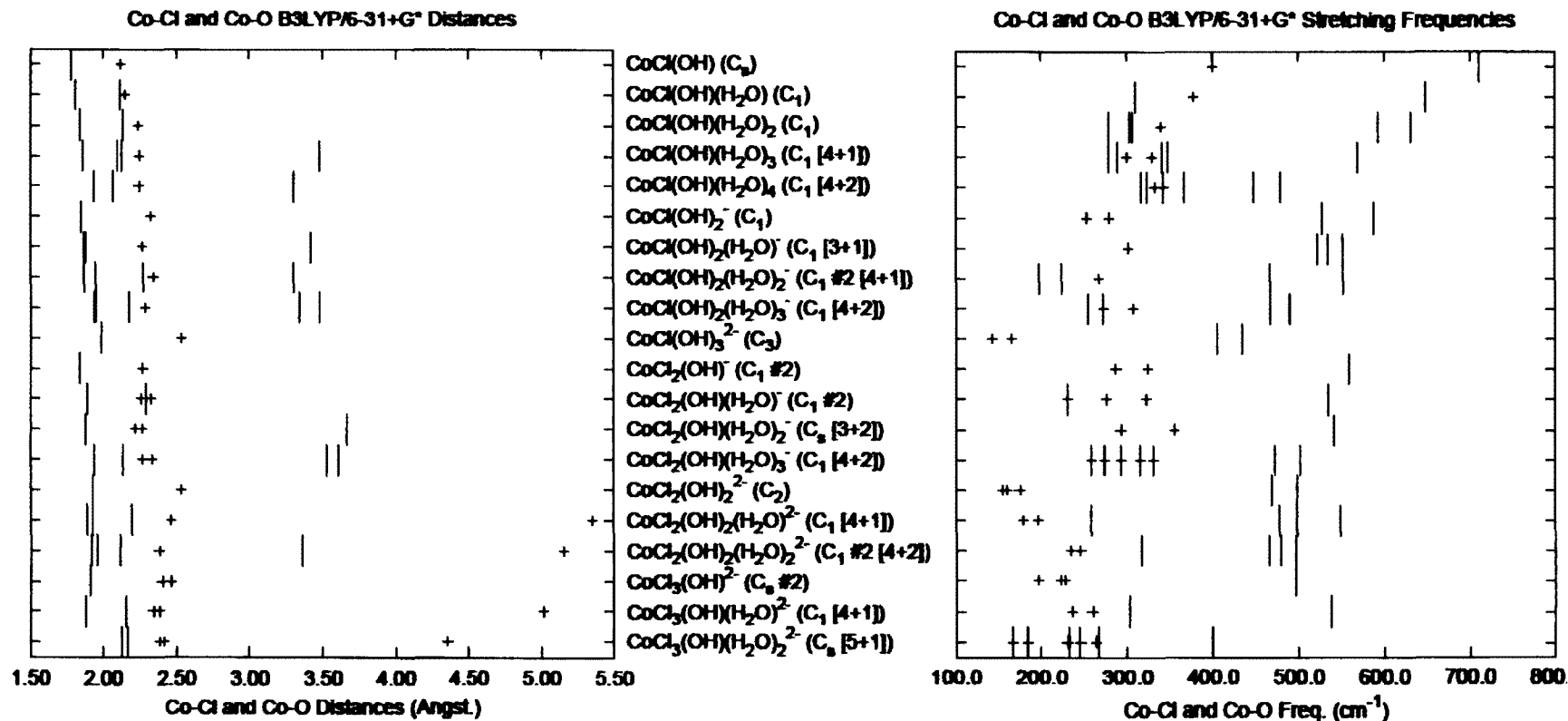


Figure 4-5: Co-Cl (+) and Co-O (|) bond lengths (left) and vibrational stretching frequencies (right) for $[\text{CoCl}_n(\text{OH})_m(\text{H}_2\text{O})_l]^{2-n-m}$, where $n=1-3$, $m=1-(4-n)$ and $l=0-(6-n-m)$, calculated at the B3LYP/6-31+G* level.

4.3 Chloroamminecobalt(II) Complexes, $[\text{CoCl}_n(\text{NH}_3)_m(\text{H}_2\text{O})_l]^{2-n}$, where $n=1-4$, $m=1-(6-n)$, $l=0-(6-n-m)$

This set of complexes was studied up to and including the six-coordinate complexes with various combinations of chloride, ammonia and water ligands. Every complex has at least one chloride and one ammonia ligand. No stable structure was found for the pentachloro monoammine complex. Stable structures were found for all of the other combinations, although a few of them were not stable as completely bound structures as they preferred to have hydrogen bonded water or ammonia ligands and in a couple of cases an ion pair was preferred. Although a couple of experimental studies have been completed, no literature data was found regarding bond length or vibrational frequency data for this set of complexes. Therefore, the discussion of the chloroammine species will be restricted to our findings regarding geometries, bond length and vibrational stretching frequency trends.

4.3.1 Results

Total energies have been collected and tabulated for all optimized geometries attempted, whether stable or not (shaded numbers indicate instability), and can be found in Table 4A.7 of the supplementary materials section for Chapter 4. The optimized MP2 and B3LYP geometries for the stable structures can be seen in Figure 4-6 for all monochloroammine complexes, Figure 4-7 for the dichloroammine complexes and Figure 4-8 for the trichloroammine and tetrachloroammine complexes. Due to the large number of stable geometries found for this set of complexes, the minimum energy structures are listed in Table 4.2. The lowest energy (most stable) structures are

Table 4.2: Stable Geometries of $[\text{CoCl}_n(\text{NH}_3)_m(\text{H}_2\text{O})_l]^{2-n}$, with lowest energy point group symmetries highlighted in yellow.

n	m	l	Stable Geometries		
1	1	0	C_{3v}	C_{3v}	C_{3v}
1	1	1	C_1	C_1	C_1
1	1	2	$C_s \#1, C_s \#2, C_1$	$C_s \#2, C_1$	C_1
1	1	3	C_s	C_s	C_s
1	1	4	C_1	C_1	C_1
1	2	0	$C_s, C_1 \#1$	$C_{2v} \#1, C_s, C_1 \#1$	$C_{2v} \#1, C_1 \#2$
1	2	1	$C_s \#2$	$C_s \#2$	$C_1 \#2$
1	2	2	$C_1 [4+1]$	$C_1 [4+1]$	$C_1 [4+1]$
1	2	3	C_2	C_2	C_2
1	3	0	$C_{3v} \#2$	$C_{3v} \#2$	$C_{3v} \#2, C_3$
1	3	1	C_s, C_1	C_1	$C_1 [4+1]$
1	3	2	C_1	C_1	C_1
1	4	0	C_{2v}, C_1	C_{2v}, C_1	C_{2v}, C_1
1	4	1	C_1	C_2, C_1	$C_2, C_s \#2, C_1$
1	5	0	C_1	C_1	C_1
2	1	0	$C_s \#1, C_1$	$C_s \#1, C_1$	$C_s \#2, C_1$
2	1	1	$C_s \#3, C_1 \#1$	$C_1 \#1$	$C_1 \#1, C_1 \#2$
2	1	2	$C_s \#1, C_1$	$C_s \#2, C_1$	$C_s \#2, C_1 [4+1]$
2	1	3	C_1	C_1	C_1
2	2	0	$C_{2v} \#2$	$C_{2v} \#1$	C_1
2	2	1	C_1	C_1	$C_1 [4+1]$
2	2	2	$C_i, C_1 \#1, C_1 \#2$	$C_s, C_i, C_1 \#1, C_1 \#2$	$C_i, C_1 \#1, C_1 \#2$
2	3	0	C_{3v}, C_3	C_{3v}, C_3	C_{3v}, C_3
2	3	1	C_1	C_1	C_1
2	4	0	$C_1 \#1, C_1 \#2$	$C_2, C_1 \#1, C_1 \#2$	$C_2, C_1 \#1, C_1 \#2$
3	1	0	$C_{3v} \#2$	$C_{3v} \#2$	$C_{3v} \#2$
3	1	1	$C_s \#2, C_s \#7 [4+1], C_1 [4+1]$	$C_s \#2, C_s \#3, C_s \#7 [4+1], C_1 [4+1]$	$C_s \#2, C_s \#7 [4+1], C_1 [4+1]$
3	1	2	$C_s \#1 [5+1]$	$C_s \#1 [5+1]$	$C_s \#1 [5+1]$
3	2	0	$D_{3h} \#1$	$D_{3h} \#1$	$D_{3h} \#1$
3	2	1	$C_1 [5+1] \text{ IP}$	$C_1 [5+1] \text{ IP}$	$C_1 [5+1] \text{ IP}$
3	3	0	$C_{3v} \#1, C_3 \#1, C_3 \#2$	$C_3 \#2$	$C_{3v} \#1, C_3 \#1, C_3 \#2$
4	1	0	$C_{3v} \#2, C_3$	$C_{3v} \#2, C_3$	$C_{3v} \#1, C_{3v} \#2, C_3$
4	1	1	$C_1 [5+1] \text{ IP}$	$C_1 [5+1] \text{ IP}$	$C_1 [5+1] \text{ IP}$
4	2	0	$C_1 [4+2] \text{ IP}$	$C_1 [4+2] \text{ IP}$	$C_1 [4+2] \text{ IP}$

highlighted in yellow. Other structures, that may have higher symmetry, have been attempted for most complexes, but contained imaginary frequencies indicating that they are not stable species. These geometries are tabulated in the supplementary materials section. The formation of ion pairs is indicated by the “IP” after the point group symmetry label.

4.3.2 Discussion/Literature Comparison

The easiest way to confirm if our calculated geometries are viable is to compare our structures with those in the literature. Specific gravity and molecular volume studies by Clark et al.⁸⁶ include the dichloroammine complexes and kinetic ligand detachment studies by Lilie et al.¹⁰⁸ include the monochloropentammine and dichlorotetrammine complexes, but no structural data was given. No structural information was found in the literature for the chloroammine complexes, therefore there is no data to compare with what we have found. However, we do have trends within our bond length and vibrational frequency plots that need to be discussed.

Within the bond distance plots three different symbols are used, +, x and |, to distinguish between the Co-N, Co-Cl and Co-O bond lengths respectively. Each of these has a trend of increasing bond length, for a given complex, when more water molecules are added to the system. The trends become less clear when there are more chloride ligands. With more chloride ligands there is a greater tendency for water and chloride ligand dissociation and subsequent hydrogen bonding to the central molecule. The effect is usually a small increase in stabilization (decrease in total energy) of the central

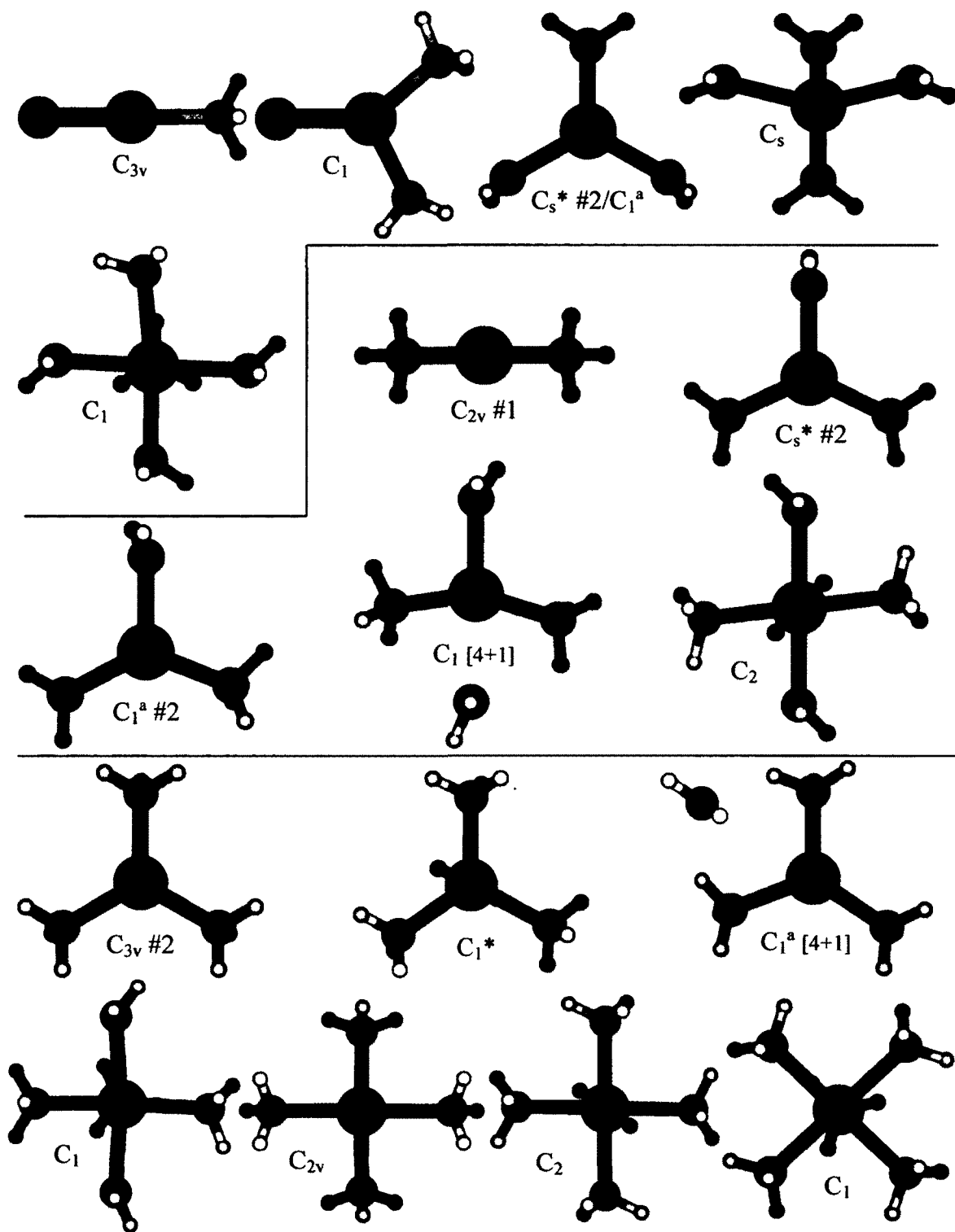


Figure 4-6: Optimized MP2 and B3LYP geometries for $[\text{CoCl}(\text{NH}_3)_m(\text{H}_2\text{O})_l]^+$, where $m=1-5$, $l=0-(5-m)$. “*” indicates only stable at MP2, “^a” indicates only stable at B3LYP.

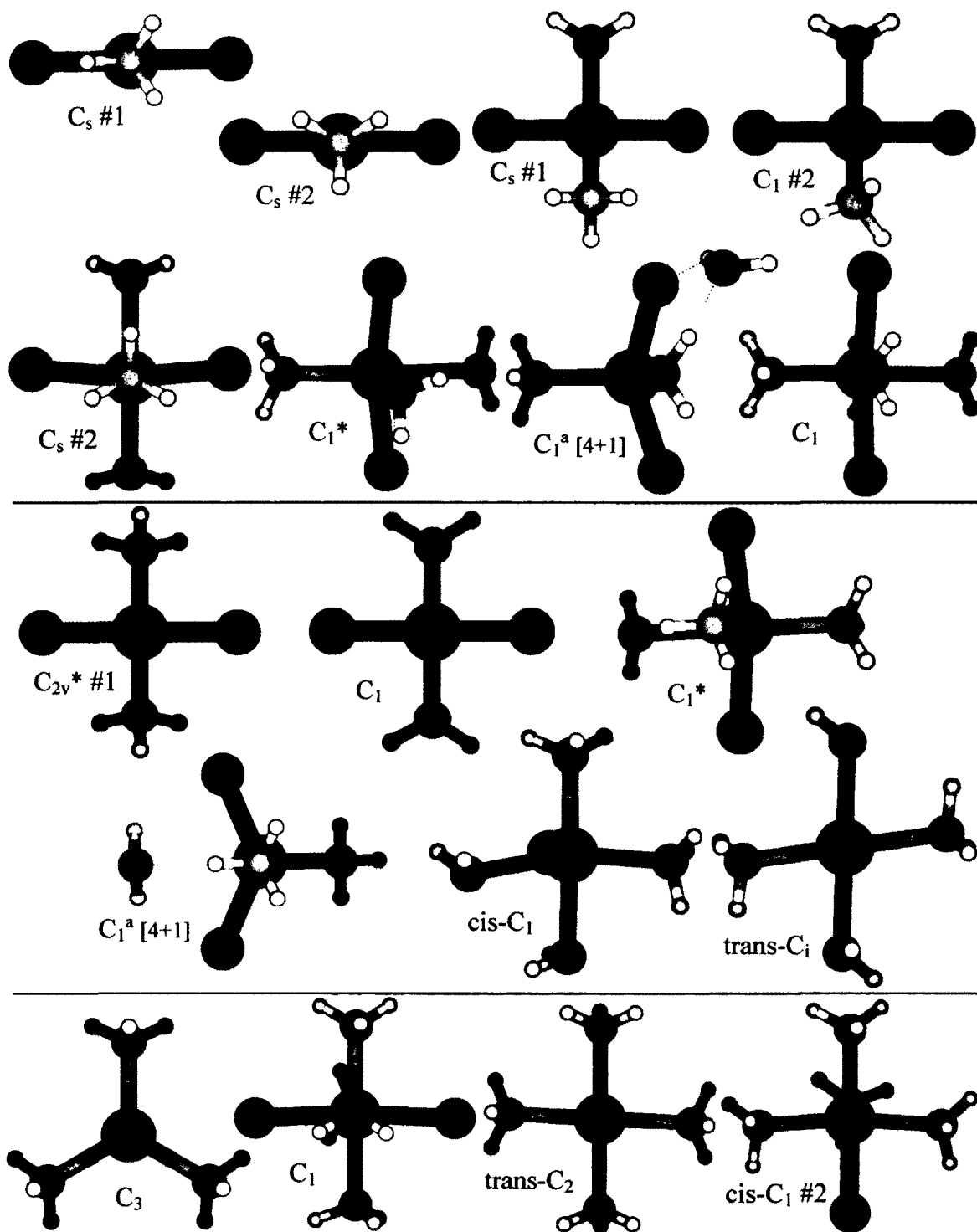


Figure 4-7: Optimized MP2 and B3LYP geometries for $[\text{CoCl}_2(\text{NH}_3)_m(\text{H}_2\text{O})_l]$, where $m=1-4$, $l=0-(4-m)$. “*” indicates only stable at MP2, “^a” indicates only stable at B3LYP.

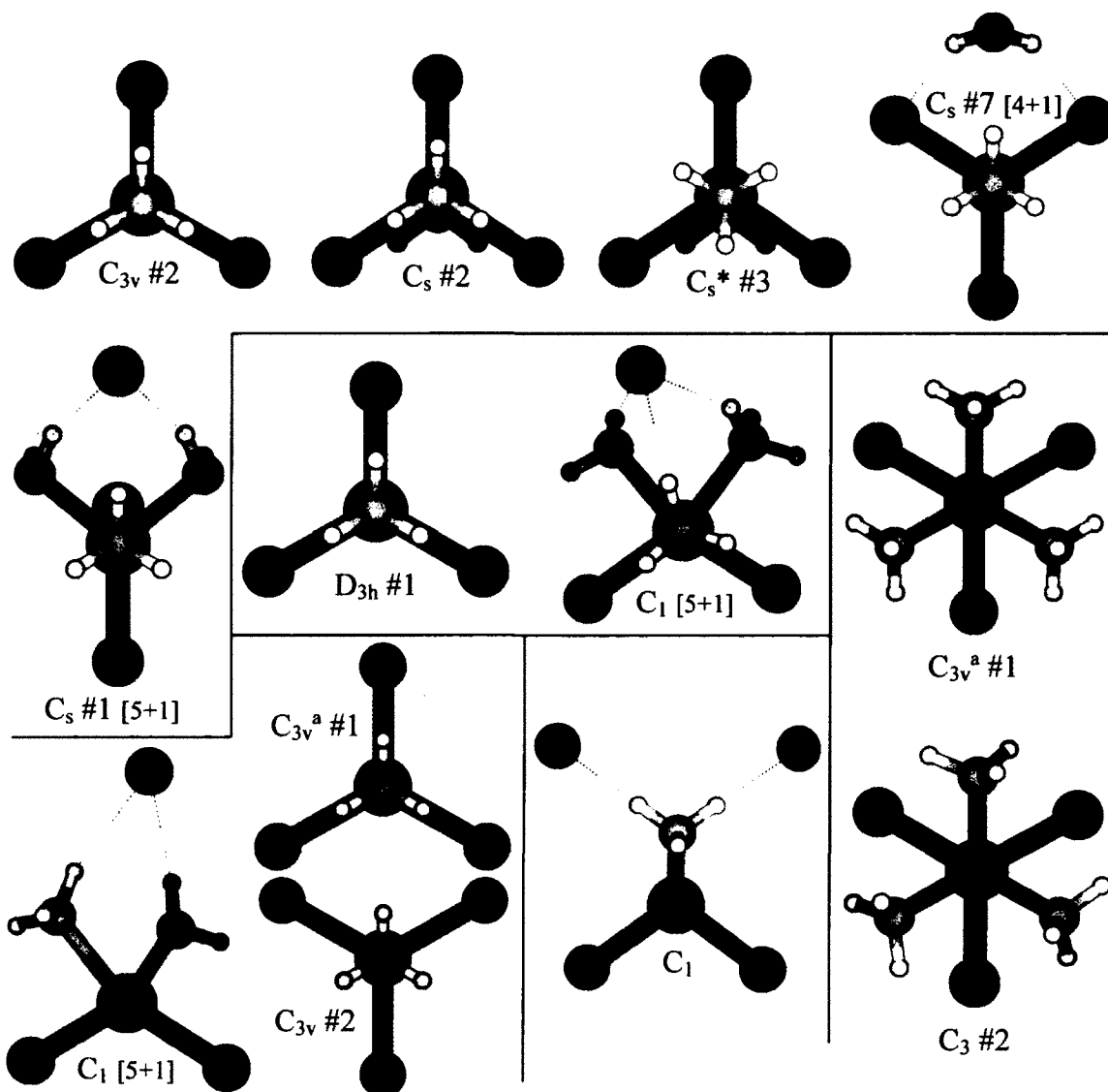


Figure 4-8: Optimized MP2 and B3LYP geometries for $[\text{CoCl}_n(\text{NH}_3)_m(\text{H}_2\text{O})_l]$, where $n=3-4$, $m=1-(6-n)$, $l=0-(6-n-m)$. “*” indicates only stable at MP2, “a” indicates only stable at B3LYP.

molecule, thereby resulting in slightly shorter bond lengths. Something to note regarding the bond distance plots is that the bond lengths of dissociated ligands were not included. This allowed for the rest of the graph to be spread out so that the trends could be easily identified. Once again the inverse relationship between bond distance and stretching

frequency is observed. A lot of the stretches were mixes of two or more of the Co-Cl, Co-N and Co-O stretches as suggested by the overlap of the characteristic symbols.

Once again, calculated Raman spectra were constructed based on the intensities calculated at the HF level. We were not able to compare with any experimental results, but these will be useful for future work that will be completed by our colleagues.

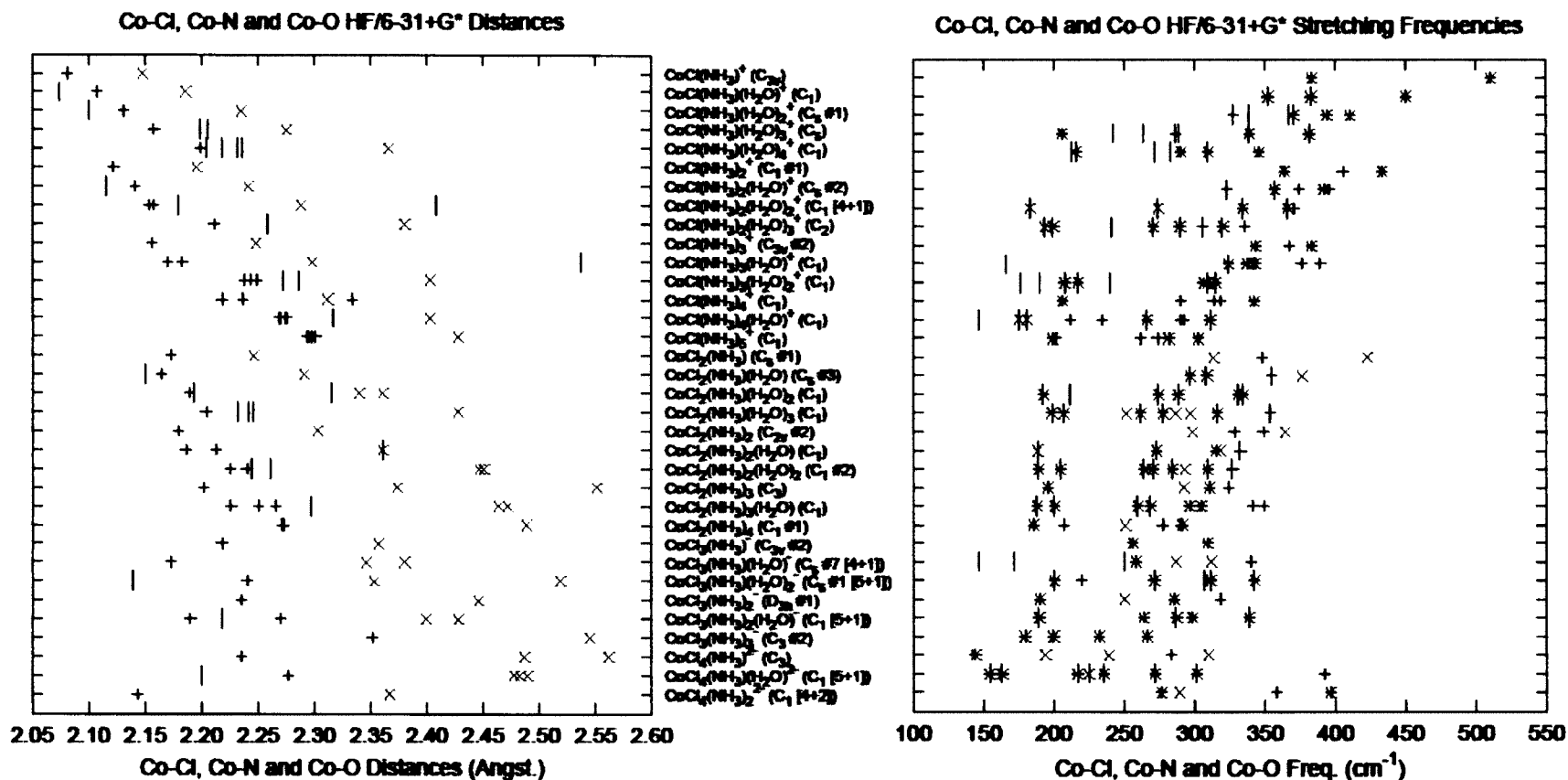


Figure 4-9: Co-Cl (+), Co-N (x) and Co-O (|) bond lengths (left) and vibrational stretching frequencies (right) for $[\text{CoCl}_n(\text{NH}_3)_m(\text{H}_2\text{O})_l]^{2-n-m}$, where $n=1-4$, $m=1-(6-n)$ and $l=0-(6-n-m)$, calculated at the HF/6-31+G* level.

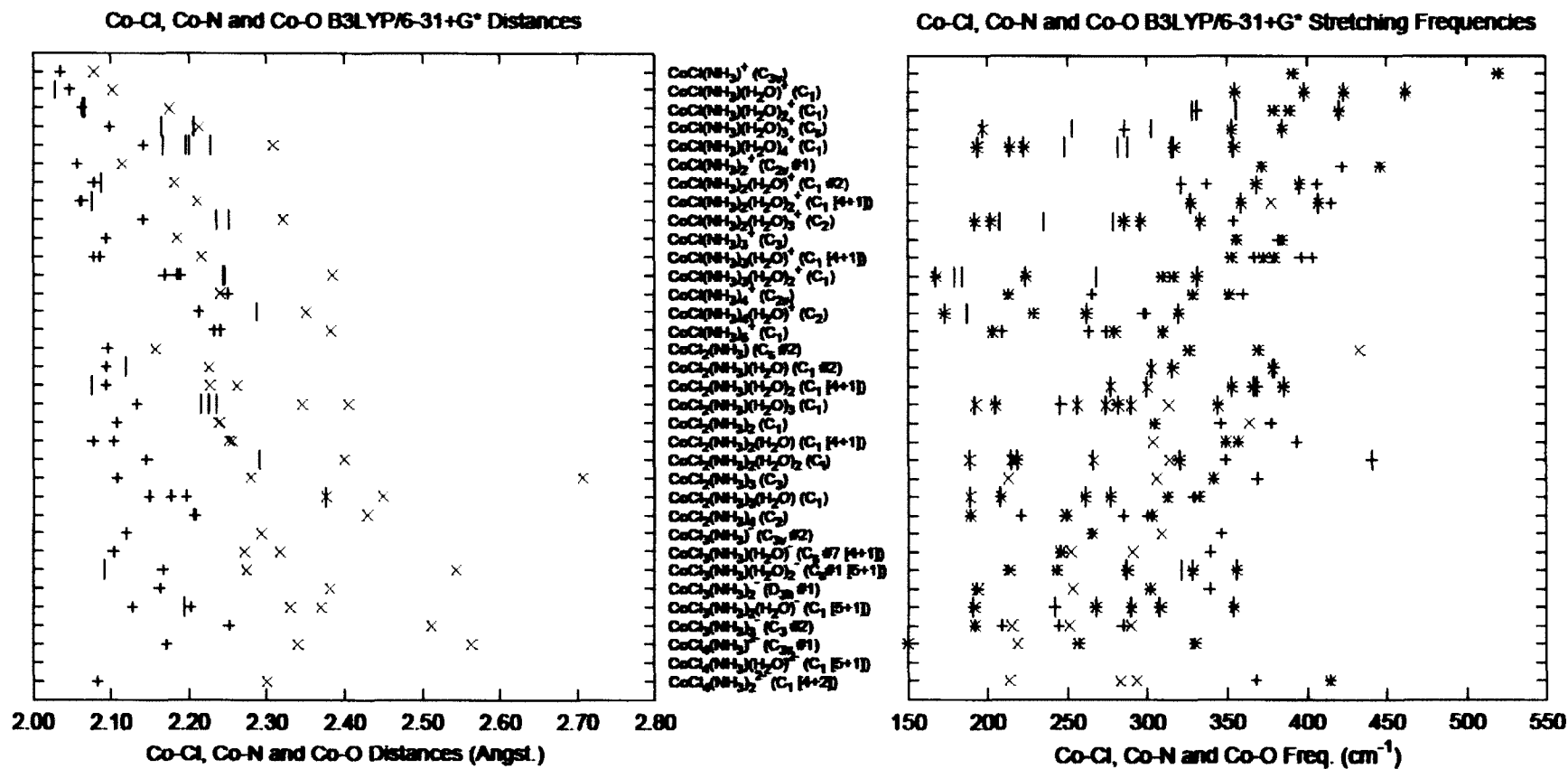


Figure 4-11: Co-Cl (+), Co-N (x) and Co-O (|) bond lengths (left) and vibrational stretching frequencies (right) for $[\text{CoCl}_n(\text{NH}_3)_m(\text{H}_2\text{O})_l]^{2-n-m}$, where $n=1-4$, $m=1-(6-n)$ and $l=0-(6-n-m)$, calculated at the B3LYP/6-31+G* level.

4.4 Hydroxoamminecobalt(II) Complexes, $[\text{Co}(\text{NH}_3)_n(\text{OH})_m(\text{H}_2\text{O})_l]^{2-m}$, where $n=1-5$, $m=1-(5-n)$, $l=0-(6-n-m)$

The hydroxoammine complexes were studied up to and including all the combinations of hexacoordinate complexes. Each molecule investigated has at least one hydroxide ligand and one ammonia ligand. Stable structures were found for all combinations of ligands with four or less hydroxide ligands. When there are more than four hydroxide ligands, there is a lot of ligand dissociation. Some of the complexes do not have a completely bound set of ligands as hydrogen bonding is sometimes more energetically favored. Very few studies were found in the literature that contained hydroxoammine complexes. Therefore, our discussion will be restricted to what we have found regarding geometries, bond length trends and vibrational frequency trends.

4.4.1 Results

The total molecular energies for all optimized structures were tabulated in Table 4A.13 of the Chapter 4 supplementary materials. The stable MP2 and B3LYP structures are in Figure 4-12 for the hydroxomonoammine complexes, Figure 4-13 for the hydroxodiammine complexes and Figure 4-14 for the remaining complexes.

The point group symmetries for the stable complexes have been recorded in Table 4.3. The energy minimum structure for each species is highlighted in yellow. Other symmetrical geometries may have been calculated, but were not stable, and are located in Table 4A.13 of the Chapter 4 appendix. No ion pair formation was seen with this set of complexes, therefore any dissociation (indicated by the brackets) seen is attributed to either water or ammonia ligands (both neutral).

Table 4.3: Stable Geometries of $[\text{Co}(\text{NH}_3)_n(\text{OH})_m(\text{H}_2\text{O})_l]^{2-m}$, with point group of the lowest energy geometry highlighted in yellow.

n	m	l	Stable Geometries		
1	1	0	C_s #2	C_s #2	C_s #2
1	1	1	C_1	C_s, C_1	C_1
1	1	2	C_s, C_1	C_1	C_1
1	1	3	C_1 #1 [4+1], C_1 #2	C_1 #1 [4+1], C_1 #2	C_1 #1 [4+1], C_1 #2
1	1	4	C_1	C_1	C_1
1	2	0	C_1	C_1	C_1
1	2	1	C_1	C_1	C_1
1	2	2	C_1 [4+1]	C_s #2 [3+2], C_1 [4+1]	C_1 [4+1]
1	2	3	C_1 [4+2]	C_1 [4+2]	C_1 [4+2]
1	3	0	C_1	C_1	C_1
1	3	1	C_1 [4+1]	C_1 [4+1]	C_1 [4+1]
1	3	2	C_1 [4+2]	C_1 [4+2]	C_1 [4+2]
1	4	0	C_1 [4+1]	C_1 [4+1]	C_1 [4+1]
1	4	1	C_1 [4+2]	C_1 [4+2]	C_1 [4+2]
2	1	0	C_1	C_1	C_s, C_1
2	1	1	C_1	C_1	C_1
2	1	2	C_1 [4+1]	C_1 [4+1]	C_1 [4+1]
2	1	3	C_1	C_1	C_1
2	2	0	C_2, C_1	C_2, C_1	C_2, C_1
2	2	1	C_1 [4+1]	C_1 [4+1]	C_1 [4+1]
2	2	2	C_i, C_1	C_i, C_1	C_i [4+2], C_1 [5+1]
2	3	0	C_1 [4+1]	C_1 [4+1]	C_1 [4+1]
2	3	1	C_1 [4+2]	C_1 [4+2]	C_1 [4+2]
2	4	0	C_1 [4+2]	C_1 [4+2]	C_1 [4+2]
3	1	0	C_1	C_1	C_1
3	1	1	C_1 [4+1]	C_s, C_1 [4+1]	C_1 [4+1]
3	1	2	C_1 #1, C_1 #2 [4+2]	C_s #1 [4+2], C_1 #1, C_1 #2 [4+2]	C_s #1 [4+2], C_1 #1, C_1 #2 [4+2]
3	2	0	C_1 [4+1]	C_1 [4+1]	C_1 [4+1]
3	2	1	C_1 [5+1]	C_1 [5+1]	C_1 [5+1]
3	3	0	C_3 [3+3]	C_3 [3+3]	C_3 [3+3]
4	1	0	C_1 #1, C_1 #2	C_1 #1, C_1 #2	C_1 #1, C_1 #2
4	1	1	C_1	C_1	C_1
4	2	0	C_i, C_1	C_i, C_s, C_1	C_i, C_1
5	1	0	C_s #2, C_1	C_s #1, C_1	C_1

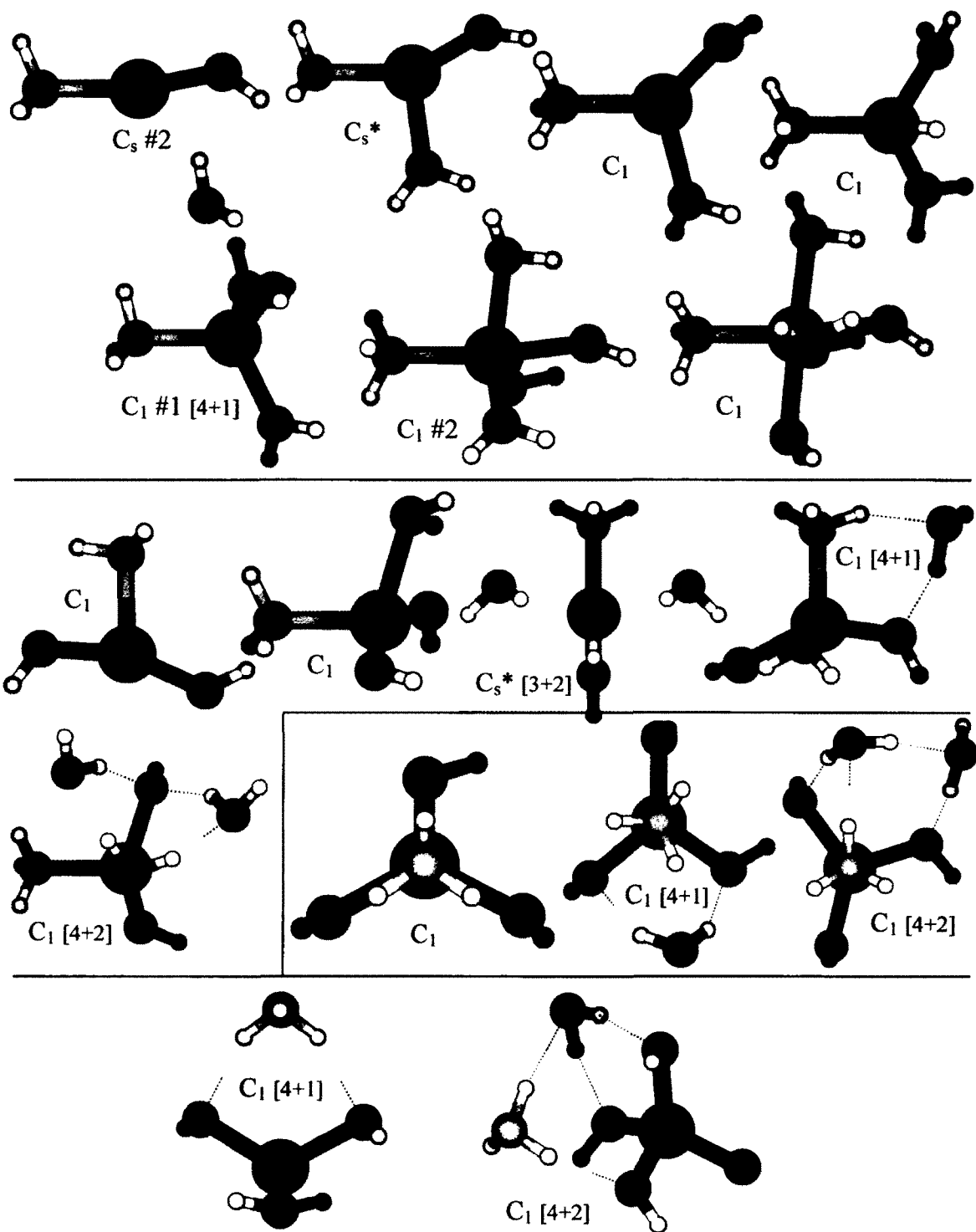


Figure 4-12: Optimized MP2 and B3LYP geometries for $[\text{Co}(\text{NH}_3)(\text{OH})_m(\text{H}_2\text{O})_l]^{2-m}$, where $m=1-4$, $l=0-(5-m)$. “*” indicates only stable at MP2, “^a” indicates only stable at B3LYP.

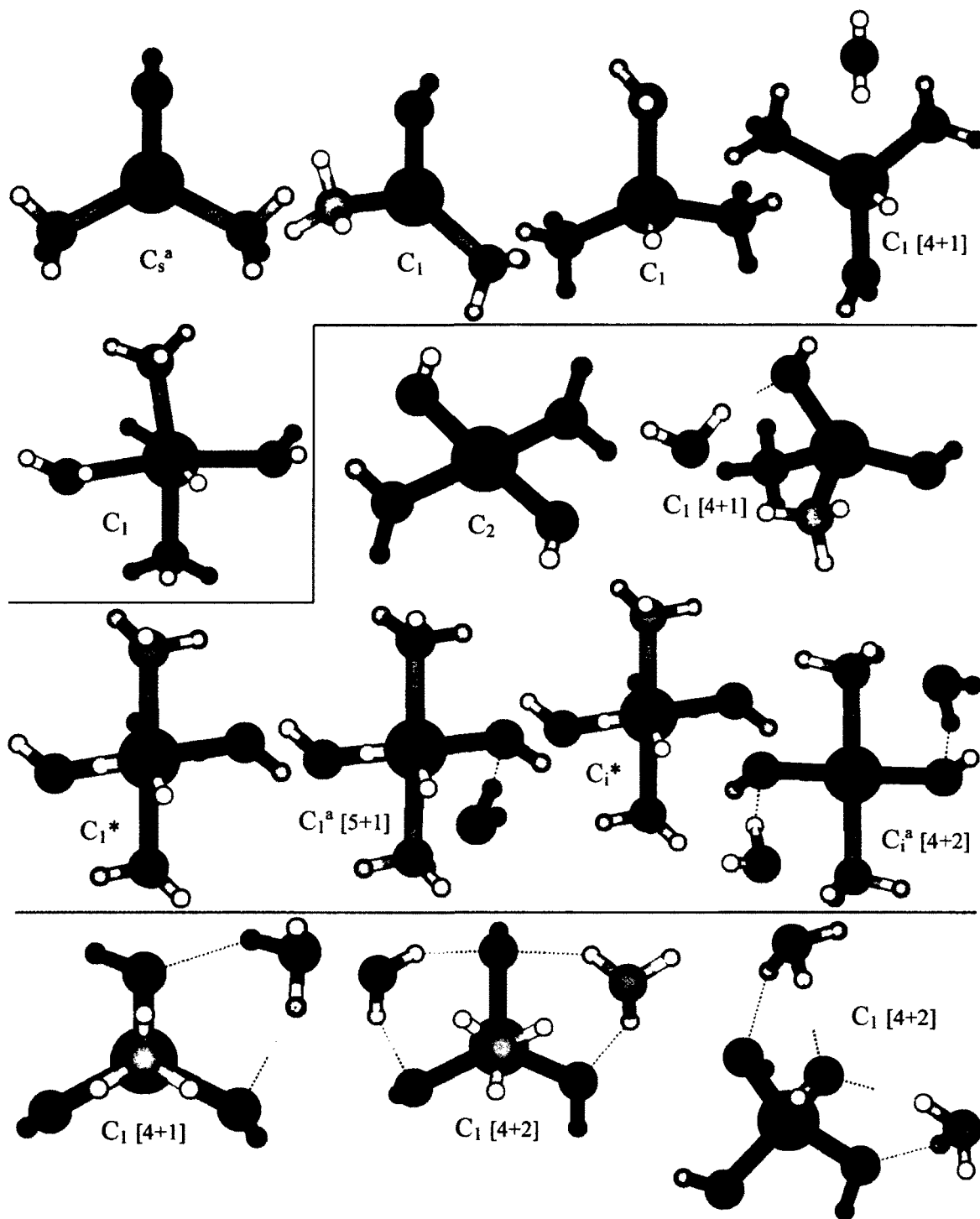


Figure 4-13: Optimized MP2 and B3LYP geometries for $[\text{Co}(\text{NH}_3)_2(\text{OH})_m(\text{H}_2\text{O})_l]^{2-m}$, where $m=1-4$, $l=0-(4-m)$. “*” indicates only stable at MP2, “^a” indicates only stable at B3LYP.

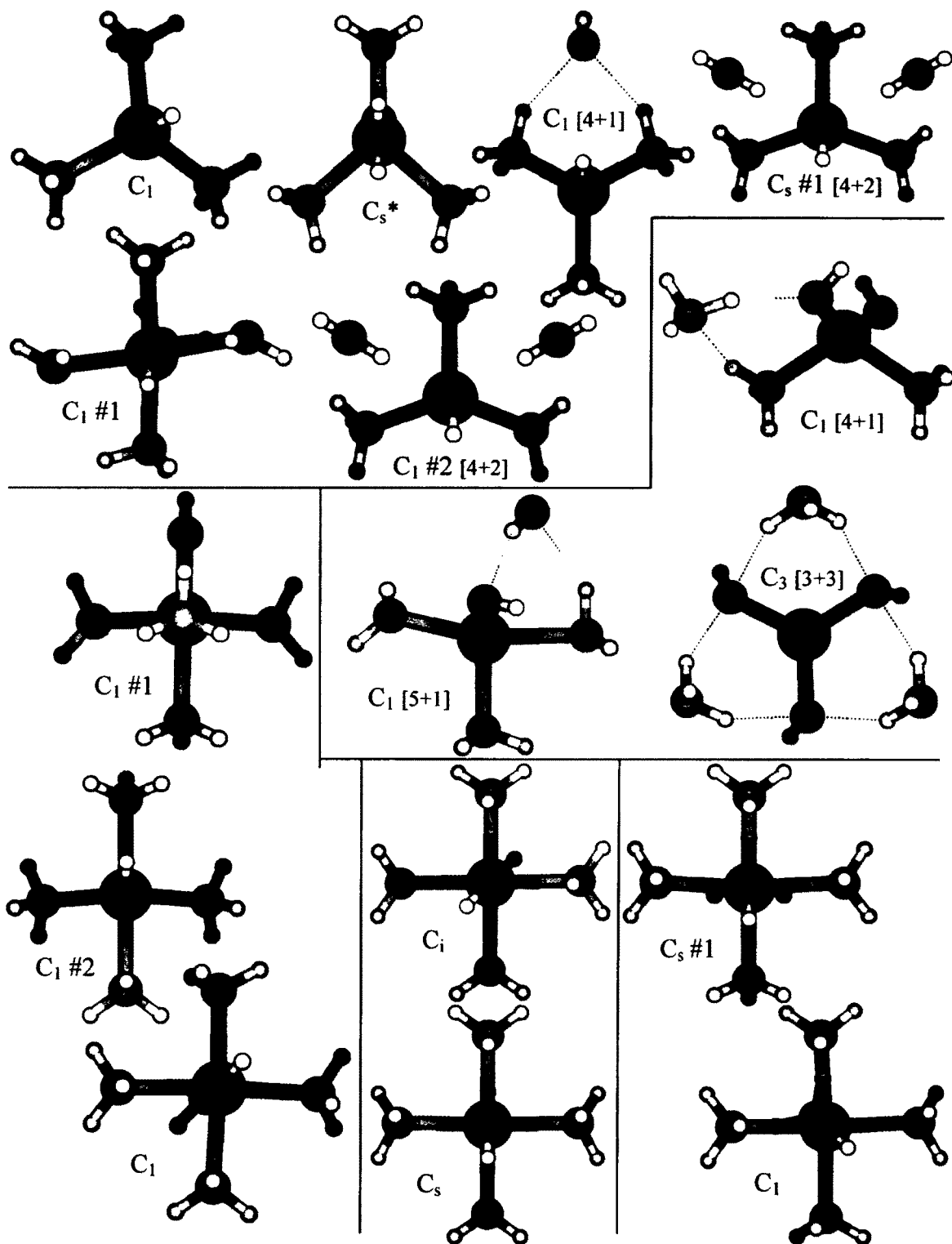


Figure 4-14: Optimized MP2 and B3LYP geometries for $[\text{Co}(\text{NH}_3)_n(\text{OH})_m(\text{H}_2\text{O})]^{2-m}$, where $n=3-5$, $m=1-(6-n)$, $l=0-(6-n-m)$. “*” indicates only stable at MP2, “a” indicates only stable at B3LYP.

4.4.2 Discussion/Literature Comparison

To confirm our geometries we would like to compare with experimental or other computational works found in the literature. However, the only mixed hydroxoamine complex that was found was contained in a study on the active site of carbonic anhydrase by Garmer and Krauss⁵⁵. Within their study they performed calculations on monohydroxo triamine using UHF/CEP-31G. Their resulting structural information included mean Co-O and Co-N bond distances of 1.86 and 2.17Å respectively which are equivalent to our HF/6-31+G* values of 1.849 and 2.171 Å. Unfortunately no other studies were found containing these mixed complexes and therefore we have nothing to compare with any of our remaining geometries.

Plots containing Co-O and Co-N bond lengths and vibrational stretching frequencies (Figure 4-15, Figure 4-16 and Figure 4-17) have been created and are located below. The general trend within all the bond distance plots is that the Co-O and Co-N bond distances increase as more water molecules are added to the given complex. There are also small clusters of bond lengths greater than 3Å, which is a result of ligand (water or ammonia) dissociation. There was no ion pair formation among this set of complexes (i.e. no dissociation of hydroxide ligands). An inverse relationship exists between the bond distances and the vibrational stretching frequencies associated with those bonds. This is evident when looking at both the bond distance and frequency plots side by side. As the bond lengths are increasing the vibrational stretching frequencies are decreasing to lower wavenumbers. Another thing to take note of in regard to the frequency plots is that

there are some frequencies which have both the “+” and the “|” label. This indicates that at this frequency there are both Co-N and Co-O stretches.

Raman intensity plots were created from the data obtained that the HF/6-31+G* level of theory. Although no experimental data could be found related to Raman activity for this set of complexes, it is still of importance to our colleagues to have this information for comparison with their experimental Raman work in the future. Plots were constructed for all the HF energy minimum structures and are located in Figure 4A-3 of the Chapter 4 appendix. Having this information will help in either assigning or confirming the experimental Raman bands.

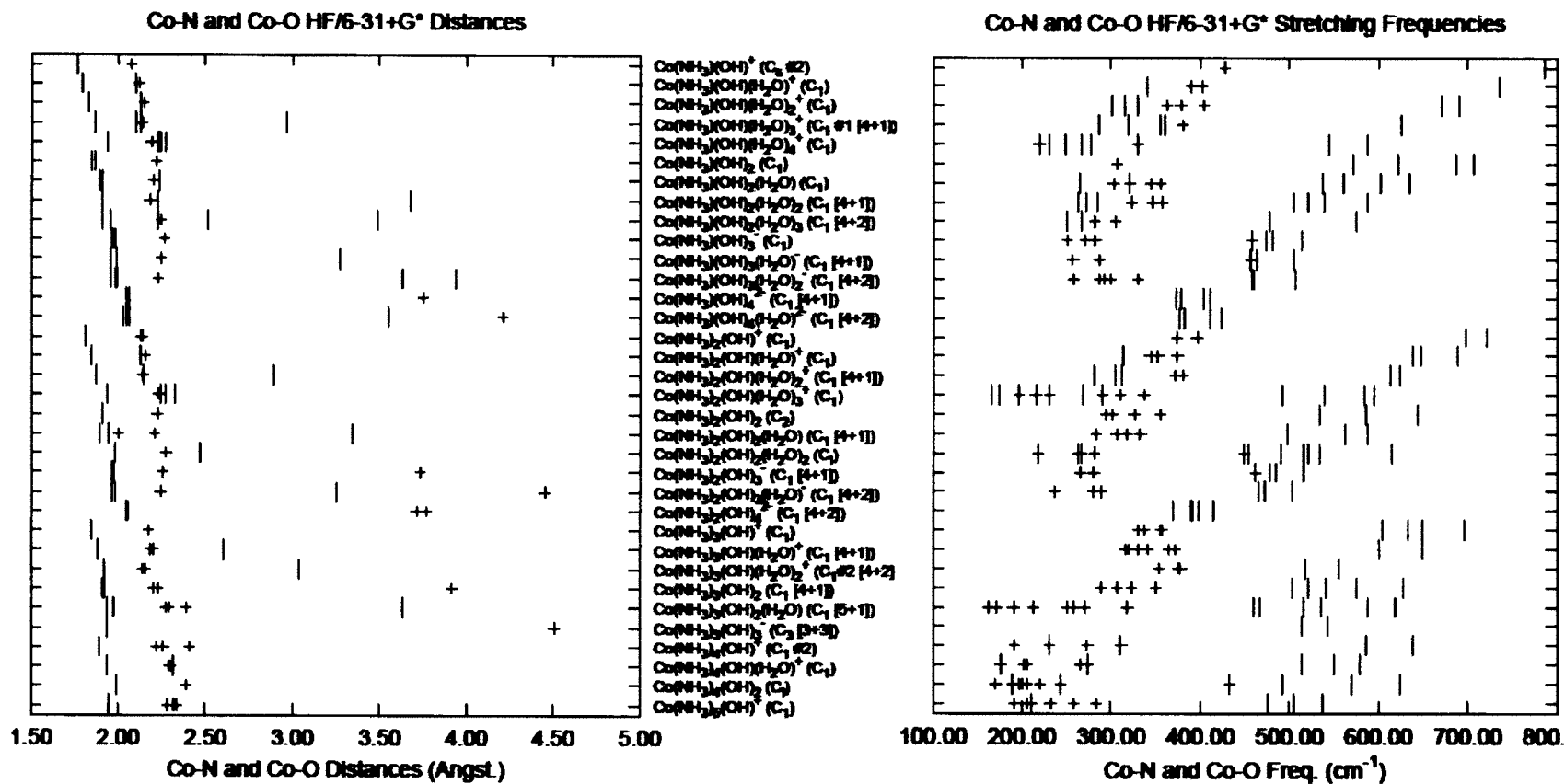


Figure 4-15: Co-N (+) and Co-O (|) bond lengths (left) and vibrational stretching frequencies (right) for $[\text{Co}(\text{NH}_3)_n(\text{OH})_m(\text{H}_2\text{O})_l]^{2-m}$, where $n=1-5$, $m=1-(5-n)$ and $l=0-(6-n-m)$, calculated at the HF/6-31+G* level.

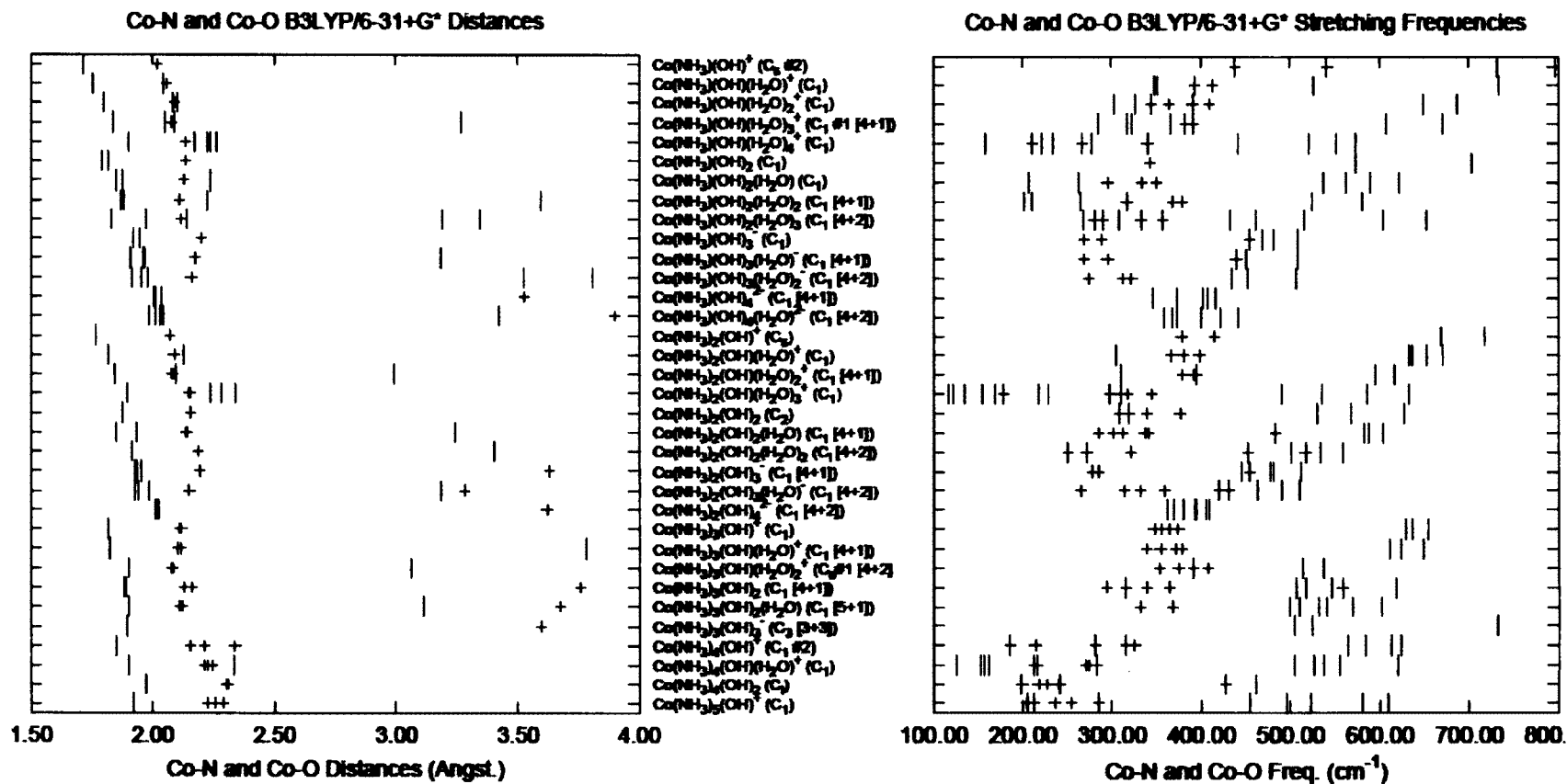


Figure 4-17: Co-N (+) and Co-O (|) bond lengths (left) and vibrational stretching frequencies (right) for $[\text{Co}(\text{NH}_3)_n(\text{OH})_m(\text{H}_2\text{O})_l]^{2-m}$, where $n=1-5$, $m=1-(5-n)$ and $l=0-(6-n-m)$, calculated at the B3LYP/6-31+G* level.

5.1 Conclusions

The primary goal of this research project was to predict possible corrosion products containing cobalt(II) that may exist inside the environment of a CANDU Gen-IV Supercritical Water-cooled Reactor (SCWR). This work will complement experimental Raman work that will be completed by our colleagues at the University of Guelph. The ligands of the cobalt(II) corrosion products were expected to be water, chloride, hydroxide, ammonia and combinations thereof and therefore any predictions would be based on *ab initio* computational chemistry calculations, in which we would model the possible combinations of ligands with the Co(II) metal center. Based on the results, some predictions could be made regarding the complexes that may be the best candidates as corrosion products in the extreme conditions of the reactor environment. Due to our study being completely computational, it would be very difficult to narrow the list of possible corrosion products to one or even 10. This is a result of corrosion being caused by a set of chemical reactions which depend on physical properties as well as radiation. Therefore all the reactions and thermodynamic conditions need to be taken into consideration before better predictions to be made. For that reason, what we will do is go through each set of complexes and provide a list of what we think might be the best candidates based on our results as well as experimental data that supports the existence of these complexes.

5.1.1 Aquacobalt(II)

Stable structures were found for all of the species studied here up to the hexaaqua complex. Due to the fact that all of these species are cations with a 2+ charge (water is a neutral ligand), they could not act alone and would require some kind of anion to form an overall neutral complex which could then be precipitated inside the pipes and valves of the reactor. However, of the six structures that we found here the most likely to be involved in a corrosion product inside the SCWR would be the hexaaquacobalt(II) ion, $[\text{Co}(\text{H}_2\text{O})_6]^{2+}$. As discussed in Chapter 3, many crystal structures have been reported that contain the hexaaquacobalt(II) ion as a part of the overall crystal structure.

5.1.2 Chlorocobalt(II)

With this set of complexes, both water and chloride ligands were added to the Co(II) center. There is a good chance that chloride will play some sort of role in the reactor because of it leaking in through the coolant system (river water). Unlike a water ligand, chloride ligands carry with them a single negative charge. Therefore, with these complexes have the possibility of having negative, neutral or positive overall charges. Due to the need of a neutral complex for precipitation to occur, the most likely complexes here are those containing cobalt(II) chloride, CoCl_2 . This includes those studied with water ligands as well, up to the six-coordinate $\text{CoCl}_2(\text{H}_2\text{O})_4$ species. This is not to say that the remaining species are not likely to exist, but they would need some kind of counter ion (i.e. anion if only one Cl^- ligand and cation if more than one Cl^- ligand). Also, based on our calculations, we can rule out any Co(II) complexes that contain more than

four chloride ligands. These complexes showed dissociation of one or more of the chloride ligands indicating their instability as a completely bound species.

5.1.3 Hydroxocobalt(II)

Once again we have a ligand that has a single negative charge. Thus the predicted complexes to be involved here include those containing neutral $\text{Co}(\text{OH})_2$. This species' insolubility in an aqueous and acidic/basic environments⁸⁹ makes it a good candidate for precipitation inside the aqueous, high temperature/pressure environment. The monohydroxo species may also be good candidates if an anion is scavenged inside the reactor to form a neutral species.

5.1.4 Amminecobalt(II)

The ammonia ligand is neutral, which means all the complexes studied here will have an overall 2+ charge. Based on cobalt(II) tending to exist in either a tetrahedral or octahedral form and on experimental evidence^{7,104-106,114} the most likely candidates here are the tetramminecobalt(II) and hexamminecobalt(II) species. We found various stable structures for these two species, with and without water ligands, and they could prove to be very likely to exist within the reactor provided they combine with some other small anionic species (i.e. chloride seems like a possible candidate) to form a neutral complex.

5.1.5 Chlorohydroxocobalt(II)

This set of mixed complexes, to a certain degree, brings together the idea that the single-ligand complexes of $\text{Co}(\text{OH})^+$ and CoCl^+ could be realistic possibilities. If the monohydroxo species combines with free chloride or the monochloro species combines

with free hydroxide in the reactor environment you would end up with some sort of mixed complex containing both ligands. The neutral complex here would contain $\text{CoCl}(\text{OH})$ with or without water ligands. Based on the calculations we have completed and the resulting stable structures we have found of this sort, the $\text{CoCl}(\text{OH})$ species seem to be a possible candidate for existence in the SCWR. The addition of more chloride or hydroxide ligands to this complex would require an additional cation to create a neutral complex. With additional Cl^- and OH^- ligands added to the central $\text{Co}(\text{II})$ the results tend to prefer the formation of ion pairs, which indicates the complexes are not stable in a completely bound form. Therefore having fewer chloride and hydroxide ligands seems to be favorable.

5.1.6 Chloroamminecobalt(II)

The ammonia complexes by themselves are all $2+$ cations. With the addition of chloride to the mix, neutral complexes can be created. Any of the complexes containing CoCl_2 plus the ammonia ligands would be neutral complexes and therefore have a possibility of existence as a corrosion product. With $\text{Co}(\text{II})$ complexes tending to exist in tetrahedral and octahedral geometries we can narrow the list down a little bit. This would leave us with four and six coordinate complexes containing two chloride ligands. These include $[\text{CoCl}_2(\text{NH}_3)_2]$, $[\text{CoCl}_2(\text{NH}_3)_2(\text{H}_2\text{O})_2]$ and $[\text{CoCl}_2(\text{NH}_3)_4]$. We have found six computationally stable complexes that fit these descriptions. These would be considered our best guess at the probable chloroammine complexes to exist in the reactor. The species with more than two chloride ligands tend to prefer ion pairs, indicating they may not be as stable as the dichloroammines.

5.1.7 Hydroxoamminecobalt(II)

Predicting the hydroxoammine complexes is similar to the chloroammine complexes. Neutral complexes in a tetrahedral or octahedral arrangement will probably be most influential, therefore we are limited to $[\text{Co}(\text{NH}_3)_2(\text{OH})_2]$, $[\text{Co}(\text{NH}_3)_2(\text{OH})_2(\text{H}_2\text{O})_2]$ and $[\text{Co}(\text{NH}_3)_4(\text{OH})_2]$. We have calculated eight different geometries that fit these descriptions in one way or another. Included in the eight are $[\text{Co}(\text{NH}_3)_2(\text{OH})_2(\text{H}_2\text{O})]$ (water has dissociated and H-bonded leaving a four-coordinate species), $[\text{Co}(\text{NH}_3)_2(\text{OH})_2(\text{H}_2\text{O})_2]$ (both waters have dissociated and H-bonded leaving a four-coordinate species) and $[\text{Co}(\text{NH}_3)_3(\text{OH})_2]$ (one of the ammonia ligands has dissociated and H-bonded, leaving a four-coordinate species). Although complexes with more ammonia ligands and one less hydroxide ligand were found to be stable, these species would have an overall positive charge thereby requiring another anion to create a neutral species that could precipitate and cause corrosion.

5.2 Future Work

Within this thesis we have completed the *ab initio* investigations of Co(II) with possible ligands of water, chloride, hydroxide, ammonia and combinations thereof. This research can be taken further by studying the complexes that contain all of these ligands (i.e. $[\text{CoCl}(\text{OH})(\text{NH}_3)]$), which were not considered here due to time restrictions. When the experimental Raman studies are completed these results will also be used for comparison and unknown Raman band assignment.

Also, cobalt(II) is not the only transition metal species that is likely to exist inside the SCWR reactor environment. The construction materials used to build the reactor will

likely be some type of metal alloy and hence there is a good chance of having nickel, iron and chromium dissolve and contaminate the reactor environment as well. If these species are existing inside the reactor they too can form corrosion products and also be a problem. There is also the potential for other ligands to be involved in the formation of corrosion products. These potential candidate ligands are carbonyl (CO), carboxylic acids (e.g. humate and formate), bisulfide (HS), porphyrins and arsenates due to their ability to form stable complexes with transition metals and also their potential availability to be present inside the reactor environment. So the *ab initio* studies that have been applied to Co(II) complexes can be extended to include these other transition metal complexes as well as some, if not all, of the other ligands mentioned. The studies of nickel(II) and iron(II) are currently being worked on in our research group.

References

- ¹ Torgerson, D.; Shalaby, B.; Pang, S. *Nucl. Eng. Des.*, **2006**, *26 (14-16)*, 1565.
- ² Was, G.; Ampornrat, P.; Gupta, G.; Teyseyre, S.; West, E.; Allen, T.; Sridharan, K.; Tan, L.; Chen, Y.; Ren, X.; Pister, C. *J. Nucl. Mater.*, **2007**, *371 (1-3)*, 176.
- ³ Schweitzer, G. K. and Pesterfield, L. L. In *The Aqueous Chemistry of the Elements*; Oxford University Press: New York, **2010**.
- ⁴ Greenwood, N. N. and Earnshaw, A. In *Chemistry of the Elements, 2nd Edition*; Elsevier: Great Britain, **1997**.
- ⁵ Young, R. S. In *Cobalt: Its Chemistry, Metallurgy and Uses*; Reinhold Publishing Corporation: New York, **1960**.
- ⁶ Young, R. S. In *Cobalt*; Reinhold Publishing Corporation: New York, **1948**.
- ⁷ Cotton, F. A. and Wilkinson, G. In *Advanced Inorganic Chemistry: A Comprehensive Text, 2nd Revised and Augmented Edition*; Wiley Interscience: New York, **1967**.
- ⁸ Revie, R. W. and Uhlig, H. H. In *Corrosion and Corrosion Control: An Introduction to Corrosion Science and Engineering, 4th Edition*; Wiley Interscience: New Jersey, **2008**.
- ⁹ Hwang, S.; Lee, B.; Kim J.; Jang, J. *J. Nucl. Mater.* **2008**, *372*, 177.
- ¹⁰ Nanstad, R.; McClintock, D.; Hoelzer, D.; Tan, L.; Allen, T. *J. Nucl. Mater.* **2009**, *392*, 331.
- ¹¹ Undefined. (July 8, 2011). Cobalt. In United States Environmental Protection Agency. Retrieved August 12, 2011, from <http://www.epa.gov/radiation/radionuclides/cobalt.html>.
- ¹² McQuarrie, D. A. In *Quantum Chemistry, 2nd Edition*; University Science Books: California, **2008**.
- ¹³ Eyring, H.; Walter, J.; Kimball, G. E. In *Quantum Chemistry*; John Wiley & Sons: New York, **1967**.
- ¹⁴ Ratner, M. A. and Schatz, G. C. In *Introduction to Quantum Mechanics in Chemistry*; Prentice Hall: New Jersey, **2001**.
- ¹⁵ Schrödinger, E., *Phys. Rev.*, **1926**, *28*, 1049.
- ¹⁶ Mueller, M. In *Fundamentals of Quantum Chemistry: Molecular Spectroscopy and Modern Electronic Structure Computations*; Kluwer Academic/Plenum Publishers: New York, **2001**.
- ¹⁷ Atkins, P. W. and Friedman, R. S. In *Molecular Quantum Mechanics, 3rd Edition*; Oxford University Press: New York, **1997**.
- ¹⁸ Born, M. and Oppenheimer, J. R., *Ann. Physik*, **1927**, *84*, 458.
- ¹⁹ Lewars, E. In *Computational Chemistry: Introduction to the Theory and Applications of Molecular and Quantum Mechanics*; Kluwer Academic: Boston, **2003**.
- ²⁰ Young, D. C. In *Computational Chemistry: A Practical Guide for Applying Techniques to Real World Problems*; Wiley Interscience: New York, **2001**.
- ²¹ Møller, C. and Plesset, M. S., *Phys. Rev.*, **1934**, *46*, 618.
- ²² Hohenberg, P. and Kohn, W., *Phys. Rev.*, **1964**, *136 (3B)*, B864.
- ²³ Kohn, W. and Sham, L. J., *Phys. Rev.*, **1965**, *140 (4A)*, A1133.
- ²⁴ Magnasco, V. In *Methods of Molecular Quantum Mechanics: An Introduction to Electronic Molecular Structure*; John Wiley & Sons: Great Britain, **2009**.
- ²⁵ Foresman, J. B. and Frisch, Æ. In *Exploring Chemistry with Electronic Structure Methods, 2nd Edition*; Gaussian, Inc: U.S.A., **1996**.
- ²⁶ Becke, A. D., *J. Chem. Phys.*, **1993**, *98 (7)*, 5648.
- ²⁷ Lee, C.; Yang, W.; Parr, R. G., *Phys. Rev. B*, **1988**, *37 (2)*, 785.
- ²⁸ Jensen, F. In *Introduction to Computational Chemistry, 2nd Edition*; John Wiley & Sons: Great Britain, **2007**.
- ²⁹ Stephens, P. J.; Devlin, F. J.; Chabalowski, C. F.; Frisch, M. J., *J. Phys. Chem.*, **1994**, *98 (45)*, 11623.
- ³⁰ Klamt, A. and Schüürmann, G., *J. Chem. Soc., Perkin Trans. 2*, **1993**, *5*, 799.
- ³¹ Cramer, C. J. and Truhlar, D. G., *Chem. Rev.*, **1999**, *99*, 2161.
- ³² Gaussian 03, Revision C.02, Frisch, M. J.; Trucks, G. W.; Schlegel, H. B.; Scuseria, G. E.; Robb, M. A.; Cheeseman, J. R.; Montgomery, Jr., J. A.; Vreven, T.; Kudin, K. N.; Burant, J. C.; Millam, J. M.; Iyengar, S. S.; Tomasi, J.; Barone, V.; Mennucci, B.; Cossi, M.; Scalmani, G.; Rega, N.; Petersson, G. A.; Nakatsuji, H.; Hada, M.; Ehara, M.; Toyota, K.; Fukuda, R.; Hasegawa, J.; Ishida, M.; Nakajima, T.; Honda, Y.;

- Kitao, O.; Nakai, H.; Klene, M.; Li, X.; Knox, J. E.; Hratchian, H. P.; Cross, J. B.; Bakken, V.; Adamo, C.; Jaramillo, J.; Gomperts, R.; Stratmann, R. E.; Yazyev, O.; Austin, A. J.; Cammi, R.; Pomelli, C.; Ochterski, J. W.; Ayala, P. Y.; Morokuma, K.; Voth, G. A.; Salvador, P.; Dannenberg, J. J.; Zakrzewski, V. G.; Dapprich, S.; Daniels, A. D.; Strain, M. C.; Farkas, O.; Malick, D. K.; Rabuck, A. D.; Raghavachari, K.; Foresman, J. B.; Ortiz, J. V.; Cui, Q.; Baboul, A. G.; Clifford, S.; Cioslowski, J.; Stefanov, B. B.; Liu, G.; Liashenko, A.; Piskorz, P.; Komaromi, I.; Martin, R. L.; Fox, D. J.; Keith, T.; Al-Laham, M. A.; Peng, C. Y.; Nanayakkara, A.; Challacombe, M.; Gill, P. M. W.; Johnson, B.; Chen, W.; Wong, M. W.; Gonzalez, C.; and Pople, J. A.; Gaussian, Inc., Wallingford CT, 2004.
- ³³ Undefined. (March 29, 2011). ACEnet: Accelerating Discovery. Retrieved September 7, 2011 from <http://www.ace-net.ca/wiki/ACEnet>
- ³⁴ Schaftenaar, G. and Noordik, J.H., *J. Comput.-Aided Mol. Design*, **2000**, *14*, 123.
- ³⁵ Swift, T. J. *Inorg. Chem.*, **1964**, *3* (4), 526.
- ³⁶ Swaddle, T. W. and Fabes, L. *Can. J. Chem.*, **1980**, *58*, 1418.
- ³⁷ Chmelnick, A. M. and Fiat, D. *J. Chem. Phys.*, **1967**, *47* (10), 3986.
- ³⁸ Matwiyoff, N. A. and Darley, P. E. *J. Phys. Chem.*, **1968**, *72* (7), 2659.
- ³⁹ Prelesnik, B. V.; Gabela, F.; Ribár, B.; Krstanović, I. *Cryst. Struct. Comm.*, **1973**, *2*, 581.
- ⁴⁰ Blackburn, A. C.; Gallucci, J. C.; Gerkin, R. E., *Acta Cryst.*, **1990**, *B46*, 712.
- ⁴¹ Kariuki, B. M. and Jones, W., *Acta Cryst.*, **1993**, *C49*, 2100.
- ⁴² Yotnoi, B.; Luachan, S.; Prior, T. J.; Rujiwatra, A., *Acta Cryst. E.*, **2009**, *E65*, i52
- ⁴³ Cotton, F. A.; Daniels, L. M.; Murillo, C. A.; Quesada, J. F., *Inorg. Chem.*, **1993**, *32*, 4861.
- ⁴⁴ Faherty, K. P.; Thompson, C. J.; Aguirre, F.; Michne, J.; Metz, R. B., *J. Phys. Chem. A*, **2001**, *105*, 10054.
- ⁴⁵ Beaver, W. D.; Trevorrow, L. E.; Estill, W. E.; Yates, P. C.; Moore, T. E., *J. Am. Chem. Soc.*, **1953**, *75* (18), 4556.
- ⁴⁶ Åkesson, R.; Pettersson, L. G. M.; Sandström, M.; Siegbahn, P. E. M.; Wahlgren, U., *J. Phys. Chem.*, **1992**, *96*, 10773.
- ⁴⁷ Åkesson, R.; Pettersson, L. G. M.; Sandström, M.; Siegbahn, P. E. M.; Wahlgren, U., *J. Phys. Chem.*, **1993**, *97*, 3765.
- ⁴⁸ Rotzinger, F. P., *J. Am. Chem. Soc.*, **1997**, *119*, 5230.
- ⁴⁹ Gilson, H. S. R. and Krauss, M., *J. Phys. Chem. A*, **1998**, *102*, 6525.
- ⁵⁰ Fedorchuck, C. and Swaddle, T. W., *J. Phys. Chem. A*, **2000**, *104*, 5651.
- ⁵¹ Gilson, H. S. R. and Krauss, M., *J. Phys. Chem. A*, **2000**, *104*, 5653.
- ⁵² Mendoza-Huizar, L. H.; Palomar-Pardavé, M.; Robles, J., *Electrochim. Acta*, **2001**, *46*, 2749.
- ⁵³ Deeth, R. J. and Randell, K., *Inorg. Chem.*, **2008**, *47* (16), 7377
- ⁵⁴ Schmiedekamp, A. M.; Ryan, M. D.; Deeth, R. J., *Inorg. Chem.*, **2002**, *41* (22), 5733.
- ⁵⁵ Garmer, D. R. and Krauss, M., *J. Am. Chem. Soc.*, **1992**, *114*, 6487.
- ⁵⁶ Rulišek, L. and Havlas, Z., *J. Chem. Phys.*, **2000**, *112* (1), 149.
- ⁵⁷ Varadwaj, P. R. and Marques, H. M., *Phys. Chem. Chem. Phys.*, **2010**, *12*, 2126.
- ⁵⁸ Magnusson, E. and Moriarty, N. W., *Inorg. Chem.*, **1996**, *35*, 5711.
- ⁵⁹ Irish, D. E. and Brooker, M. H. In *Advances in Infrared and Raman Spectroscopy, Vol. 2*; Heyden: London, **1976**.
- ⁶⁰ Pye, C. C. and Corbeil, C. R., *Can. J. Chem.*, **2002**, *80*, 1331.
- ⁶¹ Pye, C. C.; Corbeil, C. R.; Rudolph, W. W., *Phys. Chem. Chem. Phys.*, **2006**, *8*, 5428.
- ⁶² Mishra, S. K. and Kanungo, S. B., *J. Therm. Anal.*, **1992**, *38*, 2437.
- ⁶³ Morosin, B. and Graeber, E. J., *Acta Cryst.*, **1963**, *16*, 1176.
- ⁶⁴ Gamo, I., *Bull. Chem. Soc. Jap.*, **1961**, *34* (10), 1430.
- ⁶⁵ Waizumi, K.; Kouda, T.; Tanio, A.; Fukushima, N.; Ohtaki, H., *J. Solution Chem.*, **1999**, *28* (2), 83.
- ⁶⁶ Mizuno, J.; Ukei, K.; Sugawara, T., *J. Phys. Soc. Japan*, **1959**, *14*, 383.
- ⁶⁷ Tesarowicz, I.; Oleksyn, B. J.; Nitek, W., *Chirality*, **2007**, *19*, 152.
- ⁶⁸ Skórska, A.; Stadnicka, K.; Oleksyn, B. J., *Chirality*, **2005**, *17*, 73.
- ⁶⁹ Girma, K. B.; Lorenz, V.; Blaurock, S.; Edelman, F. T., *Z. Anorg. Allg. Chem.*, **2005**, *631*, 1419.
- ⁷⁰ Orpen, A. G. and Quayle, M. J., *J. Chem. Soc., Dalton Trans.*, **2001**, 1601.

- ⁷¹ Porai-Koshits, M. A., *J. Struct. Chem.*, **1961**, 2 (2), 207.
- ⁷² Powell, H. M. and Wells, A. F., *J. Chem. Soc.*, **1935**, 359.
- ⁷³ Figgis, B. N.; Gerloch, M.; Mason, R., *Acta Cryst.*, **1964**, 17, 506.
- ⁷⁴ Smithson, J. M. and Williams, J. P., *J. Chem. Soc.*, **1958**, 457.
- ⁷⁵ Bjerrum, J.; Halonin, A. S.; Skibsted, L. H., *Acta Chem. Scand. A*, **1975**, 29, 326.
- ⁷⁶ Migdisov, A. A.; Zezin, D.; Williams-Jones, A. E., *Geochim. Cosmochim. Acta*, **2011**, 75, 4065.
- ⁷⁷ Nagayama, H.; Hojo, M.; Ueda, T.; Nishimori, Y.; Okamura, M.; Daike, C., *Anal. Sci.*, **2001**, 17, 1413.
- ⁷⁸ Skibsted, L. H. and Bjerrum, J., *Acta Chem. Scand. A*, **1978**, 32, 429.
- ⁷⁹ Carunchio, V.; Ceipidor, U. B.; Messina, A., *Inorg. Chim. Acta*, **1972**, 6 (4), 613.
- ⁸⁰ Cotton, F. A.; Goodgame, D. M. L.; Goodgame, M., *J. Am. Chem. Soc.*, **1961**, 83 (23), 4690.
- ⁸¹ Ferraro, J. R. and Walker, A., *J. Chem. Phys.*, **1965**, 42 (4), 1278.
- ⁸² Srivastava, B. K.; Khandelwal, D. P.; Bist, H. D., *Appl. Spectrosc.*, **1975**, 29 (2), 190.
- ⁸³ Grindstaff, W. K. and Fogel, N., *J. Chem. Soc., Dalton Trans.*, **1972**, 1476.
- ⁸⁴ Lucasse, W. W. and Abrahams, H. J., *J. Phys. Chem.*, **1933**, 37 (4), 511.
- ⁸⁵ Katzin, L. I. and Ferraro, J. R., *J. Am. Chem. Soc.*, **1953**, 75 (15), 3821.
- ⁸⁶ Clark, G. L.; Quick, A. J.; Harkins, W. D., *J. Am. Chem. Soc.*, **1920**, 42 (12), 2483.
- ⁸⁷ Chesnut, D. B., *J. Chem. Phys.*, **1960**, 33 (4), 1234.
- ⁸⁸ Moore, T. E.; Gootman, E. A.; Yates, P. C., *J. Am. Chem. Soc.*, **1955**, 77 (2), 298.
- ⁸⁹ Gayer, K. H. and Garrett, A. B., *J. Am. Chem. Soc.*, **1950**, 72 (9), 3921.
- ⁹⁰ Ismail, J.; Ahmed, M.; Kamath, P.; Subbanna, G. N.; Uma, S.; Gopalakrishnan, J. *J. Solid State Chem.* **1995**, 114, 550.
- ⁹¹ Jayashree, R. S. and Kamath, P. V., *J. Mater. Chem.*, **1999**, 9, 961.
- ⁹² Ramesh, T.; Rajamathi, M.; Kamath, P., *Solid State Sci.* **2003**, 5, 751.
- ⁹³ Mockenhaupt, C.; Zeiske, T.; Lutz, H. D., *J. Mol. Struct.*, **1998**, 443, 191.
- ⁹⁴ Xu, Z. P. and Zeng, H. C., *Chem. Mater.*, **1999**, 11, 67.
- ⁹⁵ Ricca, A. and Bauschlicher Jr., C. W., *J. Phys. Chem. A*, **1997**, 101, 8949.
- ⁹⁶ Trachtman, M.; Markham, G. D.; Glusker, J. P.; George, P.; Bock, C. W., *Inorg. Chem.*, **2001**, 40, 4230.
- ⁹⁷ Cassady, C. J. and Freiser, B. S., *J. Am. Chem. Soc.*, **1984**, 106, 6176.
- ⁹⁸ Bolzan, J. A. and Arvia, A. J., *Electrochim. Acta*, **1962**, 7, 589.
- ⁹⁹ Shankar, J. and De Souza, B. C., *Aust. J. Chem.*, **1963**, 16, 1119.
- ¹⁰⁰ Kishi, Y.; Shigemi, S.; Doihara, S.; Mostafa, M. G.; Wase, K., *Hydrometallurgy*, **1998**, 47, 325.
- ¹⁰¹ Ćosović, B.; Degobbis, D.; Bilinski, H.; Branica, M., *Geochim. Cosmochim. Acta*, **1982**, 46 (2), 151.
- ¹⁰² Swift, T. J. and Connick, R. E., *J. Chem. Phys.*, **1962**, 37 (2), 307.
- ¹⁰³ Gordon, S. and Schreyer, J. M., *Anal. Chem.*, **1951**, 23 (2), 381.
- ¹⁰⁴ Barnet, M. T.; Craven, B. M.; Freeman, H. C., *Chem. Commun. (London)*, **1966**, 10, 307.
- ¹⁰⁵ Newman, J. M.; Binns, M.; Hambley, T. W.; Freeman, H. C., *Inorg. Chem.*, **1991**, 30, 3499.
- ¹⁰⁶ Brumm, H. and Jansen, M., *Z Anorg. Allg. Chem.*, **2001**, 627, 1433.
- ¹⁰⁷ Simic, M. and Lilie, J., *J. Am. Chem. Soc.*, **1974**, 96 (1), 291.
- ¹⁰⁸ Lilie, J.; Shinohara, N.; Simic, M. G., *J. Am. Chem. Soc.*, **1976**, 98 (21), 6516.
- ¹⁰⁹ Geselowitz, D. A., *Inorg. Chim. Acta*, **1989**, 163, 79.
- ¹¹⁰ Banci, L.; Bencini, A.; Benelli, C.; Gatteschi, D.; Zanchini, C., *Struct. Bond.*, **1982**, 52, 37.
- ¹¹¹ Bjerrum, J. In *Metal Ammine Formation in Aqueous Solution: Theory of the Reversible Step Reactions*; P. Haase and Son: Copenhagen, **1941**.
- ¹¹² Glaeser, H. H.; Dodgen, H. W.; Hunt, J. P., *Inorg. Chem.*, **1965**, 4 (7), 1061.
- ¹¹³ Murray, R.; Lincoln, S. F.; Glaeser, H. H.; Dodgen, H. W.; Hunt, J. P., *Inorg. Chem.*, **1969**, 8 (3), 554.
- ¹¹⁴ Bertin, E. P.; Nakagawa, I.; Mizushima, S.; Lane, T. J.; Quagliano, J. V., *J. Am. Chem. Soc.*, **1958**, 80 (3), 525.
- ¹¹⁵ Simplicio, J. and Wilkins, R. G., *J. Am. Chem. Soc.*, **1969**, 91 (6), 1325.